Vol. 8 No. 2
October 2024

ISSN 2579-5821
e-ISSN 2579-5546

S3
sinta
Science and Technology Index

Jurnal Geocelebes

Published by:
Geophysics Department
Hasanuddin University
Makassar, Indonesia

JURNAL GEOCELEBES

Geophysics Department | Faculty of Mathematics and Natural Sciences | Hasanuddin University

Volume 8 Number 2, October 2024

P-ISSN: 2579-5821
E-ISSN: 2579-5546

Published by:
Geophysics Department, Math and Natural Science Faculty
Hasanuddin University

JURNAL GEOCELEBES

Volume 8 Number 2, October 2024

ISSN: 2579 – 5821 (Print)
ISSN: 2579 – 5546 (Online)
URL address: http://journal.unhas.ac.id/index.php/geocelebes

Diterbitkan berkala dua kali setahun oleh/ **Published periodically two times annually by**
Dept. Geofisika Universitas Hasanuddin/ **Geophysics Dept., Hasanuddin University**

Dewan Redaksi/ Editor Board

Sekretariat/ Secretariat:
Departemen Geofisika, FMIPA Universitas Hasanuddin
Gedung MIPA, Kampus Unhas Tamalanrea - Jalan Perintis Kemerdekaan, Makassar, Sulawesi Selatan, 90245.
E-mail: geocelebes@sci.unhas.ac.id

Jurnal Geocelebes is a scientific journal published by the Department of Geophysics, Hasanuddin University. This journal is intended as a means of scientific publication in the field of geophysics ranging from theoretical topics to geophysical applications in various fields topics. The articles are original research results, reviews of recent advances in a particular topic, case studies of geophysical applications or reviews of software related to geophysics. Papers should be sent to the editorial website in softcopy using the template provided. Each accepted paper will be reviewed for eligibility through a rigorous reviewing process by the Editorial Board.

Contents

JURNAL GEOCELEBES

Volume 8, Number 2, October 2024

ISSN: 2579 – 5821 (Print)
ISSN: 2579 – 5546 (Online)

URL: http://journal.unhas.ac.id/index.php/geocelebes

Preface

Jurnal Geocelebes managed by the Department of Geophysics, Faculty of Mathematics and Natural Sciences, Hasanuddin University Makassar has entered its eighth year. The Editorial Board expresses gratitude to God Almighty for this achievement and expresses gratitude for the commitment of the Editorial Board, in carrying out this mandate. In particular, the Editorial Board expresses its gratitude and highest appreciation to all authors who have submitted their scientific works and to the Reviewers who have been willing to take the time to provide constructive suggestions and corrections to each article in each issue of the Jurnal Geocelebes.

In the edition of Volume 8 Number 2 October 2024 there are six articles. The articles published generally discuss the implementation of the role of geosciences, especially geophysics in natural resource exploration and other fields that are in accordance with the focus and scope of the field published by the Jurnal Geocelebes. The language used in this volume and in the future is English, which shows that Jurnal Geocelebes deserves to be an international journal in the future. Jurnal Geocelebes welcomes participation from academics, researchers, industry practitioners, students, and others in the field of geosciences in both theoretical and application perspectives, both related to the subsurface (lithosphere) and above the surface (atmosphere), which of course will go through a series of processes namely submitting, editing, and reviewing.

The Editorial Board of Jurnal Geocelebes is open to suggestions and constructive criticism for future improvements. All suggestions and criticisms can be sent via email geocelebes@sci.unhas.ac.id

Makassar, October 2024

The Editorial Board of Jurnal Geocelebes

ISSN: 2579-5821 (Print)
ISSN: 2579-5546 (Online)
URL address: http://journal.unhas.ac.id/index.php/geocelebes
DOI: 10.20956/geocelebes.v8i2.25377

Jurnal Geocelebes Vol. 8 No. 2, October 2024, 123 – 131

Identification Lithology of Geothermal Potential Areas Using the Electrical Resistivity Tomography (ERT) Method

Hana Raihana[1], Suhendra[1]*, Khairun Nazli[2], Halauddin[1], Refrizon[1]

[1]Department of Geophysics, Faculty of Mathematics and Natural Sciences, Bengkulu University
[2]Department of Geophysical Engineering, Faculty of Engineering, Syiah Kuala University

*Corresponding author. Email: suhendra@unib.ac.id

Manuscript received: 9 February 2023; Received in revised form: 19 September 2023; Accepted: 27 September 2023

Abstract

The rock lithology of the potential hydrothermal area has been studied using Electrical Resistivity Tomography (ERT) in Pungguk Pedaro Village, Bingin Kuning District, Lebong Regency. Field data acquisition uses a stretch length of 480 meter with the MAE X612-EM Geoelectric tool that forms a straight line. ERT method, using Res2dinvx64 software. The study aims to determine the subsurface conditions of the potential hydrothermal area and the characteristics of the rocks that make up the hydrothermal area. The results of this study can be concluded that Pungguk Pedaro Village is dominated by clay, sandstone, sandy gravel, andesite, basalt, and granite rocks. In this study, measurements were taken with six lines to see variations in resistivity values as a reference for identifying potential geothermal lithologies. There is 1 line that cuts to five lines to validate the resistivity value of each line. Line 1 has no potential for hydrothermal distribution because there has been a mixture of hydrothermal water with mountain water, so this line will only provide groundwater.

Keywords: ERT; Hydrothermal; Lebong Regency; Lithology; Wenner.

Citation: Raihana, H., Suhendra, S., Nazli, K., Halauddin, H., & Refrizon, R. (2024). Identification Lithology of Geothermal Potential Areas Using the Electrical Resistivity Tomography (ERT) Method. *Jurnal Geocelebes*, 8(2):123–131, doi: 10.20956/geocelebes.v8i2.25377

Introduction

Geothermal energy is energy generated by the penetration of high-temperature water confined to the earth's surface at high temperatures for a long time. Geothermal energy is closely related to geothermal systems (Afandi et al., 2013).

Indonesia is one of the countries with great potential for geothermal resources. The government is developing this enormous potential to meet the country's energy needs. Based on the latest survey data from the geology, at the end of 2009, Indonesia had 265 geothermal sites resulting from volcanic and non-volcanic processes.

This situation is closely related to Indonesia's geological position at the meeting zone of three major world plates: the Indo-Australian, Eurasian, and Pacific plates, which are responsible for forming volcanoes in Indonesia (Chaidir et al., 2021).

The potential geothermal energy in Indonesia is abundant. This is inseparable from the geography of Indonesia, which is located on the Pacific Rim. This energy spreads over Sumatra, Java, Bali, Flores, North Sulawesi, and Maluku with 312 potential points. With a resource wealth that reaches 40% of the world's resources, Indonesia has the most extensive geothermal potential in the world, with a potential of more than 23.9 gigawatts

(GW) or 29 Gwe (Nurwahyudin & Harmoko, 2020).

Barrett (2013) define geothermal resources as the earth's stored heat that can be used in the future for power generation or other suitable industrial, agricultural, or domestic uses. Inadequate geological conditions can make geothermal energy expansion uneconomical in many places. The existence of geothermal potential is indicated by manifestations, such as hot springs, fumaroles, and altered rocks, caused by tectonic activity that causes faulting and allows fracture zones to exist (Tarmidzi & Setyawan, 2014).

The geothermal system includes a water system, a heating process, and system conditions under which water is heated (Basid et al., 2014). Geothermal systems include the water system, the heating process, and the conditions under which the heated water is collected. So, the geothermal system has requirements such as the availability of water, heating rock, nest rock, and cover rock (Vargemezis, 2014).

Water generally comes from rainwater or meteoric water. Hot rocks will serve as a source of hot water, which can be granite masses or other forms of batholith (Karaman, 2013). The heat generated by active fault movement is also sometimes used as a heat source, such as hot springs along active fault lines (Hidayat et al., 2021).

The potential geothermal areas are at Bengkulu Province, Bingin Kuning district, Lebong Regency, and Pungguk Pedaro village. The existence of geothermal energy is subject to secondary permeability in the form of annual faults. These faults direct hot fluids from the reservoir to the surface through hot springs, rock formations, and fumaroles (Abdillah & Malik, 2021). The rock geology of the region consists of granite, andesite, and basalt. The hydrothermal zone of Toyokuni Pedaro hot springs is also closely related to magmatic activity in the Barisan Hills (Raihana et al., 2023).

Previous research on geothermal in Lebong regency has been conducted by Fathan (2013) and Gafoer & Amin (2007). The results were obtained in the form of most of the fluid sourced from reservoirs, and some have experienced interaction with sedimentary rocks. This study aims to determine the lithology of potential geothermal areas in Lebong Regency that are thought to originate from Bukit Daun. Therefore, further research needs to be done to look if the lithology of this potential geothermal area has the potential for geothermal exploration so that it can be exploited in Pungguk Pedaro village, Bingin Kuning District, Lebong Regency, Bengkulu Province.

In geothermal reservoirs, lithology is very important to consider as it allows us to identify zones with geothermal potential (Erwin, 2016)).

Electrical Resistivity Tomography (ERT) is one of the most effective geophysical methods to map subsurface conditions and determine the lithology of the study area . This method aims to study the variation of rock resistivity under the earth's surface, both vertically and horizontally (Pitulima & Siregar, 2016). This method produces a two-dimensional profile of the resistivity pattern in the subsurface and describes the vertical and horizontal (2-D) variations in the layered structure of the subsurface resistivity (Railasha et al., 2015).

Regional Geology

The study area is structurally located in the forearc basin of the Bengkulu Basin. Neogene sediments were influenced by the tectonic evolution of the bay (Yulihanto, 1995). Sapiie et al. (2015) argues that Bengkulu Basin sedimentation is also

influenced by the activity of right-lateral strike-slip fault systems called the Mentawai Fault Zone (MFZ) and the Sumatra Fault Zone (SFZ). Therefore, fault activity is believed to influence basins' formation and sedimentary processes in basins. In the late Oligocene, the Hulusimpang Formation (Tomh) was deposited by Eocene to early Oligocene volcanic facies.

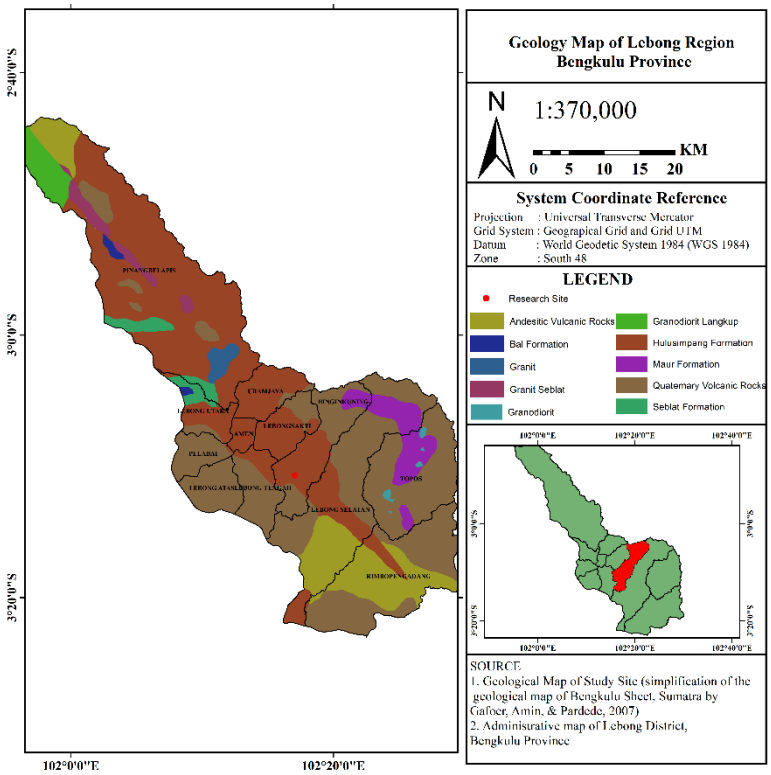

Figure 1. Geology Map of Lebong Region (Gafoer & Amin., 2007).

Materials and Methods

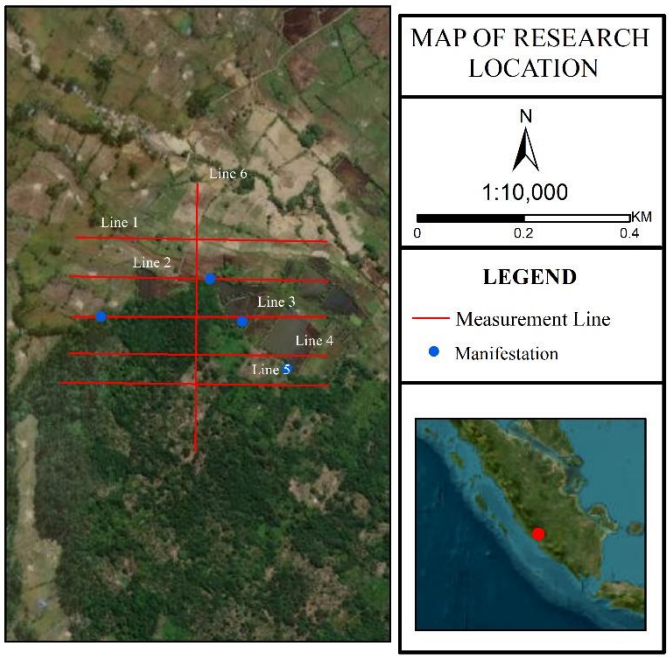

Figure 2. Map of research Location.

The study site is geographically located at the latitude and longitude coordinates (3°10'41.19" LS and 102° 17'4.98" BT). This study uses an MAE X612-EM geoelectric tool in Punguk Pedaro Village, Bingin Kuning District, Lebong Province field data collection Pungguk Pedaro with a line length of 480 meters. The measurement line takes the form of a line or a straight line by adjusting the conditions of the measurement area Pedaro Village, Bingin Kuning District. Therefore, there is 1 line that cuts five lines to validate the value of each line. The results of field measurements are in the form of 2D models, which are processed with Res2DInv.

Results and Discussion

Table 1. Resistivity value of the rock (Telford & Geldart, 1931).

Material	Resistivity (Ωm)
Air	~
Pyrite	0.01–100
Quartz	500–800000
Calcite	$1x10^{-12}$–10^{13}
Rock salt	30 – 10^{13}
Granite	200 – 10000
Andesite	$1.7x10^{2}$ – $45x10^{4}$
Basalt	200 – 1000000
Limestone	500 – 10000
Sandstone	200 – 8000
Shales	20 – 2000
Sand	1 – 1000
Clay	1 – 100
Ground water	0.5 – 300
Sea water	0.2
Magnetite	0.01 – 1000
Dry Gravel	600 – 10000
Alluvium	10 – 800
Gravel	100 – 600

Electric charge cross sections were obtained from processing resistivity geoelectric data (Pratama & Rustadi, 2019) from the field using Res2Dinvx64 software. The Wenner - beta configuration resistivity geoelectric method accepts a subsurface cross-section in 2 dimensions: the resistivity cross-section (Amir et al., 2017). Interpretation of 2D geoelectric data uses the table of resistivity values by Telford & Geldart (1931) (Table 1) and adjusts to the geological conditions of the data collection location.

Table 2. Interpretation in each line site.

Site	Resistivity (Ωm)	Lithology
Line 1	3.71	Groundwater
	7.98	Groundwater
	17.2	Silty Sand
	37.0	Clay
	79.6	Sandstone
	171	Sandy Gravel
	369	Andesite
Line 2	2.14	Hydrothermal
	5.36	Groundwater
	13.4	Tuff
	33.5	Clay
	83.7	Sandstone
	209	Basalt
	523	Andesite
Line 3	1.06	Hydrothermal
	3.01	Hydrothermal
	8.50	Groundwater
	24.0	Clay
	67.9	Sandstone
	192	Sandy Gravel
	542	Andesite
	1532	Volcanic Breccia
Line 4	1.42	Hydrothermal
	3.63	Hydrothermal
	9.25	Groundwater
	23.6	Clay
	60.1	Sandstone
	153	Sandy Gravel
	390	Andesite
	994	Granite
Line 5	1.97	Hydrothermal
	4.86	Hydrothermal
	12.0	Groundwater
	29.6	Clay
	73.0	Sandstone
	180	Sandy Gravel
	444	Andesite
	1097	Granite
Line 6	0.693	Hydrothermal
	1.70	Hydrothermal
	4.53	Groundwater
	12.1	Groundwater
	32.3	Clay
	86.1	Silt-Clay
	230	Andesite
	613	Granite

The source of geothermal energy is magma all over the earth. Magma transfers heat to surrounding rocks (Erwin, 2016). This heat also causes hot water convection within the pores of stones and rocks. This

hot water then moves upwards but is blocked by rock formations and does not reach the surface (Putriutami et al., 2014). This is because impermeable rock layers surround the character. Impermeable layers separate the hydrothermal and groundwater within the geothermal reservoir (Widiatmoko, 2019). The reservoir is isolated from shallow groundwater. So far, however, it is still being determined whether that hydrothermal fluid is from bedrock heating (in the form of magma) below the source point or simply hydrothermal flows from other regions (Suciningtyas et al., 2013). A fissure in the rock through which the hot water flows allows hot water from another area to emerge on the surface. The 2-Dimensional resistivity model can also display topographic data (Riputra & Malik, 2021).

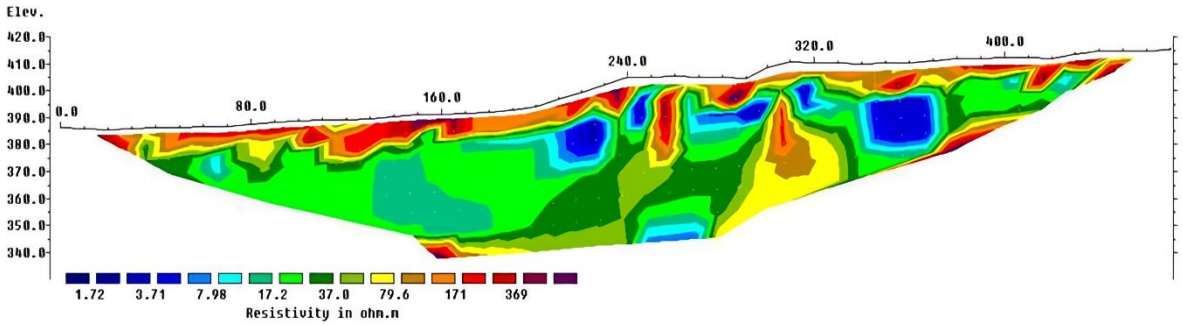

Figure 3. Data processing results of line 1 with topography.

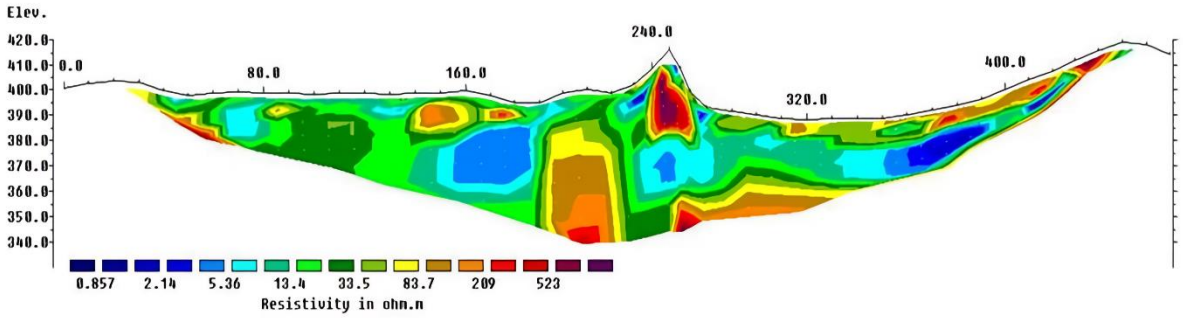

Figure 4. Data processing results of line 2 with topography.

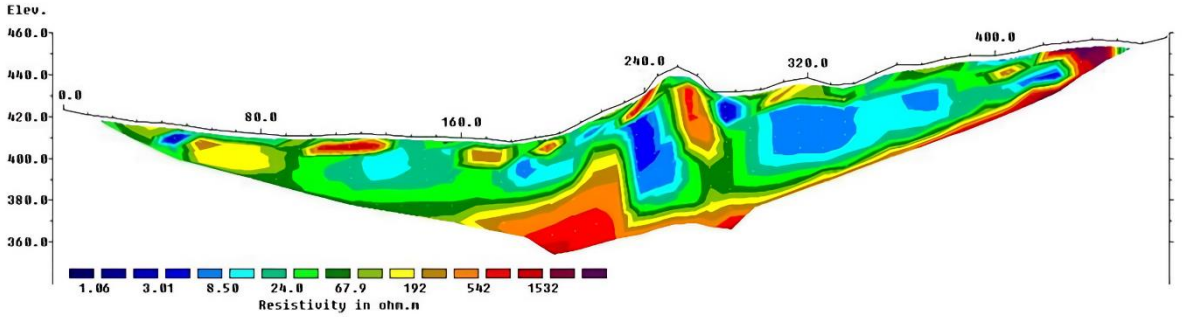

Figure 5. Data processing results of line 3 with topography.

This research was conducted in an area that has hydrothermal potential. This area has a significant perspective for geothermal exploration. This condition requires research to see this area's lithology and geothermal distribution. The results of this research are used as reference material for geothermal exploration, which is then exploited for the benefit of the community and government.

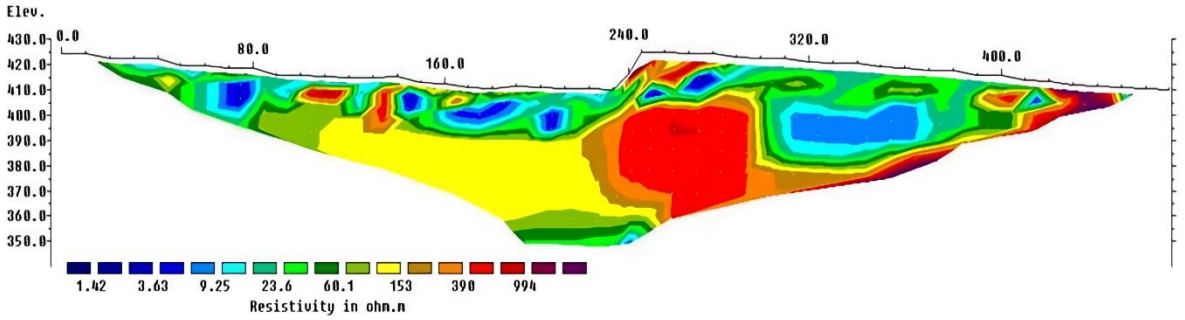

Figure 6. Data processing results of line 4 with topography.

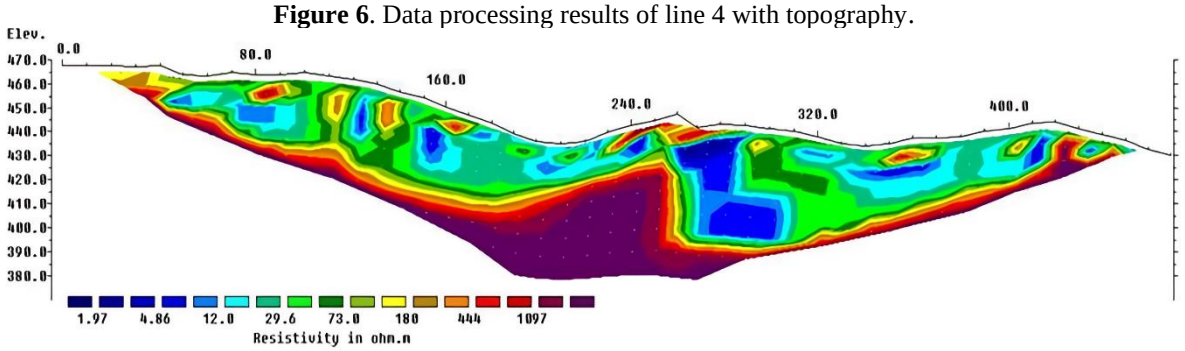

Figure 7. Data processing results of line 5 with topography.

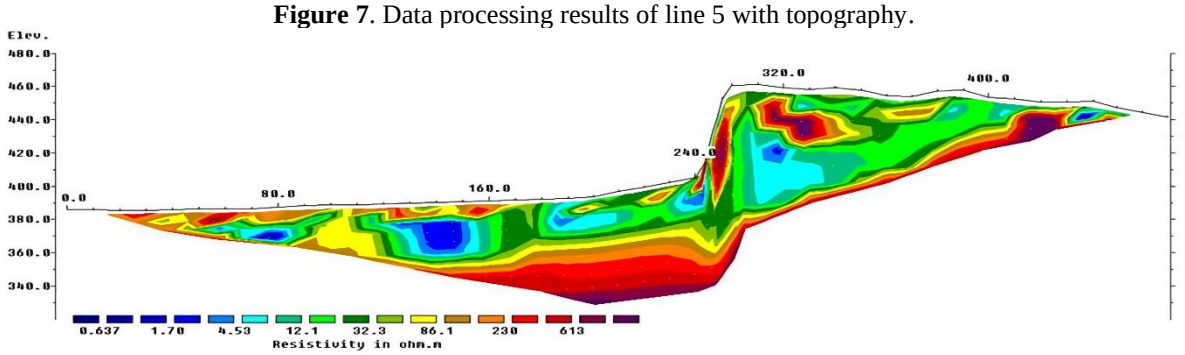

Figure 8. Data processing results of line 6 with topography.

The measurement results in each line with the potential for hydrothermal has a small resistivity value, one of which can be seen in Figure 7. The rock structures dominating this potential hydrothermal area are clay, sandstone, sandy gravel, andesite, basalt, and granite (Telford & Geldart, 1931). This rock type is an andesite-basalt volcanic rock unit, with the formation dominating the Hulusimpang formation. This rock type has low porosity, thermal conductivity, and high permeability (Adli, 2021). After surveying the research site, information was obtained that the hydrothermal potential is in lines 2, line 3, line 4, line 5, and line 6, which have small resistivity values.

In contrast, in line 1 (Figure 3), there is no visible hydrothermal potential because this line is a rice field area. Although it has a small resistivity value, it is groundwater. Line 1 is dominated by silty sand lithology. Although the water in this area is warm, it is water flowing from the hill that has appeared hydrothermal manifestations. The results of each 2D lithology on line 1 (Figure 3), line 2 (Figure 4), line 3 (Figure 5), line 4 (Figure 6), line 5 (Figure 7), and line 6 (Figure 8) are dominated by andesite rocks which are thought to be medium-composition extrusive volcanic rocks with aphanitic to porphyritic textures. Another factor causing hydrothermal is that this area is influenced by the presence of secondary permeability in the form of the Ketahun fault. This Ketahun fault controls the hot fluid in the reservoir to flow to the surface in the form of hot springs, rock alteration,

and fumaroles that appear and are also closely related to the magmatic activity in the Bukit Barisan range (Raihana et al., 2023). On line 6 (Figure 8), it made cuts between lines to validate the data of other lines to be more accurate. Line 6 is taken from the bottom of the hill to the top of the slope of the research area to get maximum results. Line 6 has a significant height because line 6 is a cut between hills, between which there are five other lines to validate different resistivity values.

Conclusion

The rock lithology of the hydrothermal area in Pungguk Pedaro Village, Bingin Kuning District, Lebong Regency, using the Electrical Resistivity Tomography (ERT) method, shows that the rock layer structure is an andesite-basalt volcanic rock unit with the Hulusimpang formation. Each line in the study area has an even distribution of hydrothermal potential and similar rock types. Still, those that appear to have considerable potential are seen in several lines. Line 1 has no potential for hydrothermal water with mountain water, so only groundwater is obtained.

Acknowledgments

Thanks to my friends who have helped with my research and my advisor for helping me do this article as well as possible. Thank the Village Head and the local community for receiving us well during the research process.

Author Contribution

Compiling this research journal, each writer was divided into several job desks for collecting literature sources and making research survey designs using QGIS by Khairun Nazli, data processing, and journal preparation by Hana Raihana. The observers in the practice of this journal are Suhendra, Refrizon, and Halauddin.

Conflict of Interest

There is no financial or personal relationship between the author and the organization or other parties in this research, so the research results are the author's responsibility.

References

Abdillah, F., & Malik, U. (2021). Pemetaan Sebaran Mata Air Panas Di Daerah Objek Wisata Desa Pawan Menggunakan Metode Geolistrik Tahanan Jenis Konfigurasi Wenner. *Komunikasi Fisika Indonesia*, 18(1), 35–41. http://dx.doi.org/10.31258/jkfi.18.1.35-41

Adli, M. (2021). *Simulasi Numerik Aliran Fluida Hidrotermal Dan Perpindahan Energi Panas Dengan Hydrotherm Interactive Pada Daerah Padang Cermin, Lampung*. Universitas Lampung.

Afandi, A., Maryanto, S., & Rachmansyah, A. (2013). Identifikasi Reservoar Daerah Panasbumi Dengan Metode Geomagnetik Daerah Blawan Kecamatan Sempol Kabupaten Bondowoso. *Jurnal Neutrino*, 6(1), 11–10. https://doi.org/10.18860/neu.v0i0.2441

Amir, H., Akmam, A., Bavitra, B., & Azhari, M. (2017). Penentuan Kedalaman Batuan Dasar Menggunakan Metode Geolistrik Tahanan Jenis Dengan Membandingkan Konfigurasi Dipole-Dipole Dan Wenner Di Bukit Apit Puhun Kecamatan Guguk Panjang Kota Bukittinggi. *EKSAKTA: Berkala Ilmiah Bidang MIPA*, 18(01), 19–30. https://doi.org/10.24036/eksakta/vol18-iss01/13

Barrett, M. (2013). *Renewable energy sources and the city*. A Handbook of Sustainable Building Design and Engineering: An Integrated Approach

to Energy, Health and Operational Performance.

Basid, A., Andrini, N., & Arfiyaningsih, S. (2014). Pendugaan Reservoir Sistem Panas Bumi dengan Menggunakan Survey Geolistrik, Resistivitas Dan Self Potensial (Studi Kasus: Daerah Manifestasi Panas Bumi di Desa Lombang, Kecamatan Batang-Batang, Sumenep). *Jurnal Neutrino*, 7(1), 57–60. https://doi.org/10.18860/neu.v7i1.2640

Chaidir, F. Y., Puspita, O. D., Rumahorbo, G., & Hamdalah, H. (2021). Analysis of Geomagnetic and Geoelectric Data to Identify the Potential of Gold Deposits (Case Study: Randu Kuning, Wonogiri, Central Java). *IOP Conference Series: Earth and Environmental Science*, 830(1), 012052. https://doi.org/10.1088/1755-1315/830/1/012052

Erwin. (2016). Pendugaan Reservoir Daerah Potensi Panas Bumi Pencong Dengan Menggunakan Metode Tahanan Jenis. *Jurnal Sains dan Pendidikan Fisika*, 12(3), 346–355. https://ojs.unm.ac.id/JSdPF/article/view/3063

Fathan, Q. (2013). Studi Potensi Panasbumi Daerah Hululais Kabupaten Lebong Provinsi Bengkulu, Sumatera. *Geosains*, 9(2), 125–134.

Gafoer, S., Amin, T. C., & Pardede, R. (2007). *Peta geologi lembar Bengkulu, Sumatera*. Bandung : Pusat Penelitian dan Pengembangan Geologi. https://geologi.esdm.go.id/geomap/pages/preview/peta-geologi-lembar-bengkulu-sumatera

Hidayat, H., Putra, A., & Pujiastuti, D. (2021). Identifikasi Sebaran Anomali Magnetik pada Daerah Prospek Panas Bumi Nagari Aie Angek, Kabupaten Tanah Datar. *Jurnal Fisika Unand*, 10(1), 48–54. https://doi.org/10.25077/jfu.10.1.48-54.2021

Suciningtyas, I. K. L. N., Maryanto, S., & Rachmansyah, A. (2013). Sebaran Mataair Panas Blawan-Ijen Berdasarkan Data Geolistrik Resistivitas. *Natural B*, 2(2), 164–171. http://dx.doi.org/10.21776/ub.natural-b.2013.002.02.11

Karaman, A. (2013). Preliminary geoelectrical identification of a low-temperature hydrothermal system in the Anzer glacial valley, İkizdere, Rize, Turkey. *Turkish Journal of Earth Sciences*, 22(4), 664–670. https://doi.org/10.3906/yer-1207-7

Nurwahyudin, D. S., & Harmoko, U. (2020). Pemanfaatan dan Arah Kebijakan Perencanaan Energi Panas Bumi di Indonesia Sebagai Keberlanjutan Maksimalisasi Energi Baru Terbarukan. *Jurnal Energi Baru dan Terbarukan*, 1(3), 111–123. https://doi.org/10.14710/jebt.2020.10032

Pitulima, J., & Siregar, R. N. (2016). Identifikasi Struktur Geologi Sumber Air Panas Non Volkanik Desa Nyelanding Bangka Selatan dengan menggunakan metode geolistrik konfigurasi Wenner. *Prosiding Seminar Nasional Riset Terapan*, D63–D70. https://e-prosiding.poliban.ac.id/index.php/snrt/article/download/64/111/

Pratama, W., & Rustadi, R. (2019). Aplikasi Metode Geolistrik Resistivitas Konfigurasi Wenner-Schlumberger Untuk Mengidentifikasi Litologi Batuan Bawah Permukaan Dan Fluida Panas Bumi Way Ratai Di Area Manifestasi Padok Di Kecamatan Padang Cermin Kabupaten Pesawaran Provinsi Lampung. *Jurnal Geofisika Eksplorasi*, 5(1), 30–44. https://doi.org/10.23960/jge.v5i1.21

Raihana, H., Sinaga, J. E. E., Cahyani, A. G., Halauddin., Suhendra., Hutauruk, A., & Sugianto, N. (2023).

Identification of Alteration Zones Based on Resistivity and Induced Polarization Geoelectric Survey. *Jambura Geoscience Review*, 5(2), 119–126. https://doi.org/10.34312/jgeosrev.v5i2.17931

Railasha, V., Satibi, S., & Nugroho, S. A. (2015). Interpretasi Lapisan Bawah Permukaan Tanah Menggunakan Metode Geolistrik 2-D (Mapping). *Jurnal Online Mahasiswa*, 2(2), 1–7. https://jom.unri.ac.id/index.php/JOMFTEKNIK/article/view/7627/7299

Riputra, B. Y., & Malik, U. (2021). Survei Sumber Air Panas Dengan Metode Geolistrik Konfigurasi Wenner (Studi Kasus: Wisata Air Panas Pawan, Pasirpangaraian). *Komunikasi Fisika Indonesia*, 18(2), 146–150. http://dx.doi.org/10.31258/jkfi.18.2.146-150

Sapiie, B., Yulian, F., Chandra, J., Satyana, A. H., Dharmayanti, D., Rustam, A. H., & Deighton, I. (2015). Geology and Tectonic Evolution of Fore-Arc Basins: Implications of Future Hydrocarbon Potential in the Western Indonesia. *Proceedings of Indonesia Petroleum Association, 39th Annual Convenion and Exhibition*. https://archives.datapages.com/data/ipa_pdf/2015/ipa15-g-177.htm

Putriutami, E. S., Harmoko, U., & Widada, S. (2014). Interpretasi Lapisan Bawah Permukaan Di Area Panas Bumi Gunung Telomoyo, Kabupaten Semarang Menggunakan Metode Geolistrik Resistivity Konfigurasi Schlumberger. *Youngster Physics Journal*, 3(2), 97–106. https://ejournal3.undip.ac.id/index.php/bfd/article/view/5281/5086

Tarmidzi, F., & Setyawan, A. (2014). Study of fluid flow in gedongsongo temple manifestation geothermal based on the data of geophysics. *Energy Procedia*, 47, 101–107. https://doi.org/10.1016/j.egypro.2014.01.202

Vargemezis, G. (2014). 3D geoelectrical model of geothermal spring mechanism derived from VLF measurements: A case study from Aggistro (Northern Greece). *Geothermics*, 51, 1–8. https://doi.org/10.1016/j.geothermics.2013.09.001

Widiatmoko, F. R. (2019). Pendekatan Analisa Geokimia dengan Multivariate Analysis untuk Mengetahui Tipe Mata Air Panas: Studi Kasus Lapangan Panas Bumi Mapos, Nusa Tenggara Timur. *Jurnal IPTEK*, 23(2), 71–78. https://doi.org/10.31284/j.iptek.2019.v23i2.518

Yulihanto, B., Situmorang, B., Nurdjajadi, A., & Sein, B. (1995). Structural Analysis of the Onshore Bengkulu Forearc Basin and Its Implication for Future Hydrocarbon Exploration Activity. *24th Annual Convention Proceedings*, 1, 85–96. https://archives.datapages.com/data/ipa/data/024/024001/85_ipa024a0085.htm

ISSN: 2579-5821 (Print)
ISSN: 2579-5546 (Online)
URL address: http://journal.unhas.ac.id/index.php/geocelebes
DOI: 10.70561/geocelebes.v8i2.34588

Jurnal Geocelebes Vol. 8 No. 2, October 2024, 132 – 141

Identification of Sub-Fault Zone Using Magnetotelluric Inversion (Case Study: Ketaun Fault, Lemeu Village, Lebong Regency)

Nurul Ilmi Rahmawati[1,3], M. Farid[1,2,3]*, Arif Ismul Hadi[1,2,3]*, Andre Rahmat Al Ansory[1,3]

[1]Geophysics Study Program, University of Bengkulu, Indonesia.
[2]Centre for Disaster Mitigation Studies, University of Bengkulu, Indonesia
[3]Mitigation and Exploration Laboratory, Floor 2, Integrated laboratory

*Corresponding author. Email: mfarid@unib.ac.id, ismulhadi@unib.ac.id

Manuscript received: 24 April 2024; Received in revised form: 10 June 2024; Accepted: 26 June 2024

Abstract

Lemeu Village, Lebong Regency, borders the Bukit Barisan Mountain range and is crossed by the Ketaun Fault, which causes a high level of seismic activity, so it is necessary to conduct research on the potential existence of the Ketaun sub-fault as one of the efforts to mitigate natural disasters such as earthquakes. The Magnetotelluric method utilises the earth's natural electromagnetic field, which is used to determine the distribution of resistivity in the subsurface using the ADU-07e Magnetotelluric tool with two horizontal electrical sensors (Ex, Ey) and three horizontal (Hx, Hy) and vertical (Hz) magnetic sensors and uses seven research points with an interval of 1 km. Data processing uses MAPROS software to convert data from the time domain to the frequency domain and ZONDMT2D to obtain subsurface resistivity values. The results obtained from this study are 2D magnetotelluric cross sections showing a zone with low resistivity values between research points P4 and P5 which is thought to be a new fault zone with resistivity values ranging from 1.3 – 6.1 Ωm from a depth of 2.5 km to a depth of 10 km. The zone is assumed to be a new fault that is a branch of the Ketaun fault.

Keywords: Fault; Lebong; Magnetotelluric; Resistivity.

Citation: Rahmawati, N.I., Farid, M., Hadi, A.I. & Al Ansory, A.R. (2024). Identification of Sub-Fault Zone Using Magnetotelluric Inversion (Case Study: Ketaun Fault, Lemeu Village, Lebong Regency). *Jurnal Geocelebes*, 8(2):132–141, doi: 10.70561/geocelebes.v8i2.34588

Introduction

Bengkulu Province is one of the provinces on the island of Sumatra that the Bukit Barisan crosses. According to Geology, Bukit Barisan was formed due to the subduction pressure of the Indo-Australian Tectonic Plate that penetrates under the Eurasian Tectonic Plate and moves at a velocity of 50-70 mm/year (Mulyati et al., 2020). This causes Bengkulu Province to have a high level of seismic activity due to the plate movement (Hadi & Brotopuspito, 2016).

Another result of the plate movement is that Indonesia is divided into many regions bounded by many active fault lines. Fractures in rocks that experience movement are referred to as faults. Faults usually form paths or lines, but they can also form fault planes or single fractures (Supartoyo et al., 2019).

Faults are divided into normal fault, reverse fault, strike-slip fault. Based on the activity level, faults are classified into active and inactive faults (Firdaus et al., 2016). One of the active faults in Indonesia is the Sumatra fault. The Sumatra fault cuts through the Bukit Barisan mountain range along 1,900 km, starting from the Sunda Strait to the Aceh region and the Andaman Sea (Lubis et al., 2019). The Sumatra fault was formed as a result of subduction between the Indo-Australian and Eurasian plate (Arisbaya et al., 2016).

The Sumatra fault is divided into several segments with varying segment lengths ranging from 60 km to up to 200 km (Natawidjaja, 2018). This makes Sumatra a lot of active faults. One of the active faults in Sumatra is the Ketaun fault. The Ketaun fault stretches from Ketaun, Lebong, Tes to Muaraaman along 85 km and 20 km wide. It has a northwest-to-southeast orientation direction and upward movement characteristics (Sieh & Natawidjaja, 2000).

Faults cause earthquakes that affect local tectonic geological conditions (Muflihah, 2014). One of the tectonic hazards is the people who live on the island of Sumatra, especially the Bengkulu Province, especially the North Bengkulu and Lebong Regencies, which are crossed by the Ketaun Segment Sumatra fault (Ardiansyah, 2018).

Lemeu Village in Lebong Regency is directly adjacent to the Bukit Barisan Mountains. These mountains are at the epicenter of active faults and are in an earthquake-prone zone (Bahri et al., 2022). In 1943, a large earthquake with a magnitude of M=7.4 occurred on the Ketaun segment and caused considerable damage to the Tes District to Muara Aman District. Another earthquake occurred in 1952 with M=6.8 (Syaputra et al., 2023). When viewed from the location of the main segment, the Ketaun segment, it is a land fault that has potential to damage in the event of a natural disaster earthquake even though the magnitude is not too large, the depth is shallow and close to settlements and community activities (Rais, 2021). So, it is necessary to research the existence of potential sub-faults in the Ketaun segment that have not been mapped as one of the disaster mitigation efforts to minimize the risk of fatal damage.

One of the geophysical methods used to determine the presence of sub-faults is the Magnetotelluric (MT) method because it is considered capable of detecting subsurface structures up to approximately 8,000 meters (Wulandari et al., 2017). This is because MT method measurements use low frequencies to detect to a greater depth than other methods. On the other hand, the top depth of the Sumatra fault is around 3 km (PUSGEN, 2017). Previous research on fault identification using the MT method was conducted by Arisbaya et al. (2023) to identify the possibility of an active fault in Garut, West Java. The MT method also mapped the Altyn Tagh fault, an Indian-Asian structure (Zhang et al., 2015). In addition, the MT method can estimate local structures and faults of geothermal fields.

This research is expected to provide comprehensive information on the existence of potential unmapped sub-faults to monitor the movement of these plates to minimize losses and impacts caused by earthquake natural disasters.

Materials and Methods

According to Van Bemmelen (1949), the physiographic zone of Sumatra is grouped into four parts, the Bukit Barisan Mountains, Semangko Fault, Tigapuluh Mountains, and undulating lowlands. The research location in Lemeu Village is included in the Bukit Barisan Mountains zone with physiographic conditions formed in the form of hills with narrow valleys composed of tertiary sedimentary rocks (Adrianda & Sutriyono, 2022). The Regional Geological Condition of Lebong Regency can be seen in Figure 1.

Based on the Geological map of Bengkulu sheet in (Al Ansory et al., 2023), fault structures that can be found in the geological structure of the study area include: joint, Air Putih slip fault and Batang Ketaun fault which have the age of late Miocene, when the main force moves relatively north-south, which is the time of formation of geological structures in the study area (Putra et al., 2017).

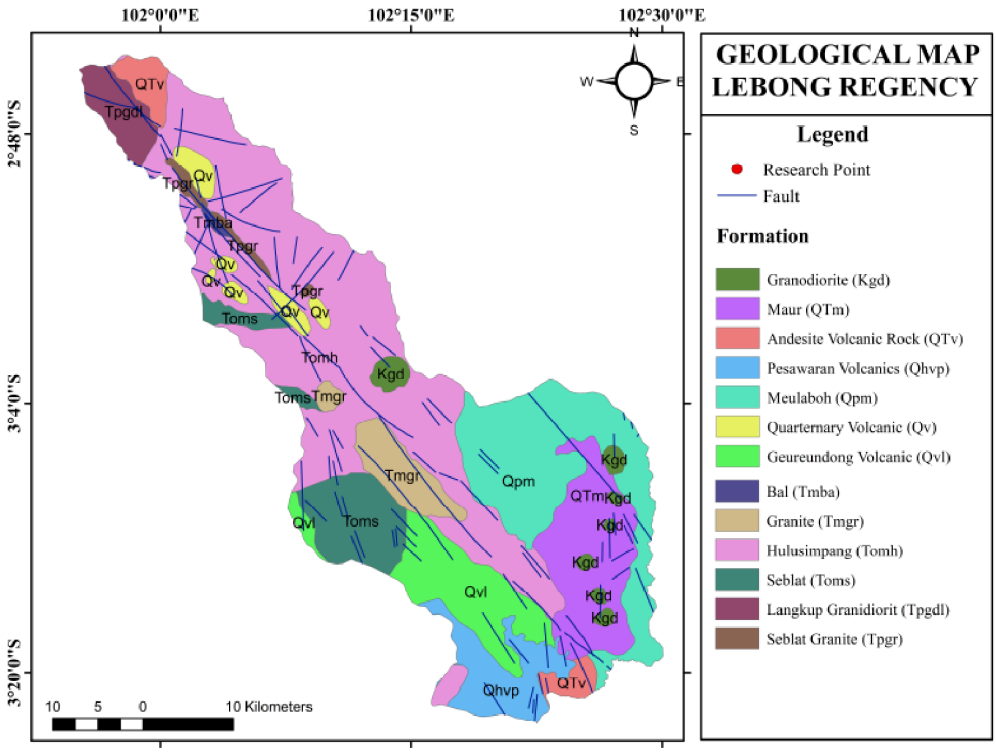

Figure 1. Regional Geological Map of Lebong Regency (Modified from ESDM, 2023).

Lebong Regency regionally has several rock formations, which are the Simpangaur Formation, which is composed of breccia and conglomerate, the Bintunan Formation, which is dominated by conglomerate, breccia, and claystone, the Hulusimpang formation which consists of lava, tuff and breccia, the Lemau Formation which is dominated by breccia and the Seblat Formation is dominated by sandstone and carbonate. At the research location, Lemeu Village, Lebong Regency, the Hulusimpang Formation is composed of lava, tuff and volcanic breccia and is composed of andesite to basalt rocks of Late Oligocene to Early Miocene age.

MT method is a geophysical exploration method that uses the earth's natural electromagnetic field to determine the conductivity distribution in the subsurface (Harahap et al., 2022). According to the frequency and duration of recording, the MT method has a reasonably deep penetration. If using a small frequency with a relatively long recording duration, the depth reached is also getting deeper up to 8 km. That is the reason of MT method can be used to determine the subsurface structure (Rizal et al., 2019).

MT method measures the orthogonal or perpendicular components of the electric (Ex, Ey) and magnetic (Hx, Hy, Hz) fields at the Earth's surface in the time domain (Setyani, 2017). Figure 2 shows a typical MT setup, with the Earth's naturally varying magnetic field as the source of a wide and continuous spectrum of electromagnetic waves. The internal coordinate system measures the electric field horizontally orthogonal and the magnetic field vertically and horizontally orthogonal (Muttaqien & Nurjaman, 2021).

The MT method utilizes the natural electromagnetic (EM) field to determine the earth's subsurface structure based on the electrical properties of rocks at relative depths (including the earth's mantle) within the earth (Hidayat et al., 2016). The MT method can describe subsurface resistivity by looking at the nature of the rock. The MT method's depth reached is inversely proportional to the signal frequency used (Türkoğlu et al., 2015).

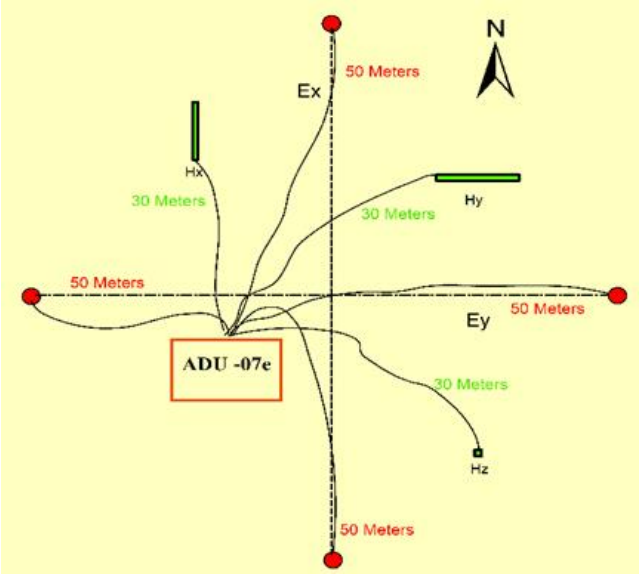

Figure 2. MT arrangement in internal coordinate system (Al Ansory et al., 2023).

These EM fields are generated by complex physical processes with a very wide frequency spectrum, ranging from 10-5 Hz to 104 Hz. Variations in the EM field at low frequencies of less than 1 Hz are caused by the interaction of the earth's permanent magnetic field with wind containing electrically charged particles, causing variations in the EM field. Furthermore, variations above 1 Hz are caused by meteorological activities such as lightning, which create EM waves that travel between the ionosphere and the earth (Fitrida et al., 2015).

To find out the nature of EM waves, the general equation is used, which is Maxwell's equation (Fitzpatrick, 2010).

$$\nabla \times \vec{E} = -\frac{\partial \vec{B}}{\partial t} \quad (1)$$

$$\nabla \times \vec{H} = \vec{J} + \frac{\partial \vec{D}}{\partial t} \quad (2)$$

$$\nabla \cdot D = q \quad (3)$$

$$\nabla \cdot B = 0 \quad (4)$$

Where :
$\vec{E}$: Electric field (Volt/m)
B : Flux or magnetic induction (Weber/m^2 or Tesla)
H : Magnetic field (Ampere/m)
J : Current density (Ampere/m^2)
D : Electrical displacement (Coulomb/m^2)
q : Current charge density (Coulomb/m^3)

Result and Discussion

This research was conducted in Lemeu Village, Lebong Regency using seven measurement points and a 1 km intervals. Figure 3 shows the map of the research location. The results of MT measurements in Lemeu Village, Lebong Regency are shown in the time series in Figure 4. The time series of electric field data has good quality because at the time of measurement, further data processing is carried out by MAPROS software. MAPROS software can reduce data.

That deviate from the main data pattern. As a result, only data with good quality will be processed using MAPROS. Figure 4 shows the measurement results for 16 hours taken with a low frequency (128 Hz) with a recording time of 13 hours because small frequencies are more susceptible to noise, therefore the recording time is longer, medium frequency (1024 Hz) with a recording duration of 2 hours, high frequency (4096 Hz) with a recording time of 1 hour because the frequency used is large.

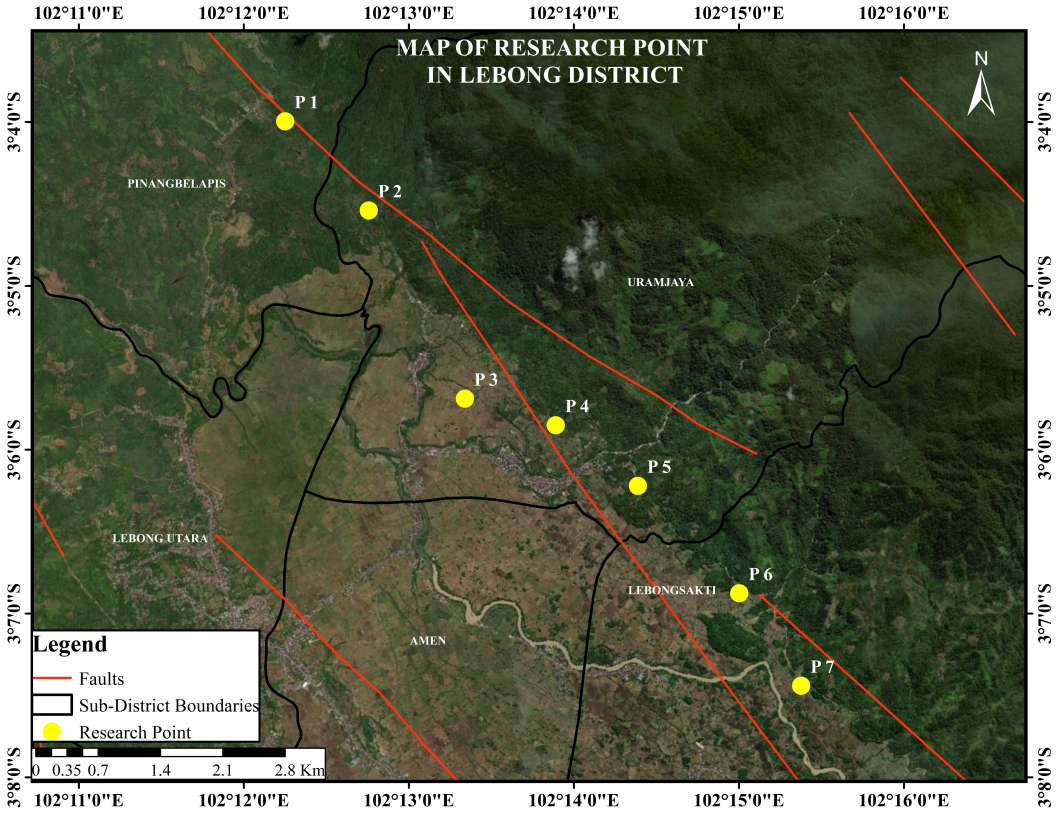

Figure 3. Map of MT research location.

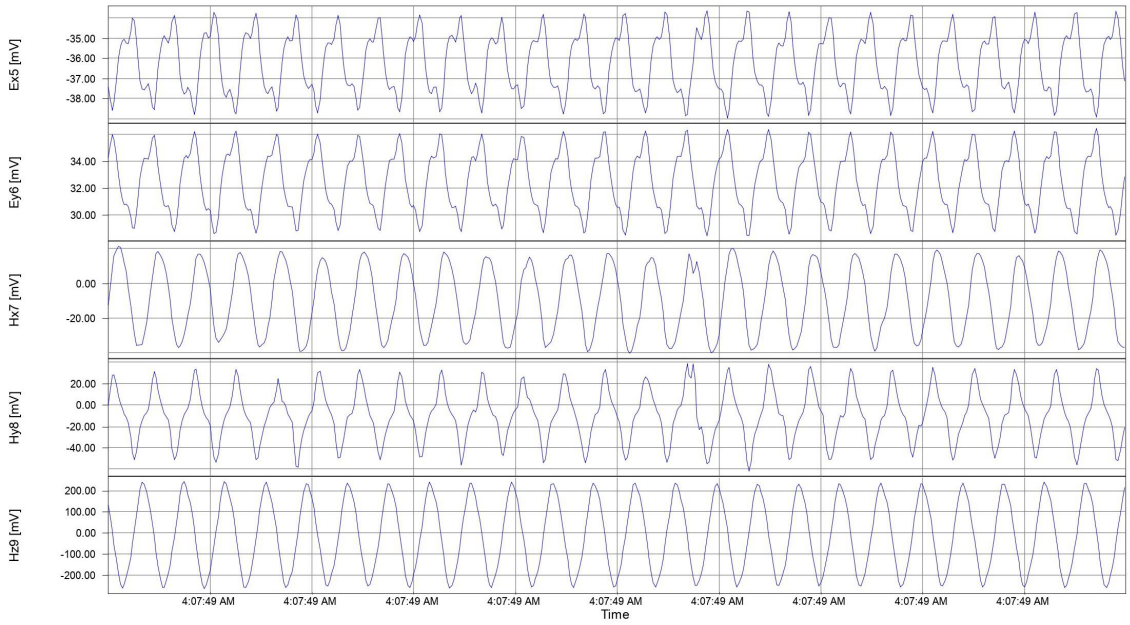

Figure 4. Time series data.

Figure 5 shows the connectivity between resistivity value and depth, from the two figures there is a difference at P5 which shows an anomaly and indicates that the zone is a fault zone because of the low resistivity value. In Figure 6 shows three 2D cross-sections of resistivity values, cross-section 1 is field data with apparent resistivity values, cross-section 2 is a calculation model between field data and model data generated by ZONDMT2D software, and cross-section 3 is the result of the actual resistivity value. The 2D resistivity model shows that the resistivity value is related to the type of rock that is there.

Research that has been conducted around this location by Al Ansory et al. (2023) which from the results of his research shows resistivity values ranging from 0.2 Ωm to 700 Ωm which from the results of the cross section shows the potential pattern of geothermal and from the results of Al Ansory et al. (2023) shows a 2D cross section of resistivity values that differ significantly when compared to this research.

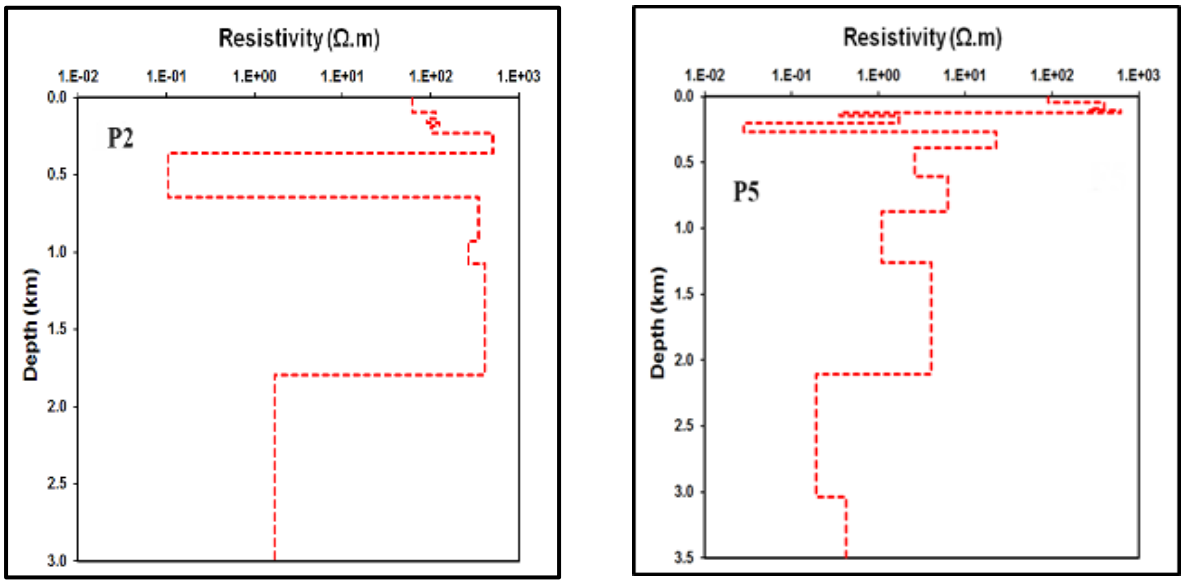

Figure 5. Connectivity of resistivity value with depth.

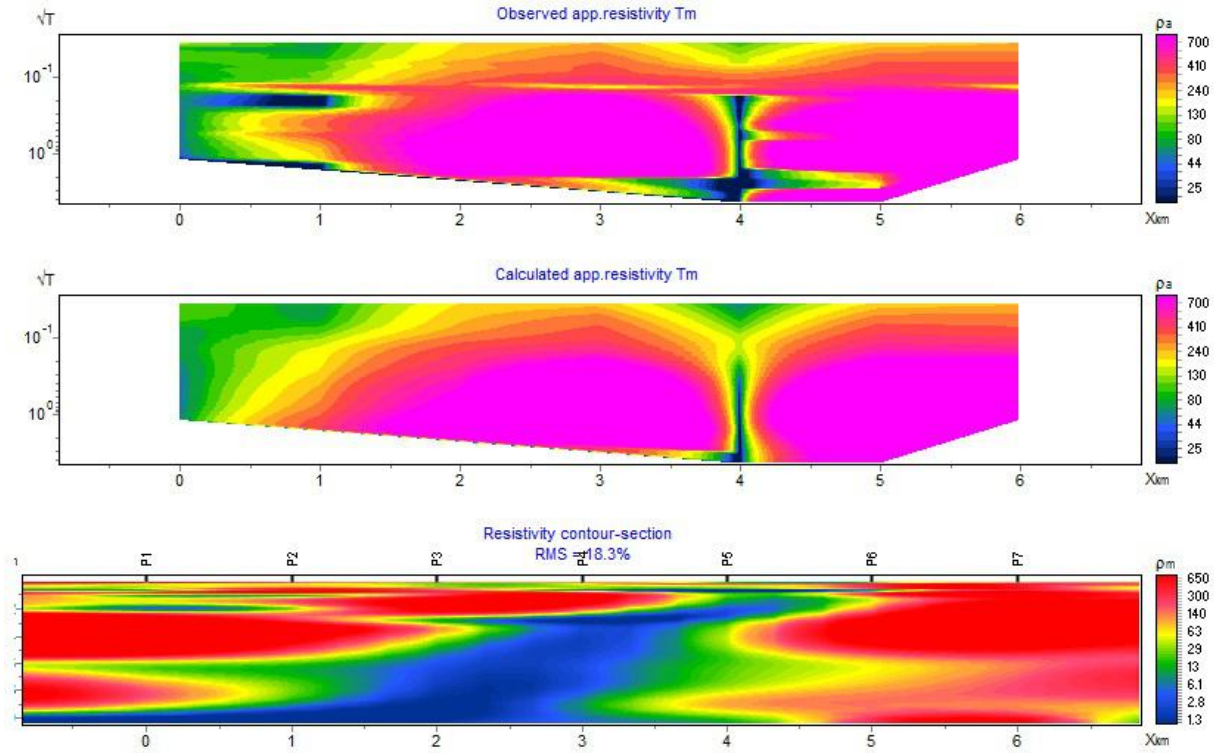

Figure 6. 2D cross-section model resistivity value.

The 2D resistivity cross-section model shows varying resistivity values, starting from 1.3 Ωm to 650 Ωm. According to Gafoer et al. (1992), the resistivity value can be classified into three groups: low, medium, and high resistivity. Low

resistivity (1.3 – 6.1 Ωm) is shown in blue color which is thought to be a caprock layer or an overlaying layer at a depth of 0.75 km. In this research area, an andesitic lava rock type was identified where this rock has undergone alteration. Some of the alterations are in the form of volcanic breccia and tuff so that they can experience fractures. Medium resistivity with resistivity values ranging from 10 - 80 Ωm is colored green to yellow and is thought to be a reservoir. The red color shows high resistivity values with resistivity values around 140 – 650 Ωm which is thought to be a hot rock layer.

The 2D cross section shows an anomaly structure in the measurements at points P4 and P5. The structure has a resistivity value that changes significantly and shows a low resistivity value of 1.3 - 6.1 Ωm which is thought to be a fault zone (Telford et al., 1990). The presence of a fault zone can generally be identified as a conductive zone by the presence of a fracture that has the potential to be filled with fluid, causing the resistivity value in the fracture to have a low resistivity value while the bedrock or basement is characterized by a resistive zone (Pratama et al., 2021). When the measurement depth is at 2.5 km, the layer is fractured which has the potential for an unmapped Ketaun sub-fault zone (Figure 7). The fault zone can be formed from the parent fault, which is the Ketaun fault, which interacts with magma intrusion, causing fluid to seep into the fractures which are then heated by the hot rock layer and produce low resistivity values.

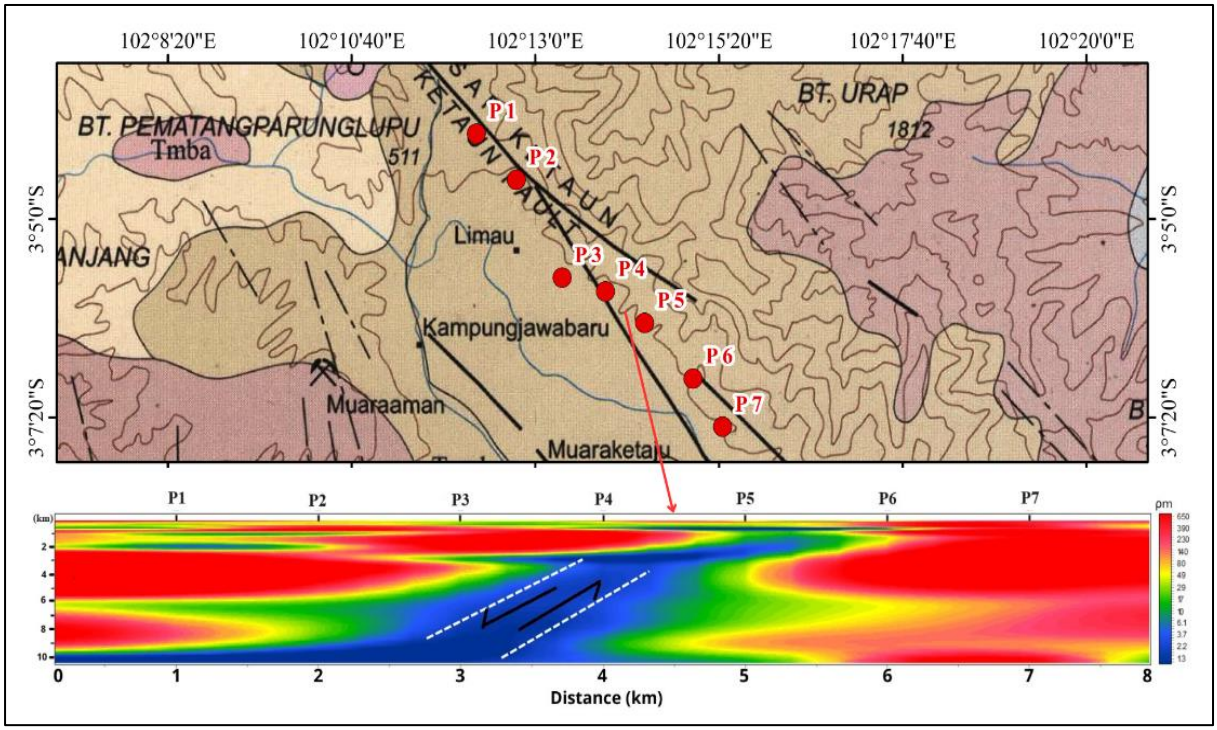

Figure 7. 2D model identified as the presence of a fault zone.

Conclusion

Based on the research conducted in Lemeu Village, Lebong Regency, on the Ketaun segment, it is concluded that the 2D MT cross section shows a zone with low resistivity values between research points P4 and P5, which is thought to be a new fault zone with resistivity values ranging from 1.3 – 6.1 Ωm from a depth of 2.5 km onwards. The zone is assumed to be a secondary fault that is a branch of the Ketaun fault. This shows that this study can

map geological structures suspected to be new faults.

Acknowledgements

Thanks to the Geophysical Laboratory of Bengkulu University for giving permission to use geophysical equipment for acquisition purposes, so that the survey in this study can be carried out.

Author Contribution

The preparation of this research journal, each author is divided into several job desks for collecting literature sources and preparing journals by Nurul Ilmi Rahmawati. Making research survey design, data processing by Nurul Ilmi Rahmawati and Andre Rahmat. Observers and supervisors in writing this journal are M. Farid and Arif Ismul Hadi.

Conflict of Interest

The authors declare that the data published in the manuscript has no conflict of interest to any parties.

References

Adrianda, R. S., & Sutriyono, E. (2022). Kajian Struktur Geologi Daerah Muaro, Kabupaten Sijunjung, Sumatera Barat. *Jurnal Geomine*, 10(3), 209–219. https://jurnal.teknologiindustriumi.ac.id/index.php/JG/article/view/1283

Al Ansory, A. R., Raihana, H., Pritama, V. L., Saputri, W., Maghribi, F. B., Farid, M., Hadi, A. I., Harlianto, B., & Sugianto, N. (2023). Delineasi Nilai Resistivitas Di Lapangan Panas Bumi Tambang Sawah Menggunakan Metode Magnetotellurik. *Buletin Sumber Daya Geologi*, 18(3), 145–154. https://doi.org/10.47599/bsdg.v18i3.386

Ardiansyah, S. (2018). *Analisis Gempabumi Merusak Kabupaten Lebong- Bengkulu 6 Desember 2017*.

Arisbaya, I., Mukti, M. M., Handayani, L., Permana, H., & Schnabel, M. (2016). Tabuan-Panaitan Ridge, Trace of Sumatran Fault in the Sunda Strait based on Geophysical Data Analysis. *Prosiding Pemaparan Hasil Penelitian Geoteknologi LIPI*, I-33–I-39.

Arisbaya, I., Wijanarko, E., Warsa, W., Sumintadireja, P., Sudrajat, Y., Handayani, L., Mukti, M. M., & Grandis, H. (2023). Magnetotellurics (MT) and Gravity Study of a Possible Active Fault in Southern Garut, West Java, Indonesia. *International Journal of Geophysics*, *2023*, 4482074 https://doi.org/10.1155/2023/4482074

Bahri, S., Hanif, M. F., Prihatiningrum, A., & Islam, M. (2022). Perilaku dan Ketahanan Struktur Rumah Vernakular Desa Gunung Alam Lebong terhadap Gempa Bumi. *Jurnal Inersia Teknik Sipil*, *14*(1), 1–10. https://ejournal.unib.ac.id/inersiajurnal/article/view/18357

ESDM, P. S. G. (2023). *SHP Peta Geologi Lebong*.

Firdaus, M. W., Setyawan, A., & Yusuf, M. (2016). Identifikasi Letak Dan Jenis Sesar Berdasarkan Metode Gayaberat Second Vertical Gradient Studi Kasus Sesar Lembang, Kota Bandung, Jawa Barat. *Youngster Physics Journal*, 5(1), 21–26. https://ejournal3.undip.ac.id/index.php/bfd/article/view/10629

Fitrida, S. M., Sampurno, J., Ivansyah, O., & Kholid, M. (2015). Identifikasi Struktur Bawah Permukaan Berdasarkan Metode Magnetotellurik di Kawasan Panas Bumi Wapsalit Kabupaten Buru Provinsi Maluku. *Positron*, 5(1), 11–18. https://doi.org/10.26418/positron.v5i1.9733

Fitzpatrick, R. (2010). Maxwells equations and the principles of electromagnetism. *Laxmi Publications, Ltd.*

Gafoer, S., Amin, T. C., & Pardede, R. (1992). *Geologi lembar Bengkulu, Sumatera*, Pusat Penelitian dan Pengembangan Geologi.

Hadi, A. I., & Brotopuspito, K. S. (2016). Estimasi Kedalaman Bidang Batas Sesar dari Data Gravitasi di Daerah Rawan Gerakan Tanah (Studi Kasus: Sesar Sumatra Segmen Musi Bengkulu). *SIMETRI, Jurnal Ilmu Fisika Indonesia*, 2(2), 2207-37–2207-42. https://jsimetri.wordpress.com/wp-content/uploads/2016/07/j-simetri-v2-no2-2016-07-arifunib-37-42.pdf

Harahap, Z. A., Haryanto, A. D., Firmansyah, Y., & Alfadli, M. K. (2022). Determinasi Zona Reservoir Dengan Data Magnetotelurik Di Zona Prospek Panas Bumi Telaga Ngebel, Jawa Timur. *Padjadjaran Geoscience*, 6(2), 803–811. https://jurnal.unpad.ac.id/geoscience/article/view/41415

Hidayat, A. R., Junursyah, L. G., & Asep, H. (2016). Analisis Deret Waktu Untuk Peningkatan Kualitas Data Magnetotelurik (Studi Kasus Lapangan Geothermal). *Proseding Seminar Nasional Fisika dan Aplikasinya*, *November*, 1–10.

Lubis, A. M., Butarbutar, D. C., Suhendra. S., & Samdara, R. (2019). Investigasi Sudut Pergerakan Sesar di Musi Kepahiang dengan Menggunakan Metode Geolistrik. *Jurnal Meteorologi dan Geofisika*, 20(2), 67–72. https://doi.org/10.31172/jmg.v20i2.543

Muflihah, I. (2014). Distribusi Dan Pola Sesar Daerah Kepala Burung (Papua Barat). *Jurnal Neutrino*, 6(2), 91–98. https://doi.org/10.18860/neu.v0i0.2588

Mulyati, R., Suryana, V. A., & Wulandari, D. A. (2020). Identifikasi Sesar Aktif Terhadap Pembangunan Bendungan Di Provinsi Aceh (NAD). *Ruang Teknik Journal*, 3(1), 94–98. https://jurnal.umsb.ac.id/index.php/RANGTEKNIKJOURNAL/article/view/1684

Muttaqien, I., & Nurjaman, J. (2021). Two-Dimensional Inversion Modeling Of Magnetotelluric (Mt) Synthetic Data Of A Graben Structure Using SimPEG. *RISET Geologi dan Pertambangan*, 31(1), 1–12. https://doi.org/10.14203/risetgeotam2021.v31.1121

Natawidjaja, D. H. (2018). Updating active fault maps and sliprates along the Sumatran Fault Zone, Indonesia. *IOP Conference Series: Earth and Environmental Science*, 118(1), 012001. https://doi.org/10.1088/1755-1315/118/1/012001

Pratama, R., Resta, I. L., Farid, F., & Joni, W. (2021). Identifikasi Lapisan Bawah Permukaan Daerah Prospek Panas Bumi Songa-Wayaua Berdasarkan Metode Magnetotelurik. *Jurnal Meteorologi dan Geofisika*, 22(2), 45–53. https://doi.org/10.31172/jmg.v22i2.786

PUSGEN. (2017). *Peta Sumber dan Bahaya Gempa Indonesia Tahun 2017 (Map of Indonesia Earthquake Sources and Hazards in 2017)*. Pusat Studi Gempa Nasional.

Putra, I. D., Nasution, R. A. F., Harijoko, A. (2017). Aplikasi Landsat 8 Oli/Tirs Dalam Mengidentifikasi Altrasi Hidrotermal Skala Regional : Studi Kasus Daerah Rejang Lebong dan Sekitarnya, Provinsi Bengkulu. *Prosiding Seminar Nasional Kebumian Ke-X*, 10, 1812–1826.

Rais, L. N. (2021). Analisis Bencana Gempa Bumi Dan Mitigasi Bencana Di Daerah Kertasari. *Jurnal Samudra Geografi*, 4(2), 14–19. https://doi.org/10.33059/jsg.v4i2.3773

Rizal, M., Ismail, N., Yanis, M., Muzakir, M., & Surbakti, M. S. (2019). The 2D resistivity modelling on north sumatran fault structure by using

magnetotelluric data. *IOP Conference Series: Earth and Environmental Science*, 364(1), 012036. https://doi.org/10.1088/1755-1315/364/1/012036

Setyani, A. (2017). *Investigasi bawah permukaan segmen cibeber zona sesar cimandiri, jawa barat dengan metode audio magnetotelurik (amt)*. Universitas Islam Negeri Syarif Hidayatullah Jakarta.

Sieh, K., & Natawidjaja, D. (2000). Neotectonics of the Sumatran fault, Indonesia. *Journal of Geophysical Research: Solid Earth*, 105(B12), 28295–28326. https://doi.org/10.1029/2000jb900120

Supartoyo, S., Suntoko, H., Bondan, A., & Alhakim, E. E. (2019). Analisis Morfotektonik dan Pemetaan Geologi pada Identifikasi Sesar Permukaan di daerah Plampang, Pula Rakit, Provinsi Nusa Tenggara Barat. *Jurnal Pengembangan Energi Nuklir*, 21(1), 45–52. http://dx.doi.org/10.17146/jpen.2019.21.1.5461

Syaputra, E. W., Refrizon, R., & Zakariya, H. (2023). Identifikasi Sesar Segmen Ketahun Berdasarkan Metode First Horizontal Derivative (FHD) dan Second Vertical Derivative (SVD) Data Anomali Gaya Berat GGMplus. *Jurnal Fisika Unand*, 12(4), 598–607.

Telford, W. M., Geldart, L. P., & Sheriff, R. E. (1990). *Applied Geophysics*. Cambridge University Press.

Türkoğlu, E., Unsworth, M., Bulut, F., & Çağlar, İ. (2015). Crustal structure of the North Anatolian and East Anatolian Fault Systems from magnetotelluric data. 241, 1–14. https://doi.org/10.1016/j.pepi.2015.01.003

van Bemmelen, R. W. (1949). *The Geology of Indonesia*, The Hague.

Wulandari, J. C., Gaffar, E.Z., Zulaikah, S., N. A. P. (2017). *Penentuan Struktur Litologi Daerah Panasbumi Probolinggo Menggunakan Metode Magnetotellurik (MT).*

Zhang, L., Unsworth, M., Jin, S., Wei, W., Ye, G., Jones, A. G., Jing, J., Dong, H., Xie, C., Le Pape, F., & Vozar, J. (2015). Structure of the Central Altyn Tagh Fault revealed by magnetotelluric data: New insights into the structure of the northern margin of the India-Asia collision. *Earth and Planetary Science Letters*, 415, 67–79. https://doi.org/10.1016/j.epsl.2015.01.025

ISSN: 2579-5821 (Print)
ISSN: 2579-5546 (Online)
URL address: http://journal.unhas.ac.id/index.php/geocelebes
DOI: 10.70561/geocelebes.v8i2.36276

Jurnal Geocelebes Vol. 8 No. 2, October 2024, 142 – 150

Study of the Digital Geological Compass in Increasing the Effectiveness and Efficiency of Measuring Geological Structure Data in the Field

Rezki Naufan Hendrawan*, Muhammad Irsyad, Aditya Gunawan, Ahmad Dennil Zainuddin, Angga Jati Widiatama

Geological Engineering Study Program, Institut Teknologi Sumatera, 35365, Indonesia.

*Corresponding author. Email: rezki.hendrawan@gl.itera.ac.id

Manuscript received: 26 July 2024; Received in revised form: 24 September 2024; Accepted: 30 September 2024

Abstract

This study compares the use of analog geological compasses and digital geological compasses in measuring fracture planes on crystalline rocks at the Lampung region. The measurement results demonstrate that using digital compasses yields higher time efficiency than analog compasses, with a reduction in measurement duration of over 50%. Although the dominant directions of the fracture planes were similar between the two methods, the inclination values and accuracies of each plane were not always consistent. Data processing using rose diagrams and stereonets indicates that the RockD application provides comparable results to measurements obtained using analog compasses. Therefore, the use of digital compass applications such as RockD can serve as an efficient alternative for geologists in collecting field data related to rock fractures, particularly in the context of quantitative data. However, analog geological compass is still recommended for measuring planes with on single-plane characteristics, such as rock bedding and fault mirrors. This study demonstrates the potential for development and transformation from analog geological compasses to digital geological compasses, and further research is needed to investigate the minimum number of fractures that can be measured with a digital geological compass to be considered statistically valid.

Keywords: Digital Geological Compass, RockD, Rocklogger, Smartphone.

Citation: Hendrawan, R.N., Irsyad, M., Gunawan, A., Zainuddin, A.D., & Widiatama, A.J. (2024). Study of the Digital Geological Compass in Increasing the Effectiveness and Efficiency of Measuring Geological Structure Data in the Field. *Jurnal Geocelebes*, 8(2):142–150, doi: 10.70561/geocelebes.v8i2.36726

Introduction

A geological compass is an essential instrument utilized by geologists for lithological and structural mapping. Field geologists are proficient in employing analog geological compasses equipped with clinometers (Assali et al., 2014) and field books that document measurements across hundreds to thousands of locations daily (Allmendinger et al., 2017). The analysis of geological structures, including fault networks, lava flow directions, sedimentary rock bedding, lineation, and foliation, necessitates the measurement of various orientations via a geological compass (Jaud et al., 2022). Consequently, field measurements utilizing a geological compass require focused study by students or aspiring geologists to present sedimentological and structural data accurately (Novakova & Pavlis, 2017; Senger et al., 2021).

Engineers generally obtain discontinuity data using a geological compass, clinometer, measuring tape and scale. This process necessitates a certain level of expertise (Ibrahim & Musa, 2020; Liu et al., 2022; Singh et al., 2021; Vöge et al., 2013), rendering it generally challenging, time-intensive, and prone to data bias (Li et al., 2019), in both scanline (1D) and window sampling (2D) measurements (Kong et al.,

2020; Watkins et al., 2015). Conversely, since 2010, there has been significant innovation in the geological compass through the development of a digital application for smartphones and tablets, which is relatively cost-effective and practical (Novakova & Pavlis, 2017; 2019). Aspiring or novice geologists can likely produce more reliable field data utilizing a digital compass compared than an analog compass, which requires greater consistency and skill (Whitmeyer et al., 2019).

Worldwide since 2016, more than 3.9 billion people have been using smartphones (Lee et al., 2018). Digital geological compasses, available as smartphone applications, offer an alternative for aspiring geologists and professionals alike to gather data effectively, much like how GPS has been replaced by applications like Avenza or digital cameras by smartphone cameras and other features (Lee et al., 2018; Wong et al., 2019). Moreover, smartphones and tablets with mapping applications that integrate digital compasses make field data collection accessible, even for those without in-depth geological knowledge (Whitmeyer et al., 2019; Whitmeyer & De Paor, 2014). This trend necessitates further examination to assess the accuracy and time efficiency provided by digital compasses.

Materials and Methods

The research was conducted quantitatively by comparing the results of fracture plane measurements using various geological structure measurement methods. The locations were selected based on the presence of abundant geological structures in the Lampung region (Figure 1). The measurement objects were crystalline rocks located at three different sites, each featuring a significant number of fracture planes (Figure 2). Shear fractures have been found on north-south and east-west direction while joint and vein tend to have a northeast-southwest orientation (Hendrawan et al., 2024). The measurements were conducted by a final-year student with excellent measuring skills who has previously conducted research in the area. Collecting data can be seen in Figure 2 (left) where the process can use a field book or clipboard placed on the plane surface, especially for rough surfaces.

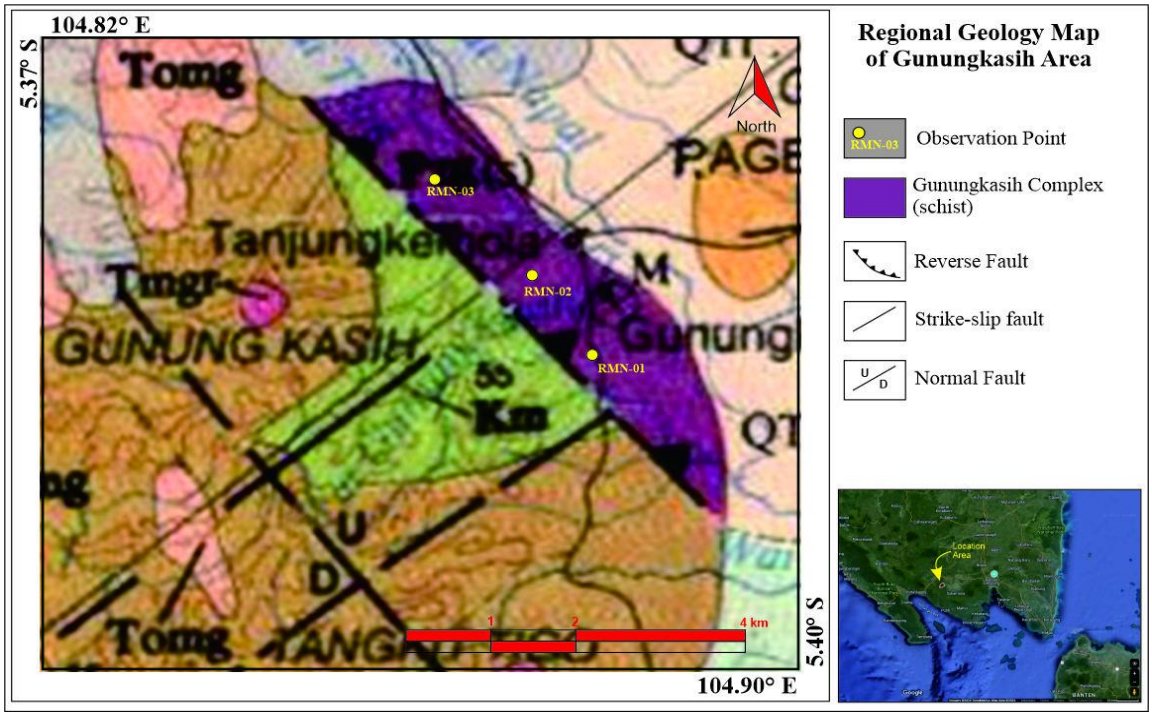

Figure 1. Observation point in Gunungkasih Area, modified Regional Geology Map (Amin et al., 1993).

Figure 2. An outcrop of rocks serves as the observation site for geological structure plane measurements.

The measurement of natural fractures at the mesoscale outcrop level in the field was conducted using the window scan method over an area of 1m² (Koesmawardani et al., 2021). At each outcrop point, measurements were taken using two different methods: the strike-dip method and the dip-dip direction method. These measurements utilized both an analog geological compass (Brunton compass) (Zewdie & Asmare, 2023) and a digital compass application on a smartphone, performed by the same individual. According to Novakova & Pavlis (2017), smartphones equipped with various sensors, such as a magnetic field sensor, accelerometer, and proximity sensor, can be used as digital compass instruments, provided they are calibrated beforehand. This study utilized the Samsung Galaxy A50, which meets the necessary specifications for these sensors (Samsung, n.d.).

There are many digital compass applications available for Android devices. FieldMove Clino has the highest number of reviews and ratings on the Play Store, followed by the Rocklogger app (Novakova & Pavlis, 2019; Whitmeyer et al., 2019; Whitmeyer & De Paor, 2014). However, in practical use, FieldMove Clino is less convenient as it requires the smartphone to always be in portrait mode. Therefore, an alternative application, RockD, was selected to function as a digital geological compass. Both applications were used for comparison in terms of data accuracy. Details of these applications are listed in Table 1.

Table 1. Geological Compass Application on Smartphones based on Android Platform (data accessed from Google Playstore on August 2024).

Name	Developer	Installation	Rating/ Review
FieldMove Clino	Petroleum Exp. Ltd.	50.000+	4.5/689
Rocklogger	RockGecko	50.000+	4.4/360
RockD	UW Macrostat	100.000+	4.5/378

The collected field data was processed using Microsoft Excel 2019 and Dips 6.0 software to generate comparison graphs, as well as distribution plots of planes and points on stereographic and rose diagrams. This data analysis will allow for evaluation of the time efficiency of each method and instrument, as well as the accuracy achieved by each method.

Results and Discussion

Data collection was conducted at three sites, designated as RNH-01, RNH-02, and RNH-03, all of which are composed of crystalline rocks. Across these three

sampling locations, a total of 292 fracture planes were measured using both analog and digital compasses. The measurements employed various methods: analog compass strike-dip (SDA), dip-dip direction (DDA), digital compass strike-dip using the RockD application (SDH), and dip-dip direction using the Rocklogger application (DDH). The details regarding the measurement duration and the amount of data collected are provided in Table 2.

The measurement duration using various methods showed consistent differences at each observation station. According to Figure 3, a pattern emerged indicating that the more fracture planes measured, particularly using analog compasses (SDA and DDA), the longer the measurement duration. However, the DDA method was more time-efficient compared to the SDA method. On the other hand, the use of digital compasses did not significantly affect the measurement duration relative to the number of fractures measured. Furthermore, the graph in Figure 2 demonstrated a significant difference in measurement duration between the SDA-DDA and SDH-DDH methods, with an average reduction of more than 50%. This indicates that measurements using digital compasses (smartphones) are considerably more efficient than those using analog compasses.

Table 2. Fracture planes data measurement recap from observation points.

Measurement Duration	Minutes		
	RNH-01	RNH-02	RNH-03
SDA	14 min	17 min	16 min
DDA	13 min	16 min	12 min
SDH	6 min	8 min	8 min
DDH	5 min	8 min	7 min
Total Fractures	88 planes	132 planes	72 planes

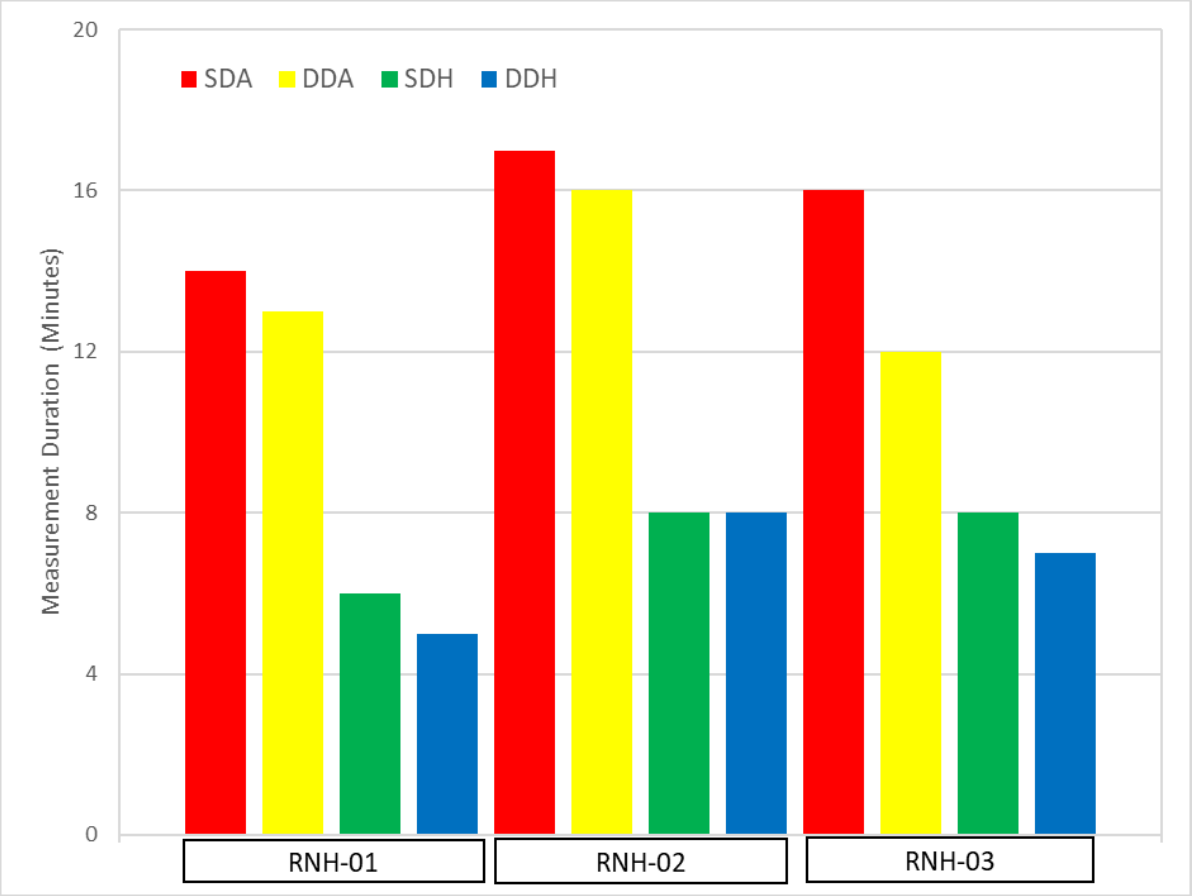

Figure 3. Comparison graph of measurement duration with several methods at each observation point.

Figure 4 shows a comparison graph between strike and dip values of planes present on the outcrop using several methods. Based on Figure 4, it indicates that the structural plane data obtained are not always the same from each method. In RNH-01 and RNH-03, some points only have one point or method, including RNH-02 although not as many as the other points. This is caused by the difference in strike and dip values measured by each method. In general, the difference in dip values becomes an anomaly compared to the strike values. However, if we look at RMN-02, which has a larger amount of data taken, the data grouping becomes clearer. This needs to be validated by plotting the data in a rose diagram to get a complete picture of the data.

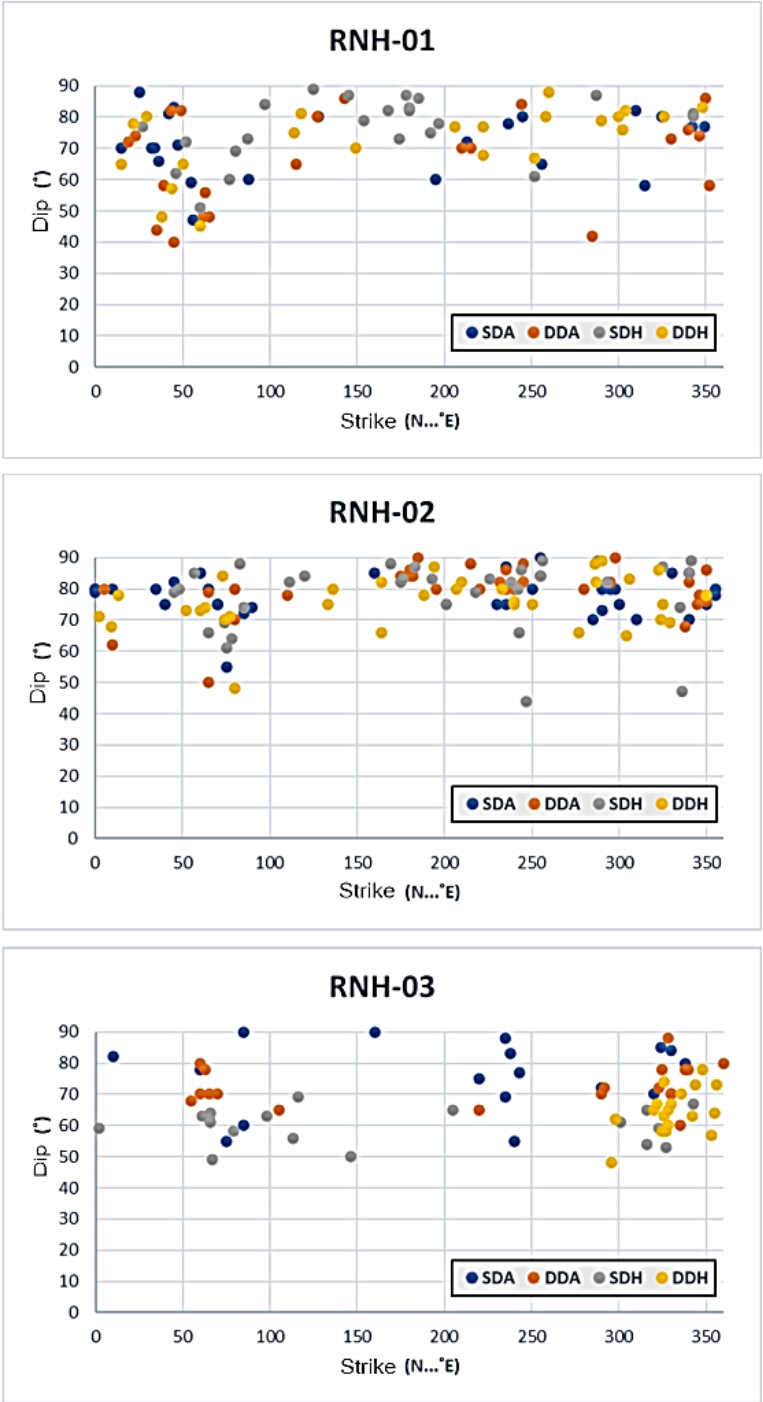

Figure 4. Strike and Dip Graph with several methods at 3 observation points.

The fracture data is then processed using a rose diagram as shown in Figure 5. Comparing each station, in general, each measurement shows a relatively similar dominant direction or trend of strike and azimuth. For example, in Figure 4, station RNH-02 shows the same dominant direction from each measurement method, although not the same. Slightly different from the data at station RNH-01, which has far fewer measurements, showing a slightly different dominance from each measurement method. This indicates that the more data measured, the more accurate it will be in seeing the dominant direction of the fracture plane, especially for the azimuth or strike direction of the fracture plane.

The stereographic contour diagram is shown in Figure 6 by entering the strike and dip data spatially. In general, each measurement at each measurement station does not show a contour concentration in the same position. As seen in Figure 5, the data distribution is still too random. This indicates that the measurements taken do not show a consistent relationship between strike and dip using either an analog compass or a digital compass.

Based on the data processing and analysis conducted using several diagrams, it is evident that the use of smartphones with the RockD and Rocklogger applications shows a high level of efficiency, particularly in terms of measurement duration. Measurements with these digital compass applications can reduce the measurement duration by more than 50%. The applications used are also relatively easy to obtain and free, making them accessible to anyone with a smartphone, whether it is an Android or iPhone. Moreover, using digital compass applications to measure fracture planes does not require specific skills or extensive experience.

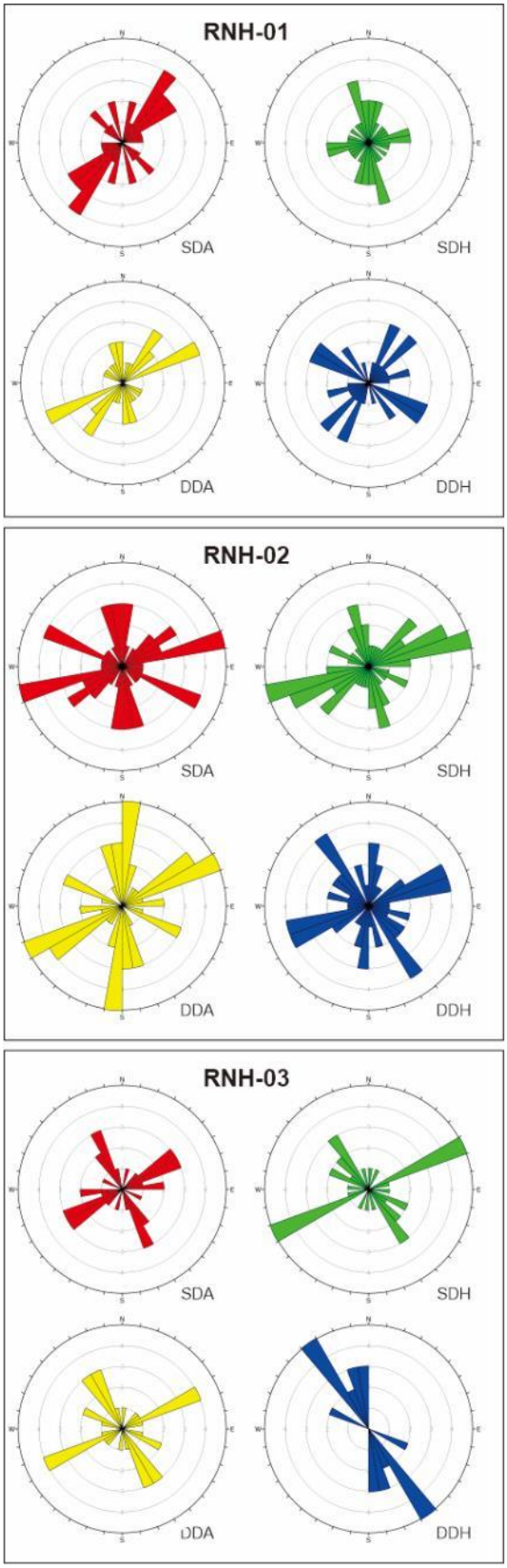

Figure 5. Rosset diagrams from observation points using data from each measurement method.

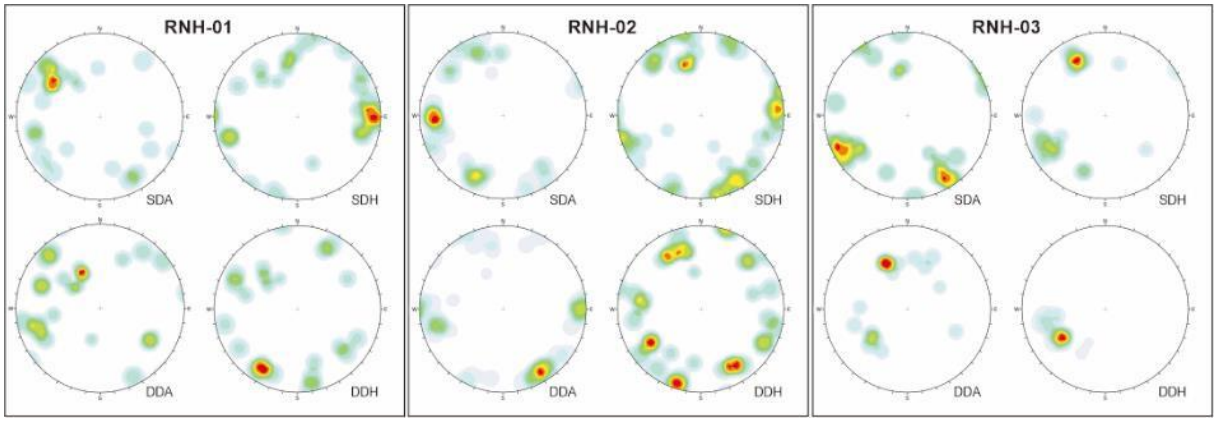

Figure 6. Contour stereonet diagrams which presented plane measurement results from outcrops with each measurement method.

Data processing using rose diagrams and stereonets shows that, in general, the use of digital compass applications on smartphones will indicate the dominance of strike and azimuth direction, showing the same dominance. However, the dip values and accuracy of each plane cannot be considered accurate. This is not suitable for measuring single planes such as bedding planes, laminations, and fault planes. Measurements using digital compass applications are suitable for measuring rocks with many geological structures like fractures and for collecting quantitative data. Based on the data processing and analysis results, the RockD application is recommended because it tends to produce results like those obtained using an analog compass.

Conclusion

The use of digital compass applications like RockD and Rocklogger greatly assists geologists in conducting fieldwork. Some conclusions drawn from this research include Smartphones with the RockD application significantly facilitate the work of geologists, particularly for quantitative data (such as shear fractures, joints, or veins). Therefore, Digital geological compass applications make field measurements more efficient, allowing geologists to measure more planes in a single day of fieldwork. The use of digital geological compass applications requires a battery with normal performance (not in battery-saving mode) and needs periodic calibration although qualitative or single-plane data (rock layers, fault mirrors) are recommended to still be measured using an analog geological compass.

This research marks the beginning of the development and transformation from using analog geological compasses to digital geological compasses. Further quantitative research is needed to determine the minimum number of fractures that should be measured with a digital geological compass at a single point to be considered valid, using a more comprehensive statistical approach.

Acknowledgements

We would like to express our sincere gratitude to the Geodynamics Engineering Geology assistant group at the Institut Teknologi Sumatera (ITERA) for their invaluable support and assistance throughout this research.

Author Contribution

RNH proposed the idea, designed the study, performed the analysis, and wrote the paper. MI, AG, and ADZ conducted the field measurements and processed the data. AJW provided brainstorming input and support for the field activities.

Conflict of Interest

The authors declare no conflict of interest.

References

Allmendinger, R. W., Siron, C. R., & Scott, C. P. (2017). Structural data collection with mobile devices: Accuracy, redundancy, and best practices. *Journal of Structural Geology*, 102, 98–112. https://doi.org/10.1016/j.jsg.2017.07.011

Amin, T. C., Sidarto, Santosa, S., & Gunawan, W. (1993). *Peta Geologi Lembar Kota Agung, Sumatera* (N. Ratman (ed.)). Geological Research and Development Centre. https://geologi.esdm.go.id/geomap/pages/preview/peta-geologi-lembar-kotaagung-sumatera

Assali, P., Grussenmeyer, P., Villemin, T., Pollet, N., & Viguier, F. (2014). Surveying and modeling of rock discontinuities by terrestrial laser scanning and photogrammetry: Semi-automatic approaches for linear outcrop inspection. *Journal of Structural Geology*, 66, 102–114. https://doi.org/10.1016/j.jsg.2014.05.014

Hendrawan, R. N., Widiatama, A. J., Irsyad, M., Zainuddin, A. D., Gunawan, A., Sanjaya, I., Nahar, R. N. F. A., Natalia, H. C., & Ogara, E. R. (2024). Geological Structure Analysis Approach to Control the Distribution of Manganese in Gunungkasih Area, Tanggamus Regency, Lampung Province. *IOP Conference Series: Earth and Environmental Science*, 1378(012009), 1–7. https://doi.org/10.1088/1755-1315/1378/1/012009

Ibrahim, A. K., & Musa, A. I. (2020). Mapping geology and structural features of Kazaure SE, NW Nigeria: Justifying groundwater potential model. *Zbornik Radova Departmana Za Geografiju, Turizam i Hotelijerstvo*, 49(1), 1–21. https://doi.org/10.5937/ZbDght2001001K

Jaud, M., Geoffroy, L., Chauvet, F., Durand, E., & Civet, F. (2022). Potential of a virtual reality environment based on very-high-resolution satellite imagery for structural geology measurements of lava flows. *Journal of Structural Geology*, 158(104569). https://doi.org/10.1016/j.jsg.2022.104569

Koesmawardani, W. T., Sapiie, B., & Rudyawan, A. (2021). Fracture characterization with fieldwork data and its implication for basement fracture reservoir at Muaro Silokek Granitic Outcrops. *IOP Conference Series: Materials Science and Engineering*, 1098(6), 1–7. https://doi.org/10.1088/1757-899x/1098/6/062019

Kong, D., Wu, F., & Saroglou, C. (2020). Automatic identification and characterization of discontinuities in rock masses from 3D point clouds. *Engineering Geology*, 265(105442). https://doi.org/10.1016/j.enggeo.2019.105442

Lee, S., Suh, J., & Choi, Y. (2018). Review of smartphone applications for geoscience: current status, limitations, and future perspectives. *Earth Science Informatics*, 11, 463–486. https://doi.org/10.1007/s12145-018-0343-9

Li, X., Chen, Z., Chen, J., & Zhu, H. (2019). Automatic characterization of rock mass discontinuities using 3D point clouds. *Engineering Geology*, 259, 105131. https://doi.org/10.1016/j.enggeo.2019.05.008

Liu, Y., Chen, J., Tan, C., Zhan, J., Song, S., Xu, W., Yan, J., Zhang, Y., Zhao, M., & Wang, Q. (2022). Intelligent scanning for optimal rock discontinuity sets considering multiple parameters based on manifold learning combined with UAV

photogrammetry. *Engineering Geology*, 309, 106851. https://doi.org/10.1016/j.enggeo.2022.106851

Novakova, L., & Pavlis, T. L. (2017). Assessment of the precision of smart phones and tablets for measurement of planar orientations: A case study. *Journal of Structural Geology*, 97, 93–103. https://doi.org/10.1016/j.jsg.2017.02.015

Novakova, L., & Pavlis, T. L. (2019). Modern methods in structural geology of twenty-first century: Digital mapping and digital devices for the field geology. In S. Mukherjee (Ed.), *Teaching Methodologies in Structural Geology and Tectonics* (pp. 43–54). Springer. https://doi.org/10.1007/978-981-13-2781-0_3

Samsung. (n.d.). *User manual Samsung Galaxy A50*. Retrieved May 25, 2023, from https://ss7.vzw.com/is/content/VerizonWireless/Catalog Assets/Devices/Samsung/samsung-galaxy-a50/samsung-galaxy-a50-ug.pdf

Senger, K., Betlem, P., Grundvåg, S. A., Horota, R. K., Buckley, S. J., Smyrak-Sikora, A., Jochmann, M. M., Birchall, T., Janocha, J., Ogata, K., Kuckero, L., Johannessen, R. M., Lecomte, I., Cohen, S. M., & Olaussen, S. (2021). Teaching with digital geology in the high Arctic: opportunities and challenges. *Geoscience Community*, 4, 399–420. https://doi.org/10.5194/gc-4-399-2021

Singh, S. K., Raval, S., & Banerjee, B. P. (2021). Automated structural discontinuity mapping in a rock face occluded by vegetation using mobile laser scanning. *Engineering Geology*, *285*, 106040. https://doi.org/10.1016/j.enggeo.2021.106040

Vöge, M., Lato, M. J., & Diederichs, M. S. (2013). Automated rockmass discontinuity mapping from 3-dimensional surface data. *Engineering Geology*, 164, 155–162. https://doi.org/10.1016/j.enggeo.2013.07.008

Watkins, H., Bond, C. E., Healy, D., & Butler, R. W. H. (2015). Appraisal of fracture sampling methods and a new workflow to characterise heterogeneous fracture networks at outcrop. *Journal of Structural Geology*, 72, 67–82. https://doi.org/10.1016/j.jsg.2015.02.001

Whitmeyer, S. J., & De Paor, D. G. (2014). Crowdsourcing digital maps using citizen geologists. *Eos, Transactions American Geophysical Union*, 95, 397–399. https://doi.org/10.1002/2014EO440001

Whitmeyer, S. J., Pyle, E. J., Pavlis, T. L., Swanger, W., & Roberts, L. (2019). Modern approaches to field data collection and mapping: Digital methods, crowdsourcing, and the future of statistical analyses. *Journal of Structural Geology*, 125, 29–40. https://doi.org/10.1016/j.jsg.2018.06.023

Wong, D., Chan, K., & Millis, S. (2019). Digital Mapping of Discontinuities. *The 39th HKIE Geotechnical Division Annual Seminar*, pp.1–12. https://www.researchgate.net/profile/Stuart-Millis/publication/332413308_Digital_Mapping_of_Discontinuities/links/5cb41110299bf12097665a9f/Digital-Mapping-of-Discontinuities.pdf

Zewdie, M. M., & Asmare, D. (2023). Investigation and mapping of geological construction materials in parts of chemoga river sub basin, debre markos, Ethiopia. *Heliyon*, 9(3), e13784. https://doi.org/10.1016/j.heliyon.2023.e13784

ISSN: 2579-5821 (Print)
ISSN: 2579-5546 (Online)
URL address: http://journal.unhas.ac.id/index.php/geocelebes
DOI: 10.70561/geocelebes.v4i2.36474

Jurnal Geocelebes Vol. 4 No. 2, October 2024, 151 – 161

Drought Analysis in Ketapang District using the Keetch-Byram Drought Index Method

Lusyndatul Massuro[1], Riza Adriat[1*], Muliadi[1], Andi Ihwan[1], Yuris Sutanto[2]

[1]Geophysics Study Program, Tanjungpura University, Pontianak 78124, Indonesia
[2]Physics Study Program, Tanjungpura University, 78124, Indonesia

*Corresponding author. Email: rizaadriat@physics.untan.ac.id

Manuscript received: 6 August 2024; Received in revised form: 4 October 2024; Accepted: 9 October 2024

Abstract

Ketapang Regency is one of the areas in West Kalimantan that is prone to drought. Drought can trigger forest and land fires. In this research, the Keetch-Byram Drought Index (KBDI) method was used to determine the level of drought in Ketapang Regency. The KBDI method relies on annual rainfall accumulation, daily rainfall, and maximum air temperature. The KBDI values obtained were correlated with the number of hotspots using Pearson correlation. This research was conducted throughout 2018-2022. Based on the monthly average KBDI value, the highest drought in Ketapang Regency occurred in August and September, while the lowest drought occurred in December and January. In terms of the annual average, the highest drought occurred in 2019. During the ENSO phenomenon in 2019, the El Niño phase experienced higher drought than the La Niña phase and normal years. In the El Niño phase, drought levels reach high to extreme categories. The correlation value between annual KBDI and the number of hotspots is 0.88, indicating a solid relationship. An increase in the KBDI value will be followed by an increasing number of hotspots.

Keywords: Drought; ENSO; KBDI; Ketapang Regency.

Citation: Massuro, L., Adriat, R., Muliadi, M., Ihwan, A., & Sutanto, Y. (2024). Drought Analysis in Ketapang District using the Keetch-Byram Drought Index Method. *Jurnal Geocelebes*, 4(2): 151–161, doi: 10.70561/geocelebes.v4i2.36474

Introduction

Indonesia has a tropical climate with the potential for drought when entering the dry season. Based on Koppen's climate classification, Indonesia is an area with a tropical rainforest climate (Af) characterized by relatively uniform air temperatures (Hidayat & Farihah, 2020). An increase in air temperature in the dry season can potentially lead to drought (Malino et al., 2022). A long dry season can cause drought because the soil air reserves will run out due to evaporation, transpiration, or other uses (Darojati et al., 2015). Drought is a natural phenomenon that is a side effect of climate variability (Auliyani & Rekapermana, 2020). Drought is included in the hydrometeorological natural disasters that occur due to reduced rainfall intensity over a long period (Fatehah et al., 2022). Drought can cause crop failure and trigger forest fires. One phenomenon affecting drought is the El Niño Southern Oscillation (ENSO). The ENSO phenomenon is divided into three phases, namely the neutral, La Niña, and El Niño phases. The La Niña phase is more synonymous with the rainy season due to high rainfall intensity and causes flooding events (Ilhamsyah, 2012). The El Niño phenomenon causes a significant decrease in rainfall in Indonesia and can cause drought in Indonesia (Astuti M. P. et al., 2024). Along with the drought that occurs, it can cause hotspots.

Hotspot is a term used to refer to pixels with temperature values above a certain threshold based on the results of satellite

image interpretation (Saharjo & Effendi, 2023). Hotspots do not necessarily describe a forest fire incident, but hotspots can be indicators used for early detection of forest fire events (Aflahah et al., 2018). The number of hotspots is a key determinant of the increase in forest fires and peat swamp forest fires (Cahyono et al., 2015). The more hotspots are distributed, the higher the potential for forest and land fires (Humam et al., 2020). Hotspots will increase in dry months or the dry season (Nahlunnisa & Sopiyandi, 2023).

Ketapang Regency is one of the regencies in West Kalimantan, with 20 sub-districts, and is the largest regency in West Kalimantan. Astronomically, Ketapang Regency is located at 0°19'26.51" South to 3°4'16.59" South and 109°47'36.55" East to 111°21'37.36" East. Forest areas and land areas still dominate the region in Ketapang Regency. Ketapang Regency has monsoon rainfall. The peak of the dry season occurs in June–July–August. During the dry season, Ketapang Regency is prone to drought, which can impact forest and land fires. In addition, most of the land in Ketapang Regency is peat, which has the potential to cause fires to spread quickly. Research by Dicelebica et al. (2022) shows that the area of peatland in Ketapang Regency has an area of 856,296.05 hectares Ketapang Regency is the region with the worst cases of forest fires in West Kalimantan.

One method that can be used to determine the value of the drought index is the Keetch-Byram Drought Index (KBDI) method. The KBDI method was first developed in 1968 to measure drought levels based on the climate of Florida, USA (Keetch & Byram, 1968). The KBDI method uses parameters of annual rainfall accumulation, maximum daily air temperature, and daily rainfall accumulation. The results of the study by Ningsih et al. (2022) showed that Ketapang Regency was the area with the highest drought index and occurred in August. Susanti et al. (2013) conducted a study on the level of drought in Pontianak City using the KBDI method. The study's results showed that during 2006-2008, the most extensive drought index in Pontianak City occurred in 2006, with an extreme KBDI level in August. 2006, the El Niño phenomenon occurred, so there was a long drought. The KBDI value and the number of hotspots show a robust correlation. Anastasia et al. (2021) conducted a study on the fire danger level in West Kalimantan using the Fire Weather Index (FWI) method. The study results showed that the FWI value had a very high correlation with the number of hotspots.

Research related to the level of drought in West Kalimantan using the Standardized Precipitation Index (SPI) method has been conducted by Qonita et al. (2019) from 1985 – 2016. Based on the research, the worst drought occurred in 2014 and 2015 in the Ketapang Regency area. Fatehah et al. (2022) conducted a study using the Standardized Precipitation-Evapotranspiration Index (SPEI) method to determine the variation of drought in West Kalimantan. The SPEI analysis showed a very dry drought severity level, which was identified in June 2004. Nahlunnisa & Sopiyandi (2023) have conducted a study on the distribution of hotspots as a predictor of forest and land fires. The study shows that Ketapang Regency has many hotspots, with 7542 in 2021-2022. The latest research on the drought index has been conducted by Tsabita (2023) using the KBDI method in West Kalimantan at 2001-2021. This study shows that Ketapang Regency is the area most prone to drought. In addition, the relationship between the drought index value and the number of hotspots shows a robust correlation.

Based on previous studies related to drought in West Kalimantan, a study related to drought was conducted that only focused on the Ketapang Regency area. The

years used in the study are 2018 - 2022 which includes the ENSO phenomenon. The research was conducted using the Keetch-Byram Drought Index (KBDI) method with parameters of annual rainfall accumulation, daily rainfall accumulation, and maximum daily temperature. The calculated KBDI value will be analyzed spatially. The purpose of this study is to determine the magnitude of the drought level in Ketapang Regency and its relationship with hotspots. The study was also conducted during the El Niño phenomenon, which is identical to the decrease in rainfall intensity. This research is expected to provide information for drought mitigation and can be a reference for further research.

Materials and Methods

The data used in this study are secondary, which are daily rainfall accumulation data, annual rainfall accumulation data, and maximum daily air temperature data in the range of 2018 - 2022. In addition, this study uses hotspot data from the MODIS satellite. Rainfall and air temperature data were obtained through Copernicus ECMWF, which can be accessed via the page Climate Data Store. Hotspot data was obtained from the Ministry of Environment and Forestry, which can be accessed through the page SiPongi^{+} (Sistem Pemantauan Karhutla). The data from Copernicus ECMWF has a resolution of 27.75 km, while the hotspot data from the MODIS satellite has a resolution of 1 km.

The research location is in Ketapang Regency, and the data collection is 50 points with a grid of 0.25° × 0.25°. The research location used is located at 109.8° E to 111.3° E and 0.3° S to 3.1° S. The research location is shown in Figure 1.

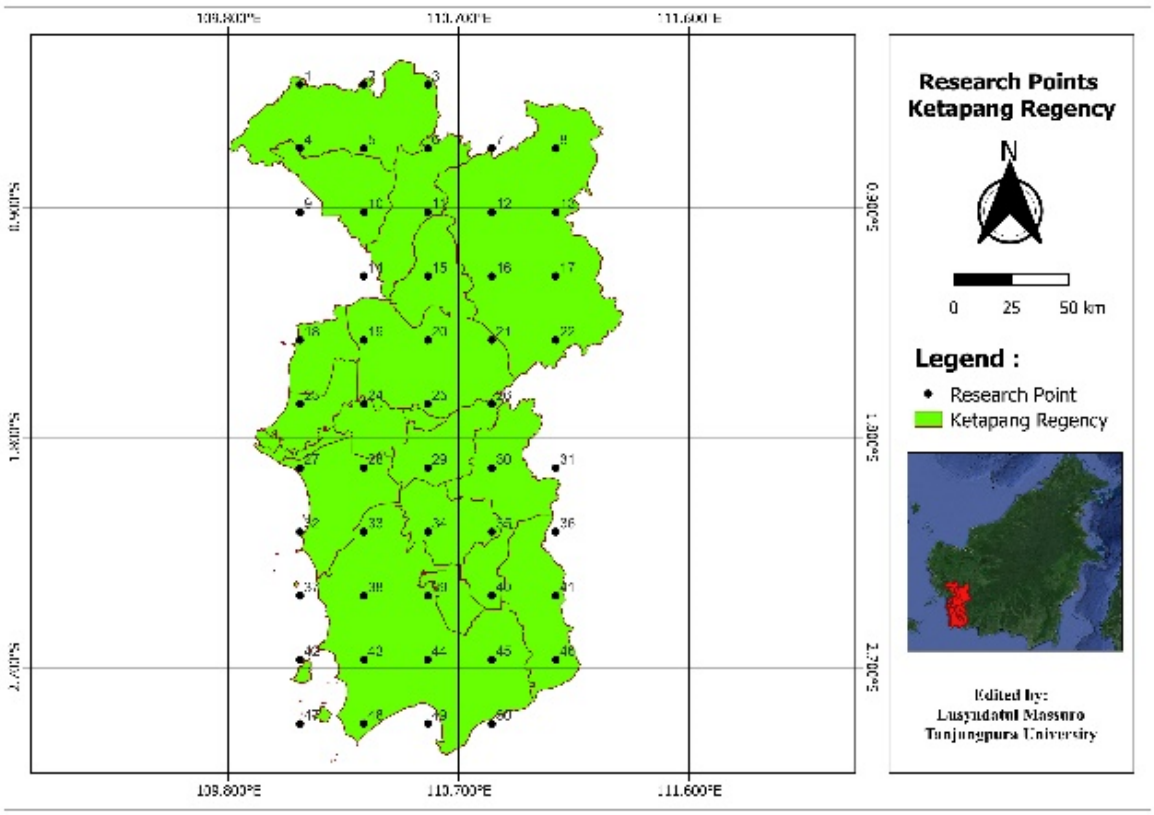

Figure 1. Research location map.

$$KBDI_{today} = KBDI^{t-1} - R_{net} + DF \qquad (1)$$

$$\frac{(203 - KBDI^{t-1})(0.4982e^{(0.0905 \times Tm + 1.6096)} - 4.268) \times 10^{-3}}{1 + 10.88e^{(-0.001736 \times R_0)}} \quad (2)$$

$$R_{net} = \begin{cases} (\mathrm{R^t} - 5{,}1), \mathrm{R^t} \geq 5{,}1 \text{ mm/day, 1st rainy day} \\ \mathrm{R^t},\ \mathrm{R^{t-1}} \geq 5{,}1 \text{ mm/day, 2nd and the next rainy day} \\ 0,\ \mathrm{R^t} < 5{,}1 \text{ mm/hari} \end{cases} \quad (3)$$

The calculation of the KBDI method requires 3 (three) parameters, including the accumulation of annual rainfall in the research area, maximum daily air temperature, and accumulation of daily rainfall. Before calculating the KBDI, it is necessary first to determine the initial KBDI value, which is zero. The initial KBDI is determined by assuming that one day after rainfall, it reaches >150 mm within one week. Taufik et al. (2015) have modified the KBDI which is adjusted to the equatorial climate. The KBDI formula can be stated as Equation (1) and (2).

The net rainfall value in Equation (1) can be obtained using the Equation (3).
Description:
KBDI : drought index
$KBDI^{t-1}$: drought index on the previous day
R_{net} : net rainfall (mm)
DF : drought factor
T_m : maximum daily air temperature (℃)
R_0 : annual accumulated rainfall (mm)

KBDI index values are grouped into four levels as in Table 1.

Table 1. KBDI value index (Taufik et al., 2015).

Range of KBDI	Interpretation
0 – 99	Low
100 – 149	Moderate
150 – 174	High
175 – 203	Extreme

Results and Discussion

Analysis of Drought Distribution Based on the KBDI Method

Spatial drought analysis was carried out by mapping KBDI values with QGIS software. Mapping was carried out using IDW interpolation. Figure 2 shows the average monthly drought index value in Ketapang Regency from 2018-2022. The varying colors on the map indicate the drought index value based on four KBDI classifications. Blue is interpreted as a low level of drought, green with a moderate drought, yellow for a high drought, and red as an extreme drought.

Figure 2 in January shows that Ketapang Regency has a low category drought index for all areas. However, it increased to a moderate category from February to March. Entering April, only a small part of Ketapang Regency has a moderate category drought index. In May, Ketapang Regency returned to a low drought category. Some areas in Ketapang Regency began to experience moderate drought when entering June. All regions of Ketapang Regency experienced moderate drought in July. The peak of drought in Ketapang Regency occurred in August with a moderate to high category. The areas experiencing high-category drought are Sungai Melayu Rayak and Pemahan Districts. However, in September, the drought in Ketapang Regency decreased again to a moderate category. In October, some areas entered the low category, but the Kendawangan area was still in the moderate category. Drought in Ketapang Regency was entirely in the low category in November and December.

Ketapang Regency is one of the regions in Indonesia that has a monsoon rainfall pattern. December–January–February is the peak rainfall, and the drought in Ketapang Regency is in the low category. March–April–May is the transition between the wet and dry seasons, so the drought in Ketapang Regency begins to increase. The dry season due to monsoons occurred in June–July–August, so in that month, the

drought in Ketapang Regency experienced a high to extreme category of drought. September-October-November is the transition month between the dry season and the wet season. Therefore, that month, the Ketapang Regency drought decreased to a low category. Based on the monthly average, the drought in Ketapang Regency generally has the same pattern, with the moderate to high drought season peak occurring in August and September.

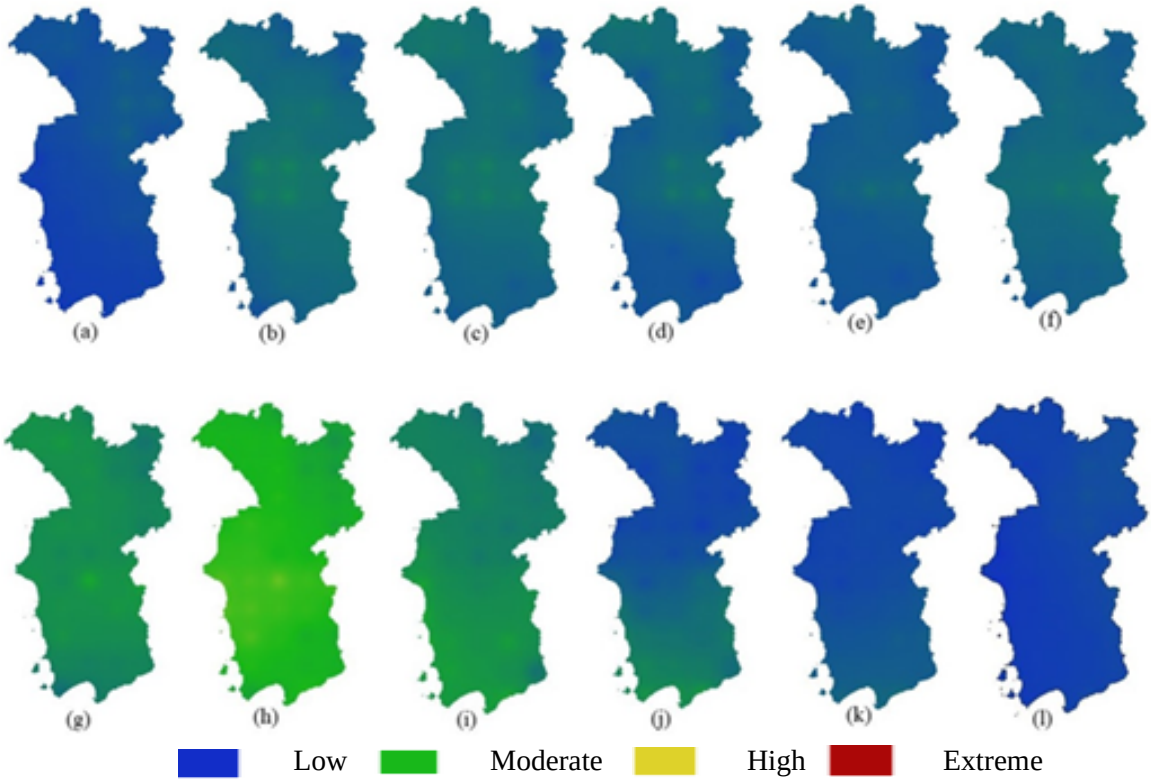

Figure 2. Map of monthly average KBDI distribution for 2018-2022 (a) January, (b) February, (c) March, (d) April, (e) May, (f) June, (g) July, (h) August, (i) September, (j) October, (k) November, (l) December

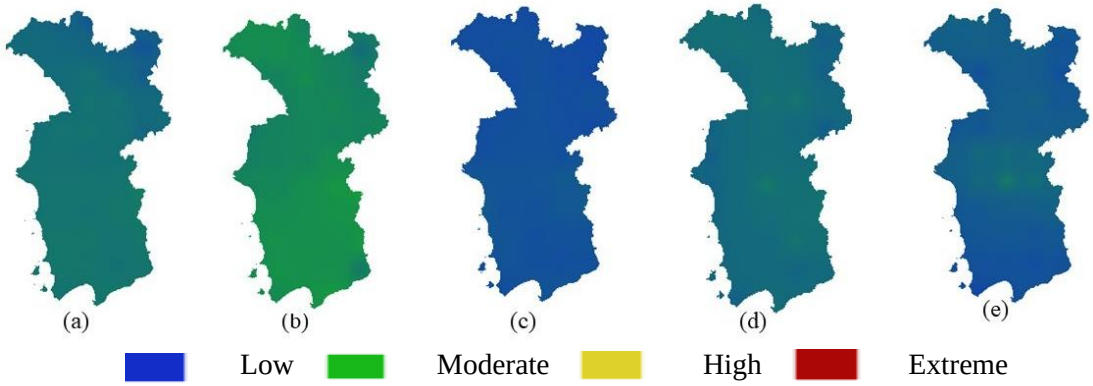

Figure 3. Map of annual average KBDI distribution (a) 2018, (b) 2019, (c) 2020, (d) 2021, (e) 2022

Figure 3 shows a map of the distribution of KBDI in Ketapang Regency in 2018-2022. The year 2018-2022 was chosen because, in the 5-year span, there have been all ENSO phenomena. The annual KBDI distribution map is obtained by averaging the KBDI values from January to December. In 2018, the KBDI distribution map of Ketapang

Regency was in the blue and green range, which means low and moderate drought. In 2019, the entire Ketapang Regency area experienced moderate drought. The drought decreased to the low category in 2020. Entering 2021, Ketapang Regency experienced drought with a dominant moderate category. In 2022, the drought again reduced to the low category, but a small number of areas remained in the mild category. Based on Figures 2 and 3, Ketapang Regency experienced the highest drought in August when entering the dry season and in 2019, the year of the El Niño phenomenon. The results obtained in Figure 3 align with research conducted by Ningsih et al. (2022), which showed that the highest drought in Ketapang Regency occurred in August. This is because the month of August in Ketapang Regency is included in the dry season. The influence of the monsoon is strong on the Ketapang Regency area.

KBDI Analysis of the El Niño Phenomenon

The El Niño is a phenomenon that can cause prolonged drought or dry season characterized by reduced rainfall intensity. The selection of months in the El Niño phase is based on the Oceanic Nino Index (ONI). ONI is one of the parameters often used to monitor El Niño and La Niña events (Nabilah et al., 2017). Figure 4 is a map of the distribution of KBDI values during the El Niño phenomenon from September 2018 to September 2019. Based on Figure 4, drought in Ketapang Regency is in the low category for December-January-February. In the transition months, drought in Ketapang Regency is in the moderate category. The highest drought that occurred during El Niño was in August and September 2019, as shown in Figure 4 (l) and (m). However, in September, there were a small number of areas with a moderate KBDI index. This can happen because September is included in the transition months from dry to wet seasons. In the future, it is necessary to carry out more complex drought studies by adding weather parameters and soil physical parameters for more comprehensive results.

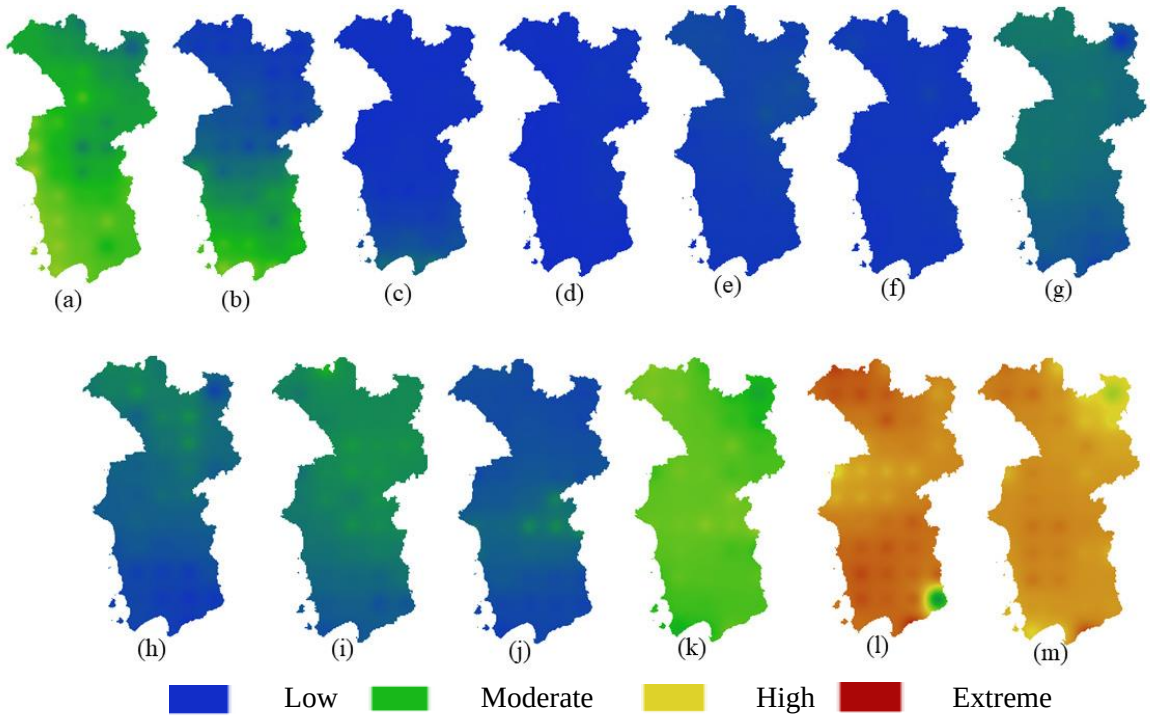

Figure 4. Map of KBDI distribution during the El Niño phenomenon (a) September 2018, (b) October 2018, (c) November 2018, (d) December 2018, (e) January 2019, (f) February 2019, (g) March 2019, (h) April 2019, (i) May 2019, (j) June 2019, (k) July 2019, (l) August 2019, (m) September 2019

The Relationship between KBDI and Hotspot

KBDI and hotspot values aim to determine the relationship between drought and the number of hotspots in Ketapang Regency. Hotspot data was obtained from the MODIS satellite with a high category. Calculations were carried out using Pearson correlation to determine the relationship between KBDI values and the number of hotspots. Pearson correlation is a popular and most frequently used correlation (Purba & Purba, 2022). The function of Pearson correlation is to determine the degree of relationship and contribution of the independent variable with the dependent variable. Pearson correlation is calculated between the average KBDI value for 2018-2022 and the number of hotspots in the same year. The correlation value obtained in that year was 0.88, which means it has a solid relationship. This shows that the number of hotspots will also increase with an increase in the KBDI value.

Based on Figure 5, the highest KBDI value was in 2019 followed by the largest number of hotspots. The phenomenon that occurred in 2019 was El Niño which of course had an impact on drought. In 2018, a normal year followed by the beginning of El Niño, the number of hotspots detected during one year was approximately 300. The KBDI value decreased in 2020, and the number of hotspots also decreased. In 2020, it was a transition year from normal to La Niña. The La Niña phenomenon occurred throughout 2021 and 2022, so the KBDI value was low, and the number of hotspots detected was not significant.

Figure 6 shows the relationship between the average monthly KBDI in 2018-2022 and the accumulation of monthly hotspots. The correlation value based on the average monthly KBDI value and the number of monthly hotspots is 0.57, which has a reasonably strong relationship. A small number of hotspots will follow low KBDI values from January to June; even in May, no hotspots were detected. The KBDI value and the number of hotspots began to increase in July, with the highest KBDI value in August. However, the most significant number of hotspots was in September, reaching 1.638, while the KBDI value in September was 66.11, which is included in the low category. An increase does not always follow an increase in the KBDI value in the number of hotspots (Tsabita, 2023). This can happen because hotspots can come from other factors, such as forest fires caused by humans. The KBDI value decreased from October to December, followed by several hotspots.

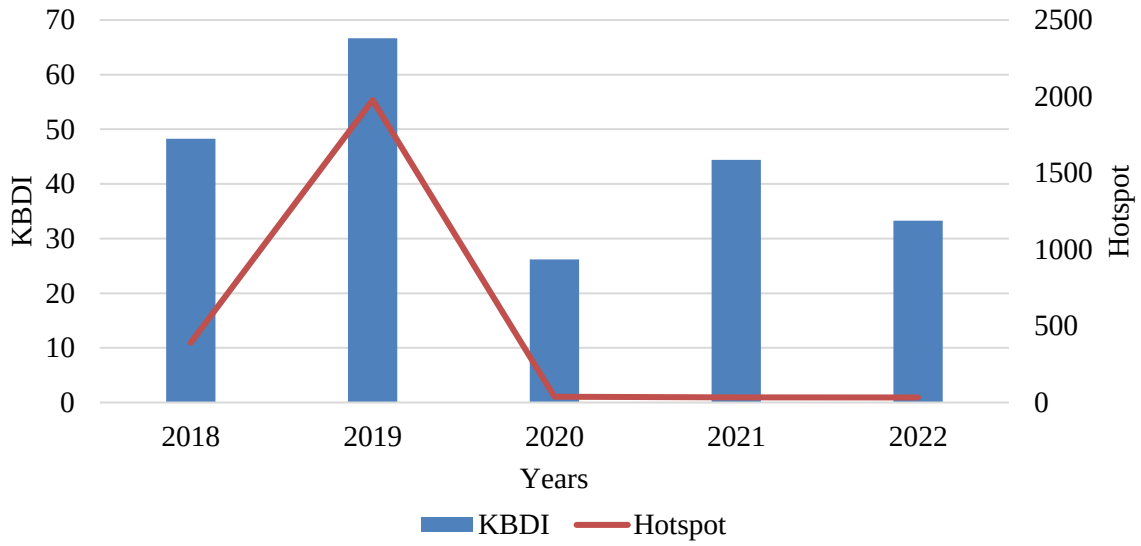

Figure 5. Graph of the relationship between KBDI and the number of annual hotspots.

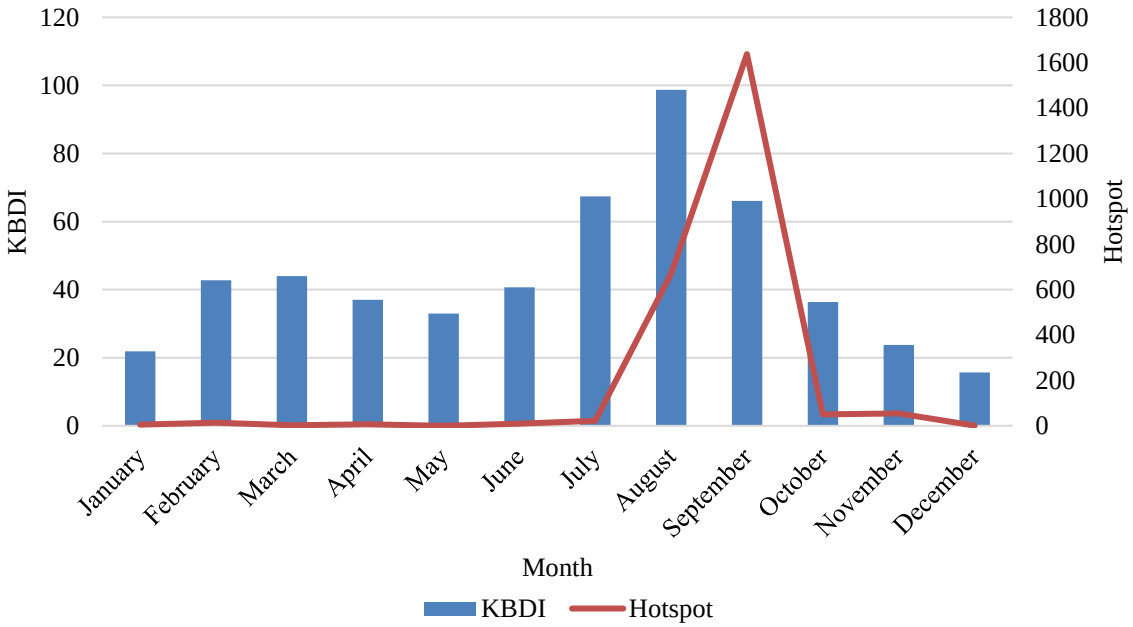

Figure 6. Graph of the relationship between KBDI and the number of monthly hotspots.

Figure 7 shows the relationship between the KBDI value and the number of monthly hotspots from 2018-2022. Based on Figure 7, the highest KBDI value occurred in 2019, followed by the most significant number of hotspots. The correlation coefficient between KBDI and the number of hotspots of 0.61 is classified as having a solid relationship. Drought in the Ketapang region is quite influenced by meteorological phenomena such as monsoons and ENSO, this can have an impact on the level of drought in the Ketapang region, thereby increasing the chances of forest and land fires.

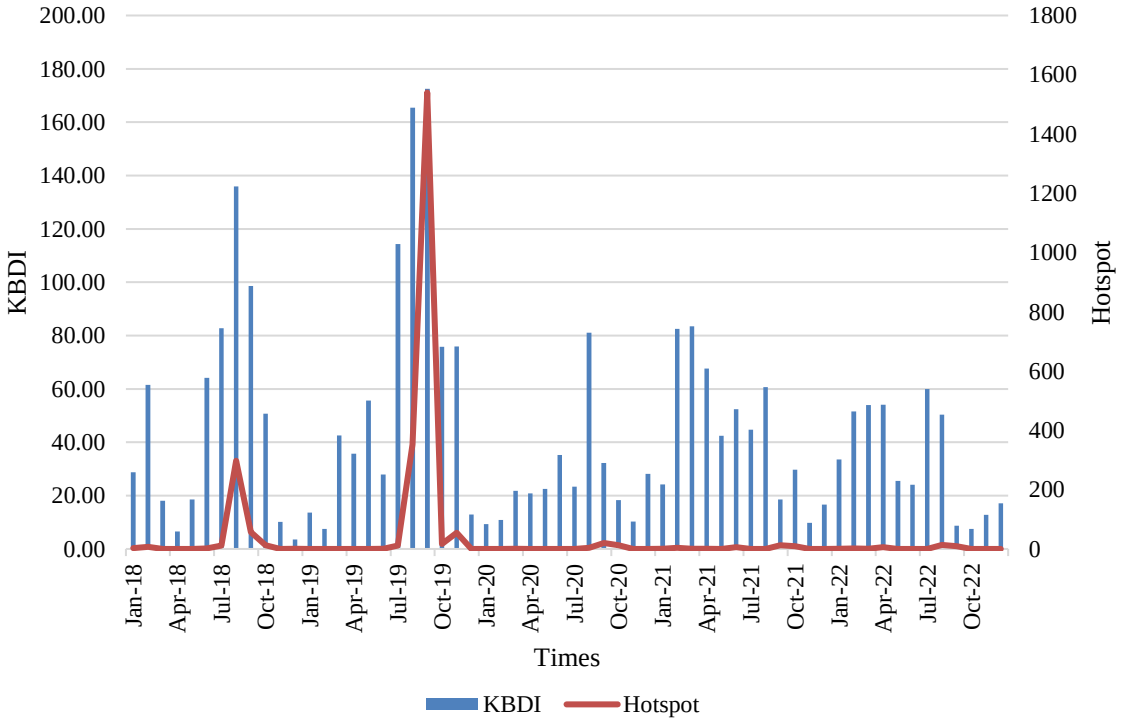

Figure 7. Graph of the relationship between KBDI and monthly hotspots from 2018-2022.

Conclusion

Based on the research that has been conducted, the conclusion that can be drawn from this study is that the level of drought that occurs in Ketapang Regency based on the monthly average has a low category from January to May. Drought began to increase in June, with the peak of drought occurring in August, and began to decline again in October. Based on the annual average, Ketapang Regency experienced the highest drought in 2019 when the El Niño phenomenon occurred. In the El Niño phase, August 2019 and September 2019 had the highest level of drought with a high to extreme category. In addition, the relationship between the KBDI value and the number of hotspots has a robust correlation, with a correlation value of 0.88, so the higher the KBDI value, the more hotspots will be followed.

Author Contribution

Lusyndatul Massuro conducted reference collection, data collection, data processing, and analysis. Riza Adriat and Muliadi supervised the interpretation of results and discussion. Andi Ihwan and Yuris Sutanto supervised the improvement of the writing.

Conflict of Interest

The authors declare no conflict of interest.

References

Aflahah, E., Hidayati, R., Hidayat, R., & Alfahmi, F. (2018). Pendugaan *Hotspot* sebagai Indikator Kebakaran Hutan di Kalimantan Berdasarkan Faktor Iklim. *Jurnal Pengelolaan Sumberdaya Alam dan Lingkungan*, 9(2), 405–418. https://jurnal.ipb.ac.id/index.php/jpsl/article/view/21248

Anastasia, A., Putra, Y. S., & Adriat, R. (2021). Studi Distribusi Tingkat Bahaya Kebakaran Menggunakan *Fire Weather Index* (FWI) di Kalimantan Barat. *Prisma Fisika*, 9(2), 179–182. https://dx.doi.org/10.26418/pf.v9i2.49509

Astuti M. P., R., Saniyah, K., Anggraeni, R., & Nur, D. M. M. (2024). Dampak *La Nina* dan *El Nino* Bagi Kehidupan Masyarakat Indonesia. *Merdeka: Jurnal Ilmiah Multidisiplin*, 1(5), 69–75. https://jurnalistiqomah.org/index.php/merdeka/article/view/1275/

Auliyani, D. & Rekapermana, M. (2020). Analisis Spasial Potensi Kekeringan di Daerah Aliran Sungai. *Jurnal Pembangunan Wilayah dan Kota*, 16(1), 61–70. https://doi.org/10.14710/pwk.v16i1.21979

Cahyono, S. A., Warsito, S. P., Andayani, W., & Darwanto, D. H. (2015). Faktor-Faktor yang Mempengaruhi Kebakaran Hutan di Indonesia dan Implikasi Kebijakannya. *Jurnal Sylva Lestari*, 3(1), 103–112. https://doi.org/10.23960/jsl13103-112

Climate Data Store. https://cds.climate.copernicus.eu/

Darojati, N. W., Barus, B., & Sunarti, E. (2015). Pemantauan Bahaya Kekeringan di Kabupaten Indramayu. *Jurnal Ilmu Tanah dan Lingkungan*, 17(2), 60–68. https://doi.org/10.29244/jitl.17.2.60-68

Dicelebica, T. F., Akbar, A. A., & Jati, D. R. (2022). Identifikasi dan Pencegahan Daerah Rawan Bencana Kebakaran Hutan dan Lahan Gambut Di Kalimantan Barat. *Jurnal Ilmu Lingkungan*, 20(1), 115–126. https://doi.org/10.14710/jil.20.1.115-126

Fatehah, T. N., Putra, Y. S., & Adriat, R. (2022). Variasi Temporal Kekeringan Menggunakan *Standardized Precipitation-Evapotranspiration Index* (SPEI) di Kalimantan Barat. *Prisma Fisika*, 10(2), 183–186.

https://dx.doi.org/10.26418/pf.v10i2.57158

Hidayat, R., & Farihah, A. W. (2020). Identification of the changing air temperature and rainfall in Bogor. *Jurnal Pengelolaan Sumberdaya Alam dan Lingkungan (Journal of Natural Resources and Environmental Management)*, 10(4), 616–626. https://doi.org/10.29244/jpsl.10.4.616-626.

Ilhamsyah, Y. (2012). Analisis dampak ENSO terhadap debit aliran DAS Cisangkuy Jawa Barat menggunakan model Rainfall-Runoff, *Depik Jurnal Ilmu-Ilmu Perairan, Pesisir dan Perikanan*, 1(3), 165–174. https://doi.org/10.13170/depik.1.3.107

Keetch, J. J. & Byram, G. M. (1968). *A Drought Index for Forest Fire Control*, *U.S.D.A. Forest Service Research Paper*, 1–32. https://www.srs.fs.usda.gov/pubs/rp/rp_se038.pdf

Malino, C. R., Arsyad, M., & Palloan, P. (2021). Analisis Parameter Curah Hujan dan Suhu Udara di Kota Makassar Terkait Fenomena Perubahan Iklim. *Jurnal Sains Dan Pendidikan Fisika (JSPF)*, 17(2), 139–145. https://doi.org/10.35580/jspf.v17i2.22167

Nabilah, F., Prasetyo, Y., & Sukmono, A. (2017). Analisis Pengaruh Fenomena El Nino dan La Nina Terhadap Curah Hujan Tahun 1998 - 2016 Menggunakan Indikator ONI (Oceanic Nino Index) (Studi Kasus: Provinsi Jawa Barat). *Jurnal Geodesi Undip*, 6(4), 402–412. https://ejournal3.undip.ac.id/index.php/geodesi/article/view/18170

Nahlunnisa, H. & Sopiyandi, S. (2023). Identifikasi Sebaran Titik Panas (*Hotspot*) sebagai Penduga Kebakaran Hutan dan Lahan di Kabupaten Ketapang dan Kayong Utara, Kalimantan Barat. *Jurnal Silva Samalas*, 6(1), 1–5. https://doi.org/10.33394/jss.v6i1.8362

Ningsih, S. R., Putra, Y. S., & Zulfian, Z. (2022). Studi Daerah Rawan Kebakaran Lahan Gambut Berdasarkan Nilai *Keetch Byram Drought Index* di Kalimantan Barat. *Prisma Fisika*, 10(3), 227–233. https://dx.doi.org/10.26418/pf.v10i3.57844

Purba, D. & Purba, M. (2022). Aplikasi Analisis Korelasi dan Regresi menggunakan *Pearson Product Moment* dan *Simple Linear Regression*. *Citra Sains Teknologi*, 1(2), 97–103.

Qonita, I. R., Putra, Y. S., & Kushadiwijayanto, A. A. (2019). Pola Distribusi Kekeringan Menggunakan Metode Standardized Precipitation Index (SPI) di Kalimantan Barat. *Prisma Fisika*, 7(2), 139–142. https://dx.doi.org/10.26418/pf.v7i2.35574

Saharjo, B. H. & Effendi, D. A. (2023). Pengaruh Curah Hujan dan Terjadinya Kebakaran Hutan dan Lahan Gambut di Kabupaten Tanjung Jabung Timur, Provinsi Jambi. *Jurnal Silvikultur Tropika*, 14(02), 126–131. https://doi.org/10.29244/j-siltrop.14.02.126-131

SiPongi^{+} (Sistem Pemantauan Karhutla). https://sipongi.menlhk.go.id/

Susanti, S., Ihwan, A., & Jumarang, M. I. (2013). Analisis Tingkat Kekeringan Menggunakan Parameter Cuaca di Kota Pontianak dan Sekitarnya. *Prisma Fisika*, 1(2), 75–81. https://jurnal.untan.ac.id/index.php/jpfu/article/view/2644/0

Taufik, M., Setiawan, B. I., & van Lanen, H. A. J. (2015). Modification of a fire drought index for tropical wetland ecosystems by including water table depth. *Agricultural and Forest Meteorology*, 203, 1–10. https://dx.doi.org/10.1016/j.agrformet.2014.12.006

Tsabita, T. K. (2023). *Hubungan Tingkat Kekeringan dengan Kebakaran Hutan pada Kejadian* El Nino *dan* Dipole Mode *Positif di Kalimantan Barat*. Universitas Tanjungpura.

Ullum, I. T. N. H., Fitria, A., & Widodo, W. (2024). Variasi Hasil Analisis Data Hasil El Nino-Southern Oscillation (ENSO) terhadap Iklim Global. *JSN: Jurnal Sains Natural*, 2(2), 40–47. https://doi.org/10.35746/jsn.v2i2.528

ISSN: 2579-5821 (Print)
ISSN: 2579-5546 (Online)
URL address: http://journal.unhas.ac.id/index.php/geocelebes
DOI: 10.70561/geocelebes.v8i2.36380

Jurnal Geocelebes Vol. 8 No. 2, October 2024, 162 – 177

Estimation of Subsurface Structure Using Euler Deconvolution Method of Magnetic Data at the Geothermal Area of Sonai Village and its Surroundings, Konawe Regency

Sariani[1], Abdul Manan[1]*, Bahdad[2], Rani Chahyani[3]

[1]Department of Geophysical Engineering, Universitas Halu Oleo (UHO), 93232, Indonesia.
[2]Department of Geology Engineering, Universitas Halu Oleo (UHO), 93232, Indonesia.
[3]Study Program of Physics Education, Institut Agama Islam Negeri (IAIN) Kendari, 93116, Indonesia.

*Corresponding author. Email: amanan@uho.ac.id

Manuscript received: 1 August 2024; Received in revised form: 13 September 2024; Accepted: 29 October 2024

Abstract

It has been carried out research with the aim of determining the subsurface structure at the geothermal area of Sonai Village and its surroundings, Konawe Regency. The data used are magnetic data obtained through field measurements at 126 points in the N180^{o}S direction. After the data were subjected to diurnal and IGRF corrections, a residual (local) magnetic field anomaly of around -150 nT to 90 nT was obtained. On the residual magnetic anomaly map which has been reduced to the Pole (RTP), the Euler Deconvolution (ED) method is applied to the Index Structure N=0 to estimate the subsurface structure in the form of the presence of minor faults, and it is known that there are 5 minor faults at a depth of around 9 to 38 meters. Information on the existence of these faults is then used in 2D modeling. Modeling results show that these minor faults cut through two rock layers, which are the layers composed of conglomerate rocks from the Alangga Formation and peridotites as bedrock from the Ultramafic Complex. One of the minor faults closest to the manifestation area (hot spring) is at coordinates around 4^{o}1’12.412” S and 122^{o}7’24.263” E to 4^{o}1’15.532” S and 122^{o}7’19.561” E with a distance of ±15 meters. The existence of these minor faults is thought to be the migration routes for heat flow or conduction to the surface at the geothermal area of Sonai Village and its surroundings.

Keywords: ED method; minor faults; Residual magnetic field; RTP.

Citation: Sariani, S., Manan, A., Bahdad, & Chahyani, R. (2024). Estimation of subsurface structure using Euler Deconvolution method of magnetic data at the geothermal area of Sonai Village and its surroundings, Konawe Regency. *Jurnal Geocelebes*, 8(2): 162–177, doi: 10.70561/geocelebes.v8i2.36380

Introduction

Based on geological environmental conditions, geothermal systems in Indonesia are divided into two, which are volcanic geological environments and non-volcanic geological environments. The islands of Sumatera, Java, Bali, West Nusa Tenggara, East Nusa Tenggara, Sulawesi and Maluku are areas on the volcanic geothermal route. Meanwhile, non-volcanic environments are in the areas of Bangka Belitung, West Kalimantan, South Sulawesi, Southeast Sulawesi, Central Sulawesi, Maluku and Papua (Aulia et al., 2022). For non-volcanic geothermal, it is usually related to the presence of geological structures such as faults in the subsurface (Risdianto et al., 2015).

Southeast Sulawesi has the potential to have geothermal areas spread from mainland Sulawesi to Buton Island. One of the areas in Southeast Sulawesi that has geothermal potential is at Sonai Village, Puriala District, Konawe Regency.

Geothermal is a natural resource in the form of hot fluid or steam that is formed in the earth's reservoir by heating water beneath the surface by hot rocks. Heat delivery occurs in the upper mantle and earth's crust then is delivered from a heat

source to a heat reservoir on the surface. In a geothermal system there are several things that control it, including heat sources, reservoir rocks, the presence of geological structures such as faults, and water catchment areas (Suryadi et al., 2017).

In 2015, the Ministry of Energy and Mineral Resources' Geological Agency conducted a preliminary geochemical survey at the geothermal area of Puriala District (Anonymous, 2017), and found that the hot spring pH was 7 (neutral). Then Baskara (2020) researched the distribution of hot fluid at the Sonai manifestation area using the geoelectric resistivity method of the Wenner-Schlumberger configuration, and it was found that the flow of hot fluid at this area is thought to be controlled by minor faults.

In this research, the method used is the magnetic method. The magnetic method is a geophysical method that measures variations in the magnetic field on the earth's surface caused by variations in the distribution of magnetized objects beneath the earth's surface (Utama et al., 2016). Magnetic methods can also be used to determine geological structures such as faults, folds and igneous rock intrusions (Ngoh et al., 2017).

In processing magnetic data, the Euler deconvolution method (Cooper, 2024; Daniel & Kingsley, 2020) can be used to make it easier to identify the presence of geological structures, especially to determine the existence of faults in the subsurface. This method is applied to magnetic data that has undergone corrections.

Several researches using magnetic method related to geothermal have been carried out in several locations, including by Luthfin & Jubaidah (2023) at the Banyu Biru hotspring Nganjuk Regency, Lestari et al. (2022) at Air Putih Tourism Area Lebong Regency, Hidayat et al. (2021) at Aie Angek Village Tanah Datar Regency, Nurhidayah (2019) at Awang Bangkal Village South Kalimantan, Sitorus & Tampubolon (2018) at the Tinggi Raja Area Simalungun Regency, Efendi et al. (2018) at the Bada Valley Central Sulawesi, Fatimah et al. (2017) at Gedong Songo Central Java, and Lestari et al. (2016) at Karangrejo Village Pacitan District. The results of these studies show that the magnetic method is able to provide adequate information regarding subsurface conditions, both layers and geological structures.

Materials and Methods

Regional Geology of the Puriala Area

Regionally, Puriala District is included in the Kolaka Series geological map (Simandjuntak et al., 1993). Based on the rock set and its characteristics, geology maps of Kolaka Series can be divided into two geological lanes, which are the Tinodo Lane and the Hialu Lane. The rocks found in the Tinodo Lane which are the base rocks are Paleozoic Metamorphic Rocks (Pzm) and are thought to be of Carboniferous age, consisting of mica schist, quartz schist, chlorite schist, graphite mica schist, slate and gneiss. The rocks found in the Hialu Lane are Ophiolite (Ku) rocks which consist of peridotite, harzburgite, dunite and serpentinite. The youngest rock on this series is Alluvium (Qa) which consists of river, swamp, and beach sediments (Zakaria & Sidarto, 2015).

Based on the regional geological map, the research area is in the central part of the Southeast Arm of Sulawesi which is still influenced by the Konaweha fault which trends Northwest-Southeast. The formations in the research area based on Figure 1 are Alluvium Sediment, Alangga Formation and Ultramafic Complex.

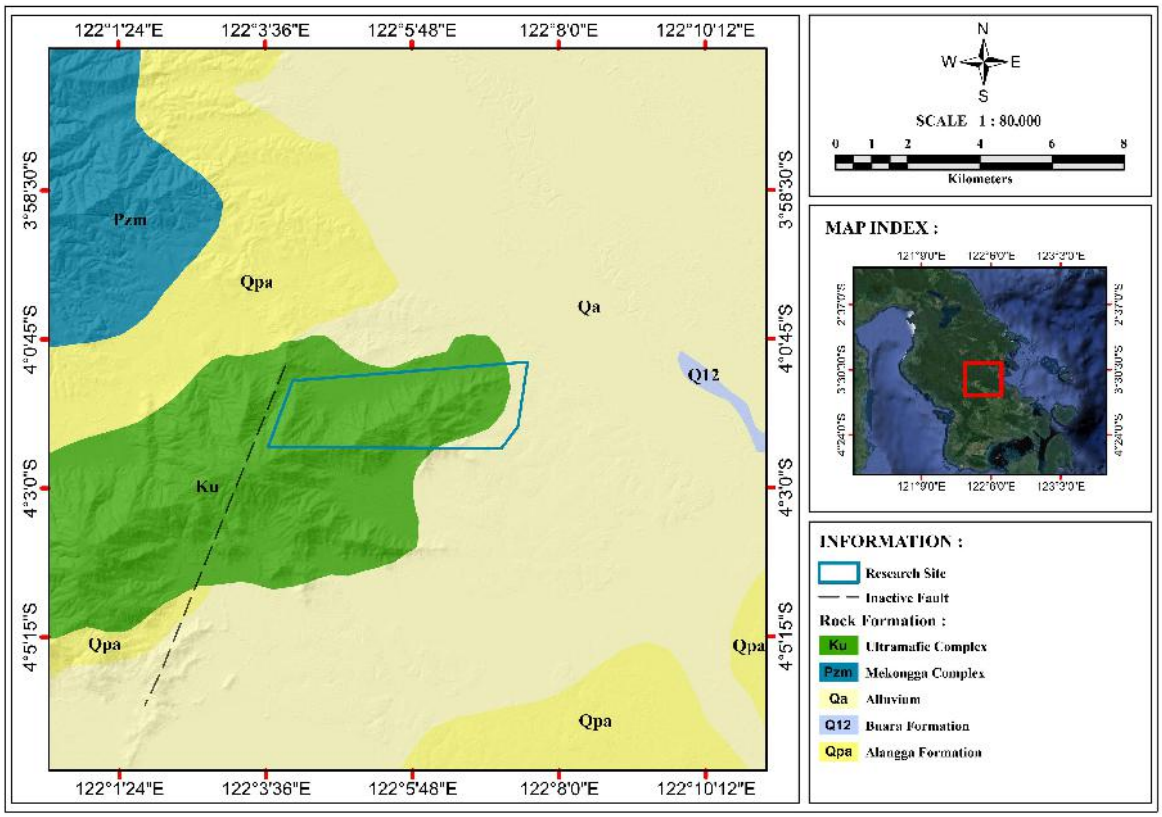

Figure 1. Geological map of the research area.

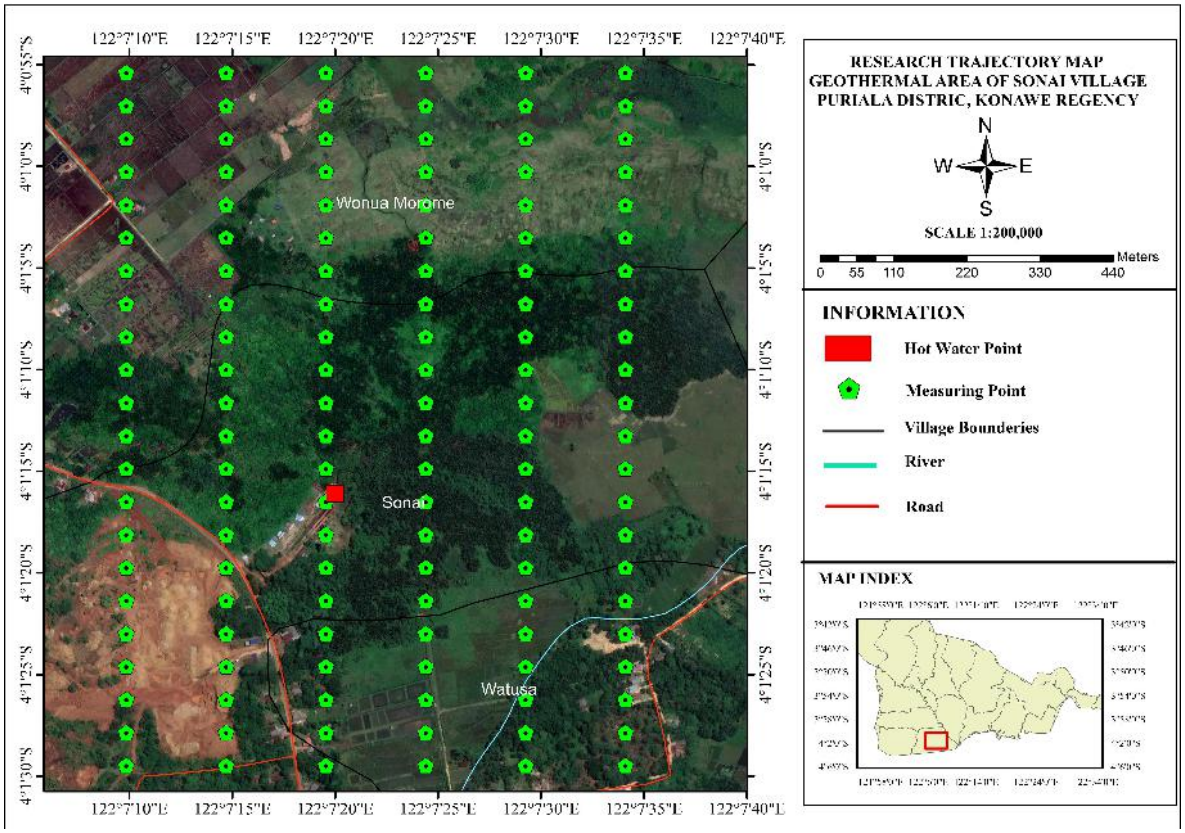

Figure 2. Research setting map.

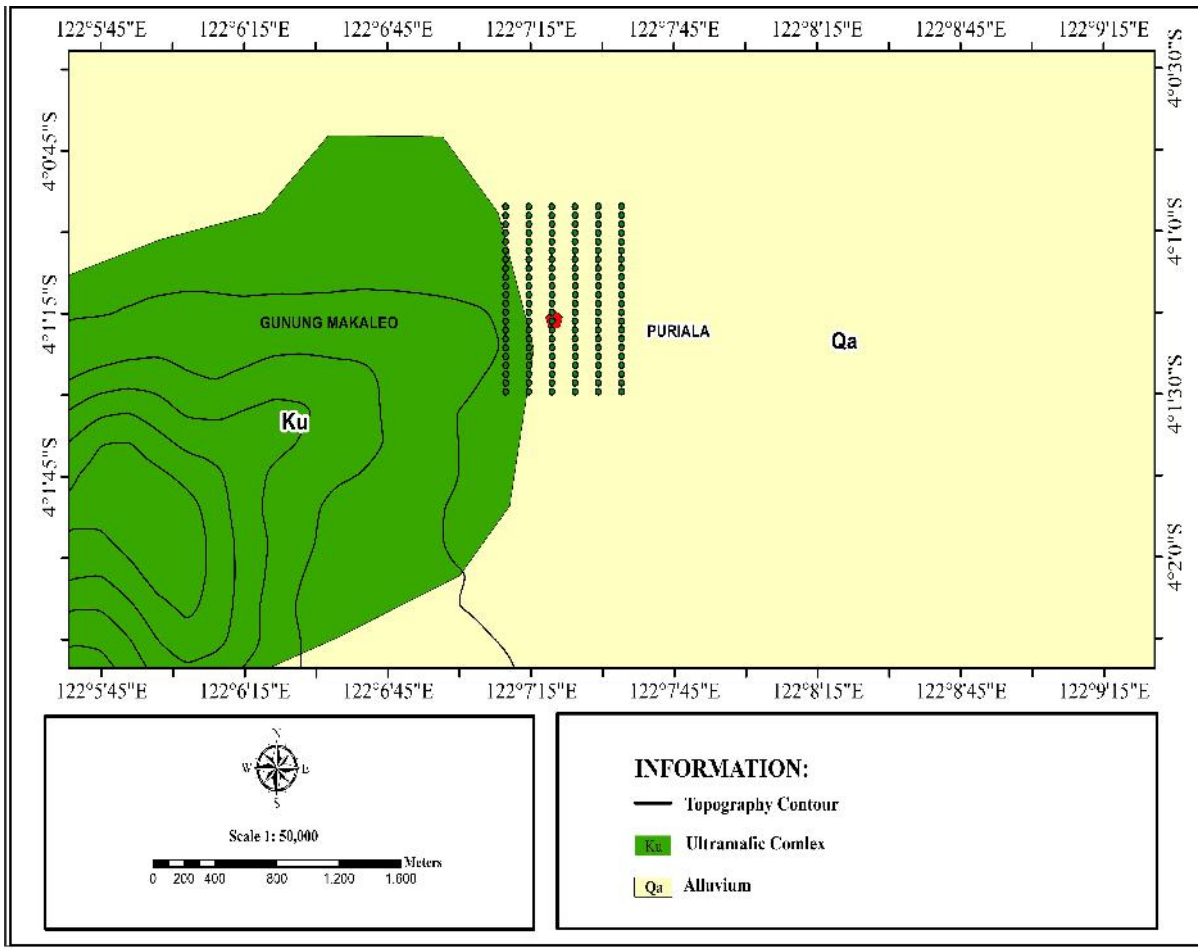

Figure 3. Research setting on geological map.

Research Setting

This research has used magnetic data as primary data. Data collection in the field was carried out using 1 set of Proton Magnetometer and Gradiometer (PMG)-2 equipment from 12 to 13 November 2023 at the geothermal area of Sonai Village and its surroundings, Puriala District, Konawe Regency. The number of measurement points is 126 points with a distance of ±50 meters on 6 trajectories in the direction of N180°S. The area of the research is approximately 1,050×900 meters. The research setting map can be seen in Figure 2 and the research setting map on the geological map can be seen in Figure 3. Apart from that, secondary data was also used in the form of an inclination angle of -23.75° and a declination of 0.36° at the research location.

Data Processing

1. Diurnal Correction

Diurnal Correction is a correction made to magnetic field data measured in the field to eliminate the influence of external magnetic fields or diurnal variations. Calculation of Diurnal Correction is carried out using the formula (Telford et al., 1990):

$$\Delta_{d} = \left(\frac{-}{1-}\right)\left(_{1} - \quad\right) \qquad (1)$$

with ΔH_d is the Diurnal Variation Correction, H_1 is the magnetic field value at the end point, H_o is the magnetic field value at the starting point, t_o is the measurement time at the starting point, t_1 is the measurement time at the end point, and t_n is the measurement time at point n.

2. IGRF Correction

IGRF (International Geomagnetic Reference Field) correction is a correction made to measured magnetic field data that has been corrected for diurnal variations to remove the influence of the Earth's main magnetic field. IGRF values for the research area were obtained from The International Association of Geomagnetism and Aeronomy (IAGA) via www.ngdc.noaa.gov/. IGRF correction is calculated using the formula (Sirait, 2021; Utama et al., 2016):

$$\Delta_{t} = {}_{d} \pm \Delta_{d} - \quad (2)$$

where ΔH_t is the total magnetic field anomaly, H_d is the H value at each measurement point, ΔH_d is the Diurnal Variation Correction, and H_o is the IGRF correction for the Sonai village geothermal area and its surroundings.

3. Upward Continuation

After performing the two corrections above, the total magnetic anomaly data is then transformed using Upward Continuation ($\Delta H_{continuation}$). This stage functions to separate regional magnetic field anomalies from total magnetic field anomalies (Kamureyina et al., 2019; Setiani et al., 2019; Pancasari et al., 2020). In Fikar et al. (2019) it is stated that this process is to eliminate local influences originating from surface sources and clarify the influence of regional magnetic field anomalies.

4. Residual Magnetic Field Anomaly

In this research, the target is the residual (local) magnetic field anomaly. The anomaly is obtained following the equation (Telford et al., 1990):

$$\Delta_{l} = \Delta_{t} - \Delta_{continuation} \quad (3)$$

where ΔH_l is the residual magnetic field anomaly, ΔH_t is the total magnetic anomaly and $\Delta H_{continuation}$ is the magnetic anomaly resulting from Upward Continuation.

5. Reduction to Pole (RTP)

The residual magnetic field anomaly data that has been obtained is then carried out by the RTP process on it. It is hoped that the magnetic field anomaly is located directly above the body of the object causing the anomaly. This transformation process changes dipole magnetic anomaly data into monopole data (Sehah et al., 2023).

6. Euler Deconvolution Method

The Euler Deconvolution method is used to estimate the location and depth of anomaly sources in the subsurface (Ghanbarifar et al., 2024; Cooper, 2024), especially the presence of minor faults.

The Euler Deconvolution method is based on the degree of Euler homogeneity which is interpreted as the Index Structure (N). The Index Structure for several anomaly models can be seen in Table 1 (Stavrev and Reid, 2007). The Euler Deconvolution equation at (x,y,z) coordinate is (Pham et al., 2024; Daniel & Kingsley, 2020):

$$(-) \frac{}{} + (-) \frac{}{} + (-) \frac{}{}$$

$$= N(B\text{-}H) \quad (4)$$

where ($_o$, $_o$, $_o$) is the coordinate of the anomaly source, H the total magnetic field detected at (, ,), and B the regional magnetic field.

Table 1. Index Structure (N) for several magnetic anomaly models (Stavrev & Reid, 2007).

N	Magnetic Anomaly Model
0	Contact/ fault
1	Sill/ dike
2	Cylinder

Results and Discussion

The Total Magnetic Field Measured at the Research Area

Magnetic field measurements at the Sonai geothermal area and its surroundings were carried out using 1 set of PMG-2 equipment. The measurement results are in the form of uncorrected magnetic anomaly

contour as shown in Figure 4. The magnetic field values obtained ranged from 42,220.59 nT to 42,469.21 nT.

Figure 4 shows that there are tighter and looser contour closures. This situation is caused by the inhomogeneous distribution of the magnetic susceptibility of the material or layer in the subsurface.

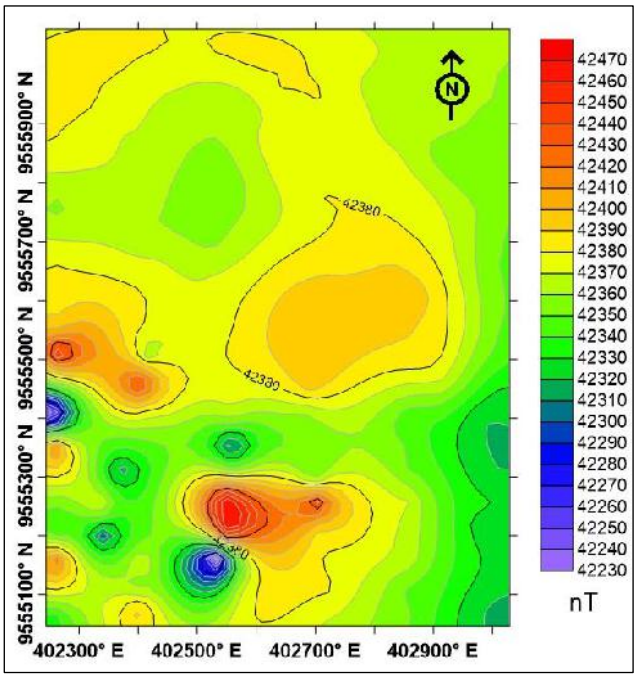

Figure 4. Measured magnetic field distribution.

Total Magnetic Field Anomaly

The total magnetic field anomaly value in an area can be calculated using equation (4). After performing Diurnal and IGRF Corrections, it is known that the magnetic anomaly values at the research area are between -171.17 nT and 82.47 nT. This result can be seen in Figure 5.

Based on Figure 5, qualitatively the distribution of total magnetic field anomalies in the research area is divided into three different anomaly trends, which are high, medium, and low anomalies. The distribution of high anomalies with an anomaly range of around 10 nT to 82 nT is dominant in the Northern part with a West-Northeast direction. The distribution of this anomaly pattern decreases towards the West. The medium anomaly pattern with an anomaly range of around -90 nT to 10 nT is in the Southern part of the research area. This medium anomaly has a downward trend from North-Northwest to West-Northwest. Meanwhile, the low anomaly pattern with an anomaly range of around -171 nT to -90 nT is dominant in the South-Southwestern part of the research area.

Upward Continuation Results

Through a trial-and-error process, Upward Continuation was carried out 6 times, which are at a height of 150 meters, 200 meters, 250 meters, 300 meters, 350 meters, and 400 meters, and the results are shown in Figure 6. Based on the contour map, it can be seen that the lifting process stopped at a height of 300 meters because at this height the shallow anomalies tended to disappear leaving regional anomalies as marked with contour changes that tend to stabilize if the lifting process continues at a higher level.

Residual Magnetic Field Anomaly

The results of Upward Continuation are still in the form of regional magnetic field anomalies which are not the research target, so to obtain residual (local) magnetic anomalies which are the target, further processing needs to be carried out. Residual anomaly follows equation (3).

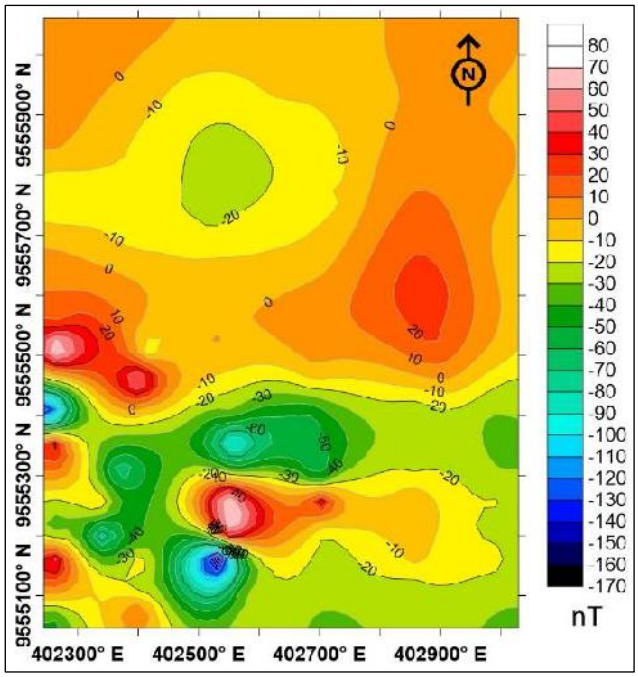

Figure 5. Corrected total magnetic field anomaly distribution.

The residual magnetic field anomaly contour map in Figure 7 shows the local geological structure pattern in the research area. This figure shows qualitatively the distribution of areas with high and low susceptibility values. The residual magnetic field anomaly contour ranges from -150 nT to 90 nT where medium to high anomalies is in the Northern part of the research area and low anomaly contours are dominant in the Southern part.

RTP Transformation of Residual Magnetic Anomaly Data

The residual magnetic field anomaly data are then subjected to RTP transformation with the aim of eliminating the influence of the magnetic inclination angle. In this research, the transformation was carried out from inclination -23.75° to 90° and from declination 0.36° to 0°. This transformation is performed on the residual magnetic field anomaly data. The results ranged from around -89.1 nT to 91 nT which can be seen in Figure 8.

Applying Euler Deconvolution Method to Residual Anomaly Contour Map

The application of Euler Deconvolution method begins with creating a synthetic fault model which is then tested for the Euler Deconvolution response. Subsurface geological structures, especially the location and depth of faults, are identified based on the use of the Index Structure N=0 with a maximum error tolerance of 15%.

The results of Euler Deconvolution can be seen in Figure 9. Based on this figure, several minor faults were found at the research location. The suspected location of minor faults is marked by a distribution of green and blue Euler points. The location is in the North-East which stretches to the Southeast, as well as in the North to North-West. A small number of faults are also in the South and Southwest,

close to area of geothermal manifestation (hot spring). These minor faults are at a depth of around 9 to 38 meters.

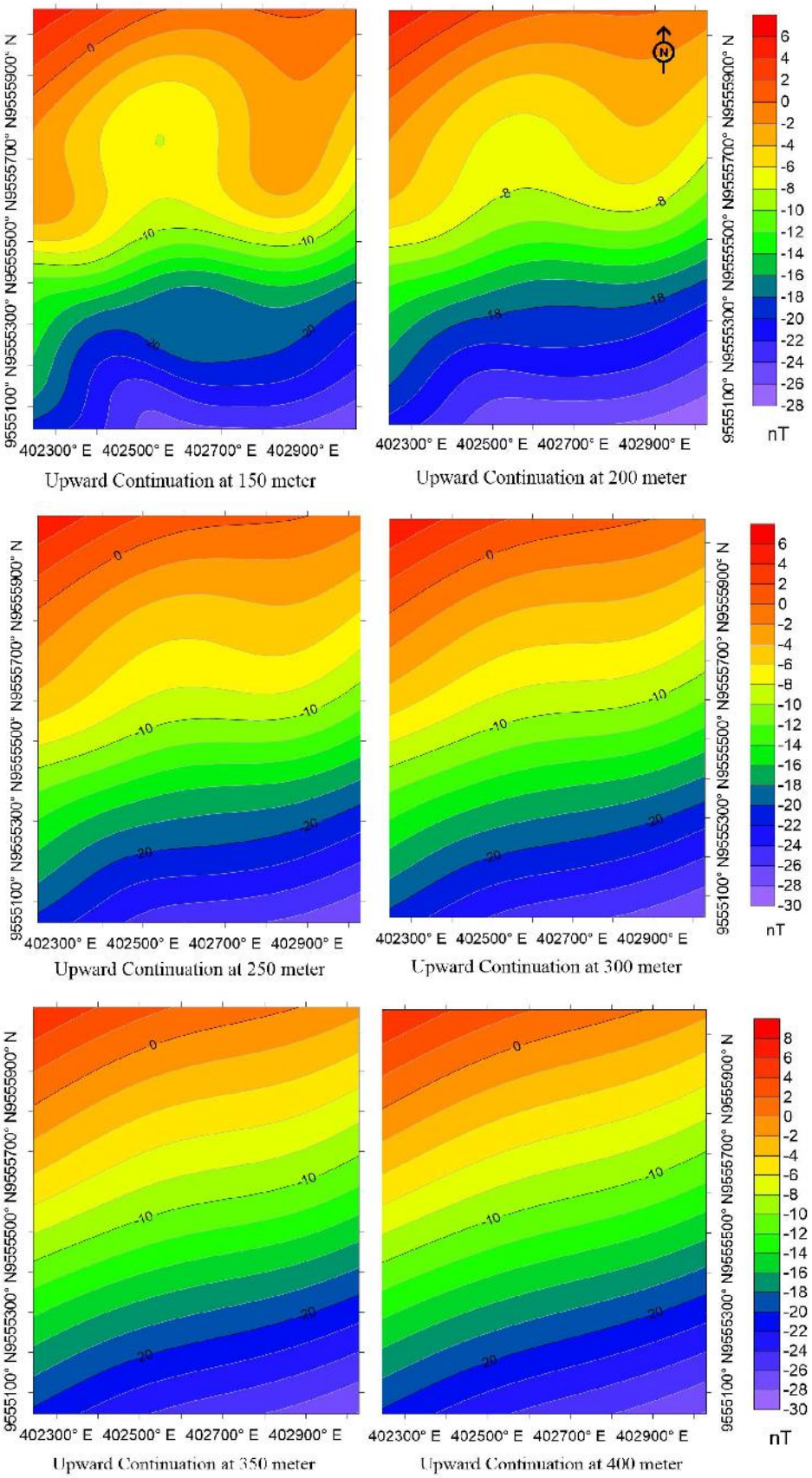

Figure 6. Upward continuation at a height of 150 to 400 meters.

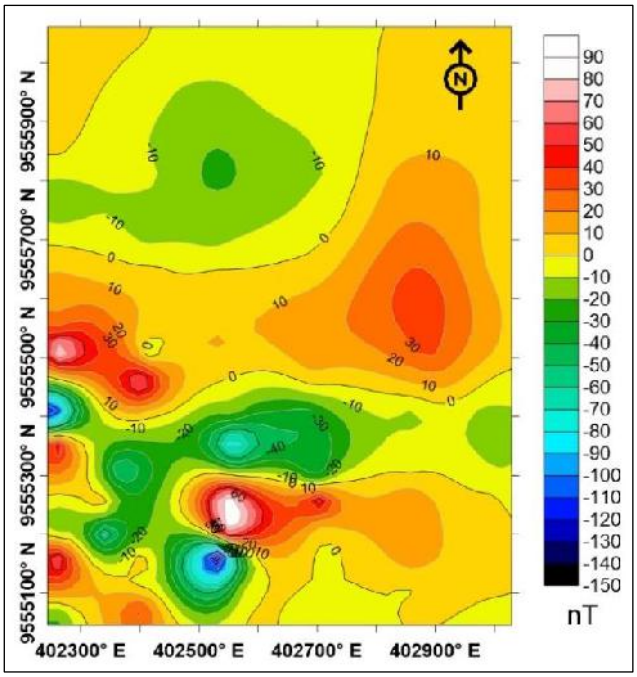

Figure 7. Residual magnetic field anomaly distribution.

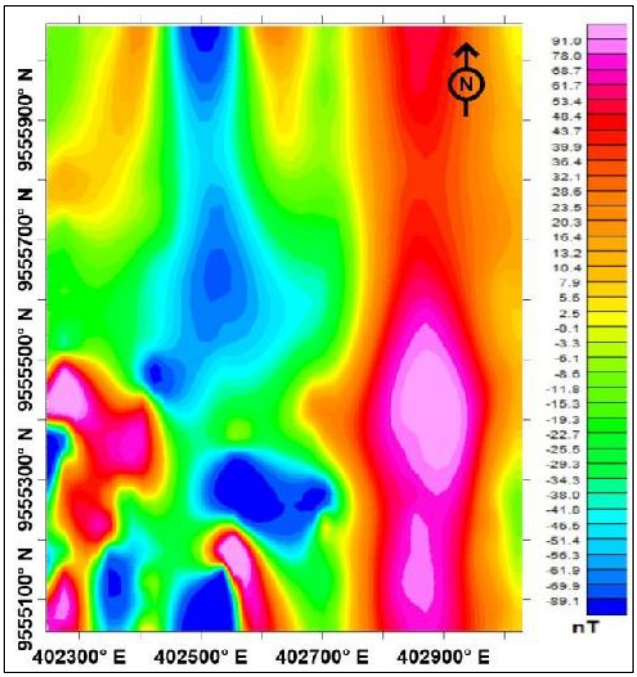

Figure 8. Residual magnetic anomaly contour that has been reduced to the Pole (RTP).

Making Slices for 2D Modeling

For 2D modeling, 2 slices were made on the residual magnetic anomaly map. These slices are A-A' and B-B' (Figure 10). For the first slice or A-A᾽ slice, it is transverse from the North-West to the Southeast through areas where 3 minor faults are thought to lie in the subsurface. Meanwhile, the second slice or B-B᾽ slice runs transversely from West to East through the geothermal manifestation (hot spring), as well as through areas where it is suspected that there are also 3 faults in the subsurface. Determining the slice paths is based on the result of Euler Deconvolution, so it will be easier to determine the presence of faults through 2D subsurface modeling.

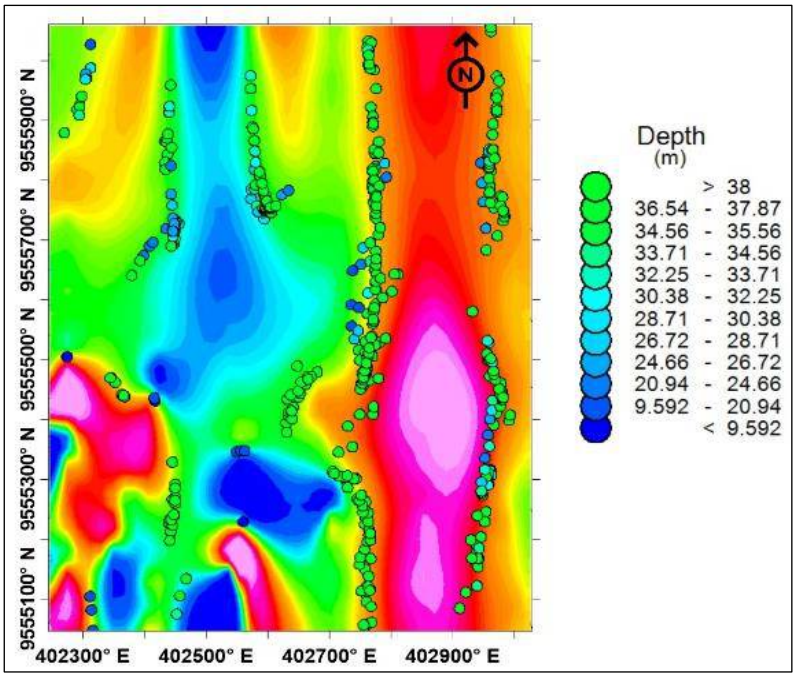

Figure 9. Euler points on the residual magnetic anomaly contour.

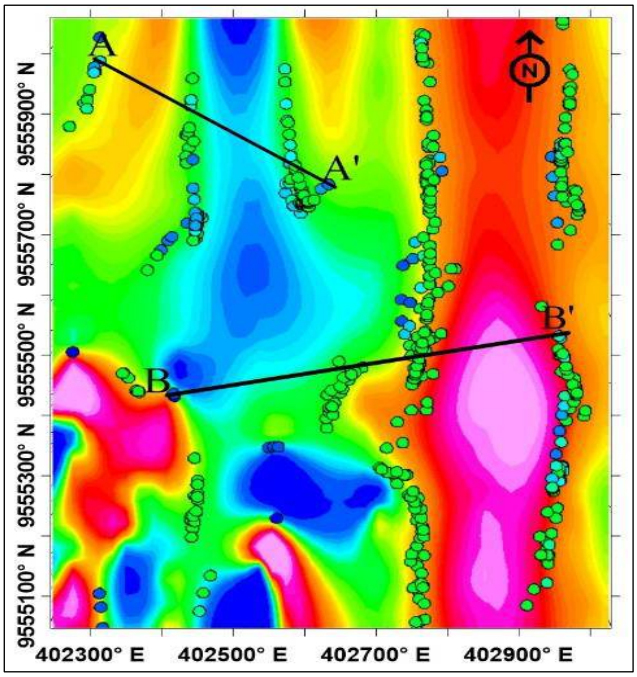

Figure 10. Direction of A-A' and B-B' slices.

2D Modeling Results of Subsurface Structure

Based on the result of 2D modeling for the A-A' slice in Figure 11, it was found that the subsurface condition consists of three layers, which are the first layer consists of three types of rocks with a susceptibility value of 0.001 which is thought to be sand, a susceptibility value of 0.002 is thought to be clay and 0.004 as sandstone. Sand and clay are included in the Alluvium Sediment which is characterized by the presence of swamps near the geothermal manifestation area, while sandstone is included in the Alangga Formation. The second layer consists of only one type of rock, which is rock with a susceptibility value of 0.005 which is thought to be conglomerate rock, and from the figure it looks relatively dominant in the Northwest

part of the research area. This rock is included in the Alangga Formation. Meanwhile, the third layer is only composed of rocks with a susceptibility value of 0.01 which is thought to be peridotite and is included in the Ultramafic Complex. This layer is relatively thinner in the Southeast of the research area.

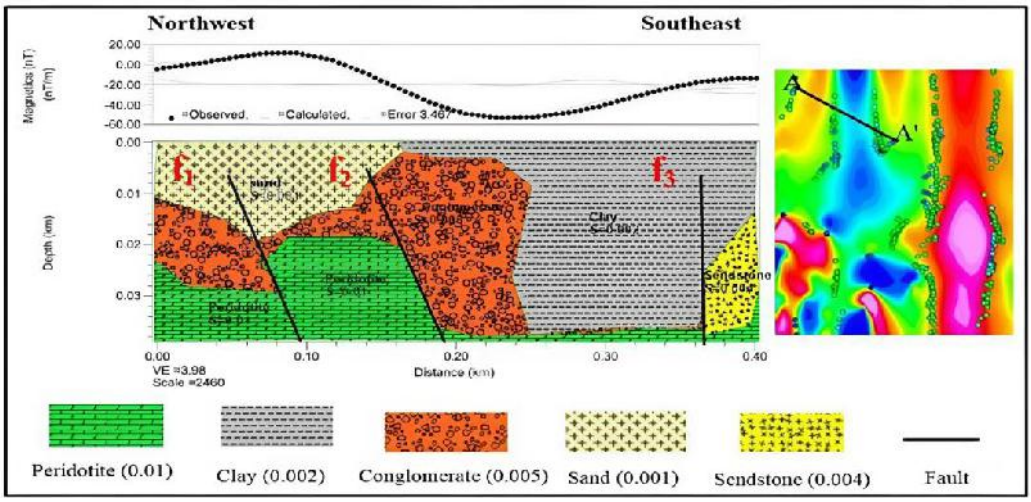

Figure 11. 2D modeling result for A-A' slice.

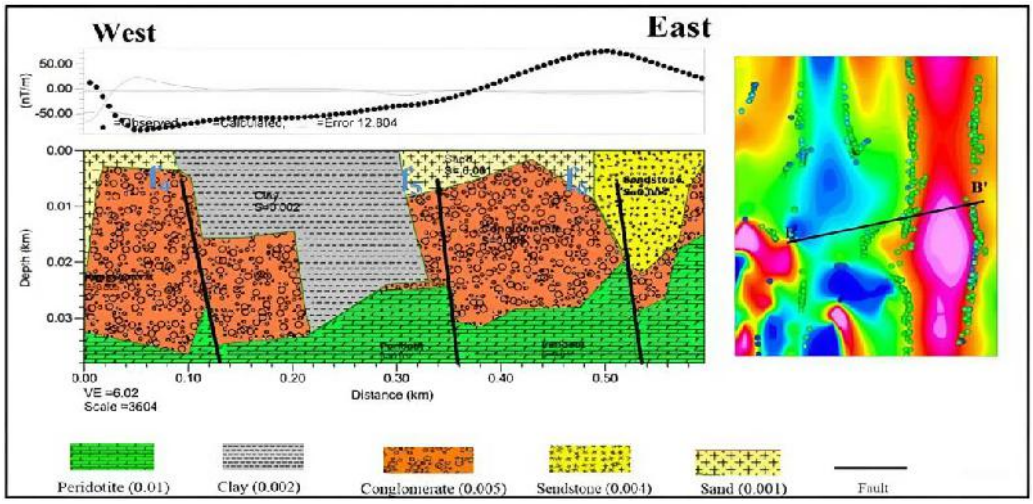

Figure 12. 2D modeling result for B-B' slice.

For the B-B' slice in Figure 12, three layers were also found. The first layer consists of three types of rocks with each susceptibility value of 0.001 which is thought to be sand, 0.002 which is thought to be clay and 0.004 which is thought to be sandstone. The first two types of rocks are the Alluvium Sediments, while the third is included in the Alangga Formation. The second layer consists only of rocks with a susceptibility value of 0.004 which is thought to be conglomerate rock, and includes the Alangga Formation. Meanwhile, the third layer also consists of only one type of rock, which is rock with a susceptibility value of 0.01, and is thought to be peridotite. This rock is part of the Ultramafic Complex. It can be seen that the thickness of this rock layer is relatively thicker than the peridotite layer in the A-A' slice.

The rocks or materials found through modeling are in accordance with the regional geological map of the research area in Figure 1. In addition, it is also in accordance with the geological conditions found directly in the research area where swamps and peridotite outcrops were found which can be seen in Figure 13.

Figure 13. (a). Alluvium sediments in the form of swamps, (b). Laterite soil, and (c). Weathered peridotite outcrop.

The first layer in Figures 11 and 12 above is a layer that can function as a fluid reservoir in geothermal area. This is because alluvium sediments such as sand and clay are loose materials and have pores that are good enough to store and pass water. It is this permeable nature that allows this layer to become a reservoir zone. The second layer is also a permeable layer because it is formed from conglomerate and sandstone from the Alangga Formation. While the third layer is a compact layer formed from peridotite. Peridotite is an igneous rock from the Ultramafic Complex that can function as a bedrock layer. This is because of its impermeable nature.

In this research, several minor fault segments were also found, as can be seen in Figures 11 and 12 above. Minor faults were found at 6 different locations, which are:

1. Fault f_1 is located at coordinates 4°0’61.041” S and 122°7’16.172” E to 4°1’5.421” S and 122°7’15.411” E, and is approximately 363 meters from the hot spring.
2. Fault f_2 is located at coordinates 4°1’2.360” S and 122°7’14.110” E to 4°1’12.168” S and 122°7’15.061” E, and is approximately 68 meters from the hot spring.
3. Fault f_3 is at coordinates 4°1’22.051” S and 122°7’19.232” E to 4°1’9.371” S and 122°7’19.640” E, and is approximately 30 meters from the hot spring.
4. Fault f_4 is at coordinates 4°1’18.345” S and 122°7’13.177” E to 4°1’27.255” S and 122°7’17.363” E, and is approximately 32 meters from the hot spring.
5. Fault f_5 is at coordinates 4°1’12.412” S and 122°7’24.263” E to 4°1’15.532” S and 122°7’19.561” E, and is approximately 15 meters from the hot spring.
6. Fault f_6 is at coordinates 4°1’17.610” S and 122°7’27.189” E to 4°1’27.431” S and 122°7’35.240” E, and is approximately 57 meters from the hot spring.

Regionally, the research area is influenced by the Konaweha strike-slip fault which trends Northwest-Southeast (Tamburaka, 2019). As a result of this fault shift, minor faults were formed which caused the emergence of manifestation such as hot spring in the research area. This fault was formed based on the deformation relationship between the horizontal fault system and the formation of a basin called a pull-apart-basin so that the conglomerate layer in the Northwest (NW) and Southeast (SE) of the research area tends to be thinner than the conglomerate layer in the middle.

The minor faults found in this research cut through the Alangga Formation and bedrock layer as shown in Figures 11 and 12. This condition shows that the type of geothermal at Sonai Village and its surroundings is non-volcanic geothermal where the fluid comes from surface water, and the heat source is controlled by fractures in the form of minor faults formed in the rocks. The fracture zone is a permeable zone that is capable of channeling geothermal fluid.

The fault zones in Figures 11 and 12 are thought to act as geothermal fluid migration routes to the surface. As a result of these zones, fluid is heated and moves upwards so that it accumulates in the permeable zone (alluvium sediment). The movement of the fluid is thought to also be influenced by the topography of the research area where fluid originating from surface water will move and accumulate in lower area. Because the area is close to minor fault zones, hot spring emerges in the area. The area in question is now known by the local population as the Sonai hot spring, Puriala.

Conclusion

Based on the research results, it can be concluded that the Sonai area and its surroundings are composed of 3 formations, which are Alluvium Sediment, Alangga Formation and Ultramafic Complex. For Alluvium Sediment, it was found to be sand with a susceptibility value of 0.001 and clay with a susceptibility value of 0.002. For the Alangga Formation, it consists of sandstone with a susceptibility value of 0.004 and conglomerate rock with a susceptibility value of 0.005. Meanwhile, the Ultramafic Complex consists of peridotite rock with a susceptibility value of 0.001.

Apart from that, in the research area geological structures were found in the form of minor faults at a depth of around 9 to 38 meters which are thought to be the cause of the emergence of geothermal manifestation such as hot spring. Of the several faults found, one of the minor faults closest to the manifestation is at coordinates $4^o1'12.412"$ S and $122^o7'24.263"$ E to $4^o1'15.532"$ S and $122^o7'19.561"$ E with a distance of ±15 meters. The formation of these faults is thought to be caused by the activity of the Konaweha fault which is close to the manifestation area. These minor faults cut through two rock layers, which are a layer composed of conglomerate rock from the Alangga Formation and a rock layer composed of peridotite from the Ultramafic Complex. This peridotite layer functions as bedrock at the Sonai geothermal area, Puriala District, Konawe Regency.

The existence of minor faults found at the area Sonai geothermal is thought to be the pathways of geothermal migration to the surface through conglomerate rock and peridotite layers, both in the form of heat flow and conduction. These minor faults act as heat controllers. At the same time, it proves that the type of geothermal in this area is non-volcanic.

Acknowledgements

Thank you to all parties who have helped this research, especially to the Geophysical Engineering Laboratory that has allowed the use of PMG-2 equipment for data acquisition in the field, laboratory assistants and friends of the magnetic-geothermal research team who have worked together in collecting data in the field.

Author Contribution

In compiling this research article, each author is divided into several job desks. The one responsible for procuring literatures, collecting and processing data

is Sariani, while the design of the research survey and preparation of the article are done by Rani Chahyani. The supervisors and observers in the research and writing of this article are Abdul Manan and Bahdad.

Conflict of Interest

We declare that there is no conflict of interest in the preparation and publication of this paper.

References

Anonymous. (2017). *Potensi Panas Bumi Indonesia Jilid 2*. Direktorat Panas Bumi, Kementerian Energi dan Sumber Daya Mineral.

Aulia, R. N., Nur, I., & Ilyas, A. (2022). Karakteristik Fluida Panas Bumi Berdasarkan Analisis Geokimia Air Panas Wawolesea Kabupaten Konawe Utara Sulawesi Tenggara. *Jurnal Geocelebes*, 6(1), 64–71. https://doi.org/10.20956/geocelebes.v6i1.19672

Baskara, M. Y. (2020). *Identifikasi Sebaran Fluida Panas Daerah Panasbumi Puriala, Kabupaten Konawe Menggunakan Metode Geolistrik Resistivitas Konfigurasi Wenner Schlumberger*. Universitas Halu Oleo.

Cooper, G. R. J. (2024). Using Euler Deconvolution as Part of a Mineral Exploration Project. *Minerals*, 14(4), 393. https://doi.org/10.3390/min14040393

Daniel, O. B., & Kingsley, K. T. (2020). Application of 3D Euler Deconvolution and 2D Inverse Modelling to Basin Depth Estimation, the Case of the Keta Basin, Ghana. *NRIAG Journal of Astronomy and Geophysics*, 9(1), 393–401. *https://doi.org/10.1080/20909977.2020.1743019*

Efendi, R., Fazri, M., Rusydi, H., & Kasim, S. (2018). Interpretasi Data Magnetik Menggunakan Dekonvolusi Euler, Studi Kasus: Lembah Bada Poso Sulawesi Tengah. *Jurnal Geosains Kutai Basin*, 1(1), 1–5. https://jurnal.fmipa.unmul.ac.id/index.php/geofis/article/view/169

Fatimah, F., Lavanto, T. A., Gunawan, B., & Febriarto, O. (2017). Analisis Potensi Panas Bumi dengan Metode Geomagnetik di Daerah Gedong Songo Ungaran Jawa Tengah. *KURVATEK*, 2(2), 35-43.

Fikar, M., Hamimu, L., Manan, A., & Suyanto, I. (2019). Pemodelan 2D Data Magnetik Menggunakan Transformasi RTP untuk Pendugaan Sesar di Daerah Kasihan, Pacitan, Jawa Timur. *Jurnal Rekayasa Geofisika Indonesia (JRGI)*, 01(02), 33–42. https://ojs.uho.ac.id/index.php/jrgi/article/view/8721

Ghanbarifar, S., Hosseini, S.H., Ghiasi, S.M., Abedi, M., & Afshar. A. (2024). Joint Euler Deconvolution for Depth Estimation of Potential Field Magnetic and Gravity Data. *International Journal of Mining and Geo-Engineering*, 58(2), 121–134. https://ijmge.ut.ac.ir/article_95272.html

Hidayat, H., Putra, A., & Pujiastuti, D. (2021). Identifikasi Sebaran Anomali Magnetik pada Daerah Prospek Panas Bumi Nagari Aie Angek, Kabupaten Tanah Datar. *Jurnal Fisika Unand (JFU)*, 10(1), 48-54. https://doi.org/10.25077/jfu.10.1.48-54.2021

International Association of Geomagnetism and Aeronomy. *National Centers for Environmental Information.* www.ngdc.noaa.gov/.

Kamureyina, E., Omang, B. O., Simon, K., Owolabi, A., & Nur, A. (2019). Determination of Hydrocarbon Potentials Using HighResolution Aeromagnetic Data over Sokoto Basin Northwestern Nigeria. *International Journal of Geosciences*,

10, 419-438. https://doi.org/10.4236/ijg.2019.104024

Lestari, S. E., Yunita, A., Rahman, R. A., Refrizon, R., & Sugianto, N. (2022). Aplikasi Metode Magnetik Pada Pemetaan Sumber Panas Bumi di Kawasan Wisata Air Putih, Lebong, Bengkulu. *Newton-Maxwell Journal of Physics*, 3(2), 71–76. https://doi.org/10.33369/nmj.v3i2.23125

Lestari, T. E., Wibowo, B.N., & Darmawan, D. (2016). Interpretasi Bawah Permukaan Daerah Manifestasi Panas Bumi Desa Karangrejo Kecamatan Arjosari Pacitan Menggunakan Metode Geomagnet. *Jurnal Fisika*, 5(1), 1–7. https://journal.student.uny.ac.id/fisika/article/view/157

Luthfin, A., & Jubaidah, N. A. (2023). Identification of Geothermal Distribution in The Banyu Biru Hot Water Source using The Magnetic Method. *Indonesian Journal of Applied Physics (IJAP)*, 13(2), 215–225. https://doi.org/10.13057/ijap.v13i2.72305

Ngoh, J. N., Mbarga, T. N., Assembe, S. P., Meying, A., Owono, O. U., & Tabod, T. C. (2017). Evidence of Structural Facts Inferred from Aeromagnetic Data Analysis over the Guider-Maroua Area (Northern Cameroon). *International Journal of Geosciences*, 8(6), 781–800. https://doi.org/10.4236/ijg.2017.86044

Nurhidayah, A., Wahyono, S. C., & Siregar, S. S. (2019). Interpretasi Bawah Permukaan Daerah Penambangan Batuan Andesit Awang Bangkal Kabupaten Banjar Kalimantan Selatan Menggunakan Metode Magnetik. *Jurnal Fisika Flux*, 16(2), 117–123. https://doi.org/10.20527/flux.v16i2.5184

Pancasari, A., Safani, J., & Manan, A. (2020). Interpretasi Struktur Bawah Permukaan Daerah Kota Kendari Berdasarkan Data Anomali Medan Magnetik Lokal. *Jurnal Rekayasa Geofisika Indonesia (JRGI)*, 02(2), 45–53.

Pham, L. T., Oliveira, S. P., Abdelrahman, K., Gomez-Ortiz, D., Nguyen, D. V., Vo, Q. T., & Eldosouky, A. M. (2024). Selection of Euler Deconvolution Solutions Using the Enhanced Horizontal Gradient and Stable Vertical Differentiation. *Open Geosciences*, 16(1), 20220637. https://doi.org/10.1515/geo-2022-0637

Risdianto, D., Permana, L. A., Wibowo, A. E. A., Sugianto, A., & Hermawan, D. (2015). *Sistem Panasbumi Non-Vulkanik di Sulawesi.* Pusat Sumber Daya Geologi, Badan Geologi, Kementerian Energi dan Sumber Daya Mineral.

Sehah, S., Prabowo, U. N., Raharjo, S. A., & Prasetya, R. I. (2023). Two-Dimensional Modeling of Magnetic Anomaly Data Reduced to the Poles in the Andesitic Prospect Area of the Southeast Slope of Slamet Volcano, Indonesia. *Earth Sciences Malaysia (ESMY)*, 7(2), 75–82. https://doi.org/10.26480/esmy.02.2023.75.82

Setiani, N., Safani, J., & Manan, A. (2019). Interpretasi Struktur Bawah Permukaan Daerah Kota Kendari Berdasarkan Data Anomali Medan Magnetik Regional. *Jurnal Rekayasa Geofisika Indonesia (JRGI)*, 03(1), 25–32.

Simandjuntak, T. O., Surono., & Hadiwijoyo, S. (1993). *Peta Geologi Lembar Kolaka Skala 1:250.000.* Pusat Penelitian dan Pengembangan Geologi.

Sirait, R. (2021). Analisis Anomali Magnetik dalam Penentuan Struktur Geologi dan Litologi Bawah Permukaan sebagai Manifestasi Panas

Bumi di Panyabungan Selatan Sumatera Utara. *Jurnal Fisika Flux*, 18(2), 83–92. https://doi.org/10.20527/flux.v18i2.7402

Sitorus, E., & Tampubolon, T. (2018) Penentuan Struktur Bawah Permukaan Area Panas Bumi Tinggi Raja Kabupaten Simalungun Dengan Menggunakan Metode Magnetik. *Jurnal Einstein*, 6(1), 26–33. https://jurnal.unimed.ac.id/2012//index.php/einsten/article/view/12060

Stavrev, P., & Reid, A. (2007). Degrees of Homogeneity of Potential Fields and Structural Indices of Euler Deconvolution. *Geophysics*, 72(1), L1–L12. https://doi.org/10.1190/1.2400010

Suryadi, S., Haerudin, N., Karyanto., & Sudrajat, Y. (2017). Identifikasi Struktur Bawah Permukaan Lapangan Panas Bumi Way Ratai Berdasarkan Data Audio Magnetotelluric (AMT). *Jurnal Geofisika Eksplorasi*, 3(1). https://journal.eng.unila.ac.id/index.php/geo/article/view/1033

Tamburaka, E. (2019). Risiko dan Mitigasi Bencana Gempa Tektonik di Kabupaten Konawe. *Jurnal Aksara Publik*, 3(2), 222–235.

Utama, W., Warnana, D. D., Bahri, S., & Hilyah, A. (2016). Eksplorasi Geomagnetik Untuk Penentuan Keberadaan Pipa Air di Bawah Permukaan Bumi. *Jurnal Geosaintek*, 2(3), 157–159. http://dx.doi.org/10.12962/j25023659.v2i3.2099

Zakaria, Z., & Sidarto, S. (2015). Aktifitas Tektonik di Sulawesi dan Sekitarnya Sejak Mesozoikum Hingga Kini Sebagai Akibat Interaksi Aktifitas Tektonik Lempeng Tektonik Utama di Sekitarnya. *Jurnal Geologi dan Sumberdaya Mineral*, 16(3), 115–127. https://jgsm.geologi.esdm.go.id/index.php/JGSM/article/view/36

ISSN: 2579-5821 (Print)
ISSN: 2579-5546 (Online)
URL address: http://journal.unhas.ac.id/index.php/geocelebes
DOI: 10.70561/geocelebes.vxix.xxxx

Jurnal Geocelebes Vol. 8 No. 2, October 2024, 178 – 189

Identification of Peridotite Bedrock using Resistivity Geoelectric Method in Lapao Pao Estuary Area, Kolaka District

Syamsul Razak Haraty, Muhammad Gusan*, Erzam Salahuddin Hasan

Department of Geophysical Engineering, Faculty of Mathematics and Natural Sciences, Halu Oleo University, Kendari, 93132, Indonesia

Corresponding Author. Email Address: gusanmuhammad102@gmail.com

Manuscript received: 24 July 2024; Received in revised form: 3 September 2024; Accepted: 29 October 2024

Abstract

Ultramafic rocks are the main source of nickel laterite deposits. One of the areas that has an ultramafic complex is located in Muara Lapao Pao Village, Kolaka Regency. The research was conducted in the mining area of PT Tri mitra Babarina Putra using the resistivity geoelectric method of the Wenner - Schlumberger configuration, In the area it is not yet known exactly how much peridotite bedrock is present in the subsurface. Therefore, it is necessary to conduct a geophysical survey in identifying the occurrence of peridotite bedrock, and can determine the depth and thickness of peridotite bedrock in the research area. the occurrence of peridotite bedrock in the mining area of PT Tri Mitra Babarina Putra has a resistivity value between 3000 – 17984 Ohm-meters. Peridotite bedrock in the research area on all four tracks has a depth and thickness that is almost uniform. lines 1 and 2 and 4 are at a depth of 34.5 - 39.6 meters with a thickness of up to 5.1 meters. and line 3 peridotite bedrock is at a depth of 40 m to more. There are 3 layers in the study area, namely, soil/overburden layer with a resistivity value of 16.5 – 122 Ohm-meters, serpentinite rock layer with a resistivity value of 200 – 2438 Ohm-meters and peridotite bedrock layer with a resistivity value of 3000 – 17984 Ohm-meters.

Keywords: Geoelectric Method; Peridotite; Resistivity; Kolaka**.**

Citation: Haraty, S. R., Gusan, M., & Hasan, E. S. (2024). Identification of Peridotite Bedrock using Resistivity Geoelectric Method in Lapao Pao Estuary Area, Kolaka District. *Jurnal Geocelebes*, 8(2): 178–189, doi: 10.70561/geocelebes.v8i2.36239

Introduction

One of the factors that play an important role in the formation of nickel laterite deposits is the type of bedrock (Jeremiarta et al., 2022). Jeremiarta et al. (2022) explains that ultramafic rocks are rocks that are the main source for laterite nickel deposits. Some examples of ultramafic rocks include dunite, pyroxynite, hornblendite, serpentinite and peridotite. One area that has an ultramafic complex is located in Muara Lapao Pao Village, Kolaka Regency. This area is included in the ofiolite complex in the Southeast Arm of Sulawesi which is part of the East Sulawesi Ofiolite Line. The rocks forming this line are dominated by ultramafic and mafic rocks and pelagic sedimentary rocks and there is melange in several places. (Rachman et al., 2020). The research was conducted in the mining area of PT Tri mitra Babarina Putra, which is engaged in mining that produces peridotite rocks. In the mining area, it is not yet known exactly how much peridotite bedrock is found in the subsurface. Therefore, it is necessary to conduct a geophysical survey in describing the subsurface structure so that later it can be used to identify the presence of peridotite bedrock, and can determine the depth and thickness value of peridotite bedrock in the research area.

Hasria et al. (2022) explains that peridotite rocks are part of ultramafic rocks that contain many mafic minerals, including olivine. Most ultramafic rocks were originally peridotite, formed in the upper

mantle and transformed into serpentinite either partially or completely by crustal fluids during its journey to its current tectonic position (Asdar et al. 2022).

To identify the subsurface conditions of the earth in an area generally using geophysical methods. One of the suitable geophysical methods used is the resistivity geoelectric method. The resistivity method is used to study the flow of electricity in rocks under the earth's surface (Pratama et al., 2019a). The use of resistivity geoelectric method to identify bedrock has been done by previous research (Pratama et al., 2019b) in the research area around Lumpue beach, Pare-Pare city, South Sulawesi.

This research identifies peridotite bedrock using the resistivity geoelectric method with the Wenner-Schlumberger configuration. (Sapina et al., 2023) explained that to detect the subsurface structure of the earth horizontally and vertically using the Wenner-Schlumberger configuration. The Wenner-Schlumberger configuration is one of the configurations usually used for 2D resistivity measurements (Amir et al., 2022). The advantage of the Wenner-Schlumberger configuration is that it can describe lateral and vertical variations in resistivity values and its depth penetration is 10% greater than the Wenner configuration (Telford et al., 1990; Hati et al., 2022). The signal strength of the Wenner-Schlumberger configuration is lower than the Wenner configuration, but higher than the Dipole-dipole configuration (Hermawan & Putra, 2016). Wenner-Schlumberger also has slightly better horizontal data coverage compared to the Wenner configuration, although not better than the Dipole-dipole configuration (Hermawan & Putra, 2016). Therefore, the Wenner-Schlumberger configuration masks the weaknesses of each configuration (Pambudi et al., 2022).

Geology of the Research Area

Based on data from BPS Sulawesi Tenggara (2018), Kolaka Regency is geographically located between 02°00' and 05°00' southern latitude and between 120°45' and 124°06' eastern longitude. Administratively, the research area is in Wolo sub-district, Kolaka Regency. According to BPS Kabupaten Kolaka (2023), the area of Wolo Sub-district is 614.58 km².

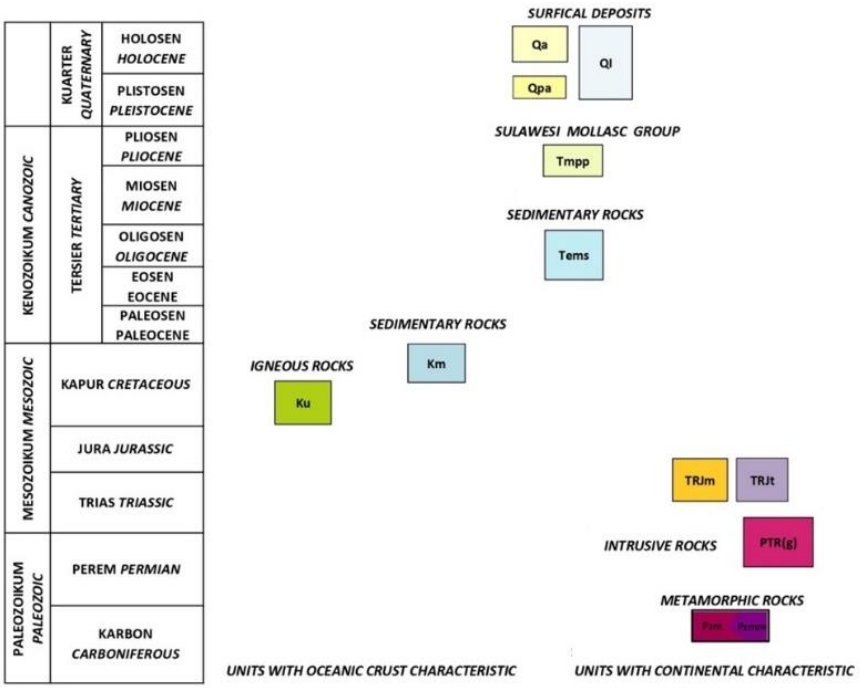

Figure 1. Regional stratigraphy of Lasusua - Kendari sheet (modified from Anggriawan et al., 2021).

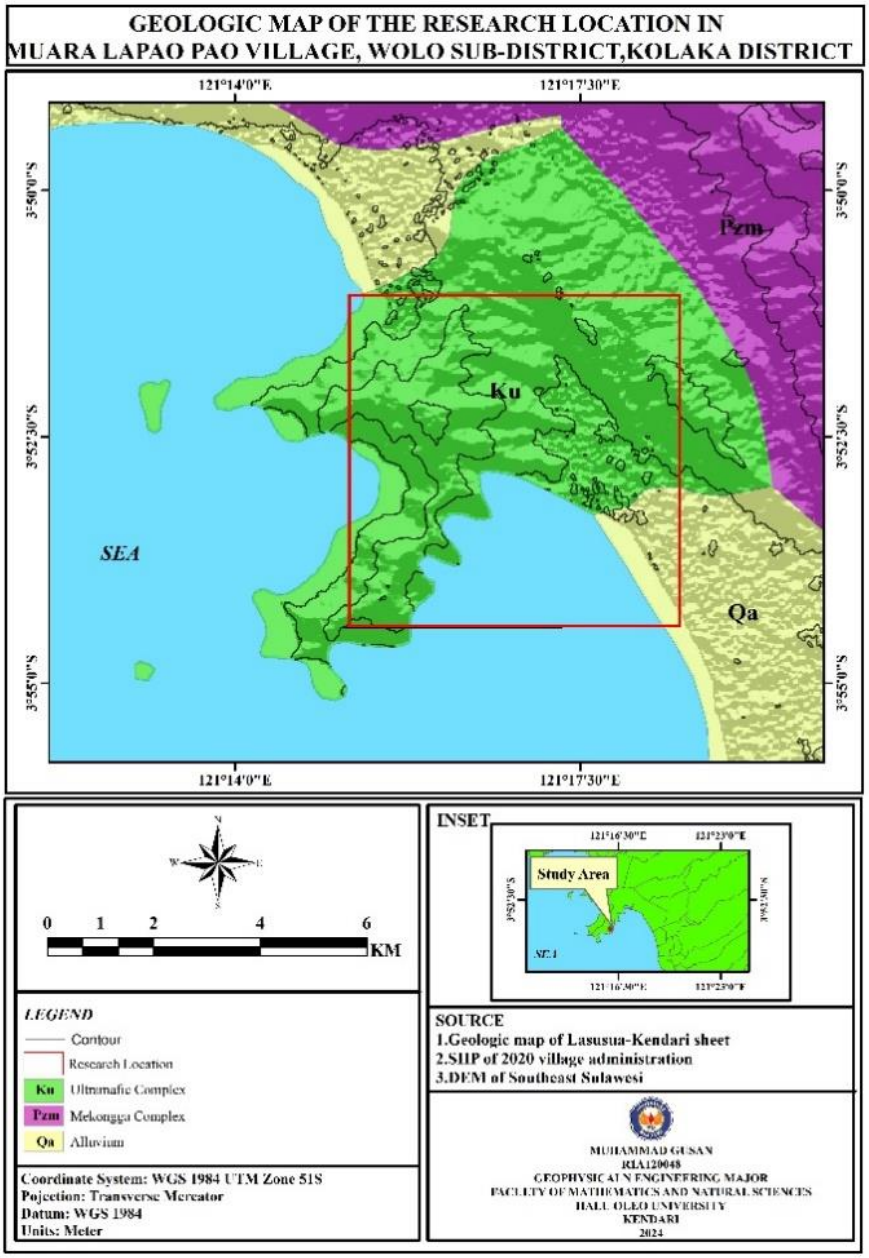

Figure 2. Geologic map of the research area.

Based on the regional stratigraphic map of the Lasusua - Kendari sheet (Anggriawan et al., 2021) in Figure 1. Wolo sub-district is dominated by the carbonaceous to perm aged Mekongga complex (Pzm) which consists of schist, genes, phyllite, quartzite, slate, and a little alabaster has a menjemari relationship with the paleozoic alabaster unit (Pzmm). The complex is overlain by Holocene-aged alluvium (Qa) consisting of gravel, pebbles, sand, clay and silt. The corresponding research area, in Figure 2, is in the ultramafic complex (Ku) which is limestone in age with constituent rocks of peridotite, harzburgite, dunite, gabbro and serpentinite.

Peridotite Rocks

According to Thorffata et al. (2022), bedrock is one aspect that determines the nickel content in nickel laterite deposits because it is the source of nickel content before enrichment occurs. Peridotite rocks consist of holocrystalline minerals with medium - coarse size and anhedral shape. The composition is composed of olivine and pyroxene, the accessory minerals consist of plagioclase, hornblende, biotite,

and garnet (Puspita et al., 2022). According to Erwin et al. (2023) explained that Peridotite is one of the nickel-bearing rocks of origin. Peridotite has a high nickel content compared to pyroxynite bedrock because peridotite rocks contain more olivine minerals, while pyroxynite bedrock is generally rich in pyroxene mineral content (Musrifin et al., 2021). The uses of peridotite rock are as building materials, floor or wall ornaments, sculpture making, half gemstones, materials for jewelry, and as emery.

Resistivity Method

Amin et al. (2023) explained that one method to describe the conditions under the earth's surface is the resistivity geoelectric method, which is by injecting electric current into the soil through two current electrodes. then two potential electrodes are used to measure the potential difference that occurs. The resistivity geoelectric method is used to measure a physical quantity such as the resistivity of a subsurface layer. The resistivity value reflects the ability of the layer to inhibit the flow of electric current. This value will be used as a basis for interpreting the condition of the subsurface layer (Ariputra et al., 2021).

Nugroho & Afiatna (2021) explained that pseudo-resistivity is the resistivity of a fictitious medium considered to be the same or homogeneous which is equivalent to the layered medium under review. For example, the layered medium under review may consist of two layers that have different resistivities ($\rho 1$ and $\rho 2$) considered as the same or homogeneous single-layer medium that has one resistivity price of ρa, thus this ρa is a pseudo price. The apparent resistivity value can be expressed in the equation:

$$\rho = 2\pi \left[\left(\frac{1}{r1} - \frac{1}{r2}\right) - \left(\frac{1}{r3} - \frac{1}{r4}\right)\right]^{-1} \frac{\Delta V}{I} \quad (1)$$

$$\rho_a = K \frac{\Delta V}{I} \quad (2)$$

ρ_a is the apparent resistivity value (Ωm), refer to Figure 3, ΔV is the potential difference between P1 and P2 (Volt) and I is the current strength (A) (Sapina et al., 2023) and r is the distance between the two current electrodes (C1C2) and potential electrodes (P1P2) (m) (Sihombing et al., 2023). By measuring ΔV and I, the resistivity value can be determined (Nugroho & Afiatna, 2021).

Table 1. Resistivity values of earth materials (Telford et al., 1990; Pratama et al., 2019b).

Rock Type	Resistivity Range (Ωm)
Granite	$3\ x\ 10^2 - 10^6$
Feldspar Porphyry	$4\ x\ 10^3$
Carbonatized Porphyry	$2.5\ x\ 10^3 - 6\ x\ 10^4$
Porphyry (Various)	$60 - 10^4$
Dacite	$2x10^4$
Diabase Porphyry	$10^3 - 1.7\ x\ 10^5$
Marble	$10^2 - 2.5\ x\ 10^8$
Lavas	$10^2 - 5\ x\ 10^4$
Gabbro	$10^3 - 10^6$
Basalt	$10 - 1.3\ x\ 10^7$
Olivine Norite	$10^3 - 6\ x\ 10^4$
Peridotite	$3\ x\ 10^3 - 6.5\ x\ 10^3$
Serpentinite	$2x10^2 - 3x10^3$
Hornfels	$8\ x\ 10^3 - 6\ x\ 10^7$
Tuffs	$2\ x\ 10^3 - 10^5$
Graphite Schist	$10 - 10^2$
Gneiss (various)	$6.8\ x\ 10^4 - 3\ x\ 10^6$

The configuration used to detect subsurface structures in mapping and sounding is the Wenner-Schlumberger configuration (Sapina et al., 2023). The Wenner-Schlumberger configuration is a configuration that applies a fixed spacing rule system with the factor "n" for this configuration as a comparison of the distance between electrodes C1-P1 (or C2-P2) with the space between P1-P2 as shown in Figure 3. If the distance between potential electrodes (P1 and P2) is a then the distance between current electrodes (C1 and C2) is 2na + a. The process of determining resistivity involves 4 electrodes with placement on a straight line (Yuristina et al., 2015).

The spacing distance between electrodes, the geometry factor of the Wenner-Schlumberger configuration becomes:

$$k = \pi (n+1)a \quad (3)$$

where, k is the geometry factor (m), n is the distance between C1 and P1 (m) and C2 and P2 (m), a is the electrode spacing distance (m), (Saputra et al., 2020). Figure 4 provides a schematic of the Wenner-Schlumberger arrangement.

Materials and Methods

Field data acquisition has been carried out on September 13 - 16, 2023 located in the mining area, in Muara Lapao Pao Village, Wolo District, Kolaka Regency, Southeast Sulawesi Province can be seen in Figure 5. Data processing, data analysis and interpretation were carried out at the Geophysical Engineering Laboratory, Faculty of Mathematics and Natural Sciences, Halu Oleo University, Kendari.

The data used is secondary data in the form of data from field measurements consisting of electric current (I) and potential difference (V). Preparation stage by preparing tools and materials that will be used during measurements in the research area. The preliminary study includes an initial study of the literature and making measurement data tables, to collect information that is relevant or related to bedrock, peridotite rock, resistivity geoelectric method, safety factor and regional geological description of the research area.

The resistivity value obtained from the interpretation results is then interpreted based on the value of the resistivity variation of earth materials (Table 1). So that data analysis is carried out qualitatively on the 2D resistivity cross section, thus it can determine the presence of peridotite bedrock in the research area based on the subsurface resistivity value of the displayed color scale.

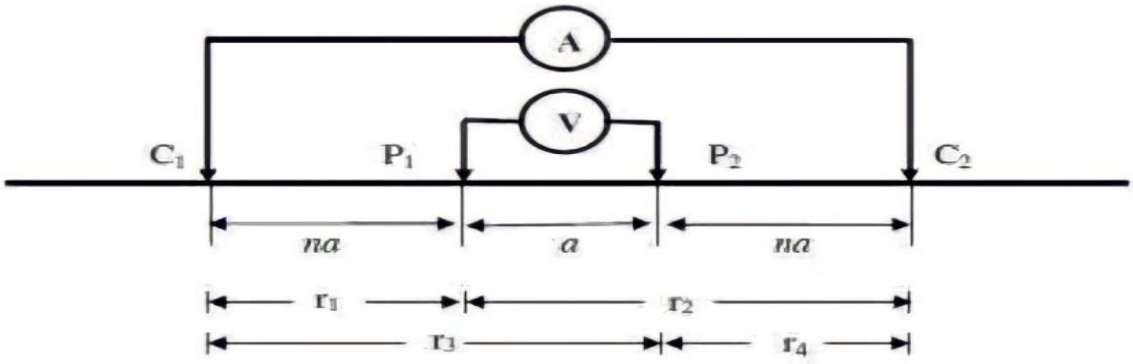

Figure 3. Wenner - Schlumberger configuration (Panjaitan & Jusfarida, 2022).

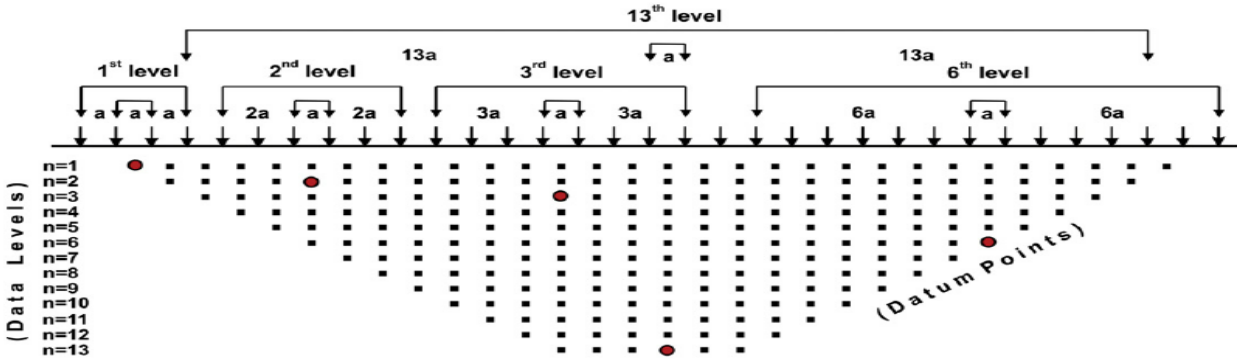

Figure 4. Schematic of the Wenner-Schlumberger array of electrode locations and datum points (Akhasanullatief & Sehah, 2022).

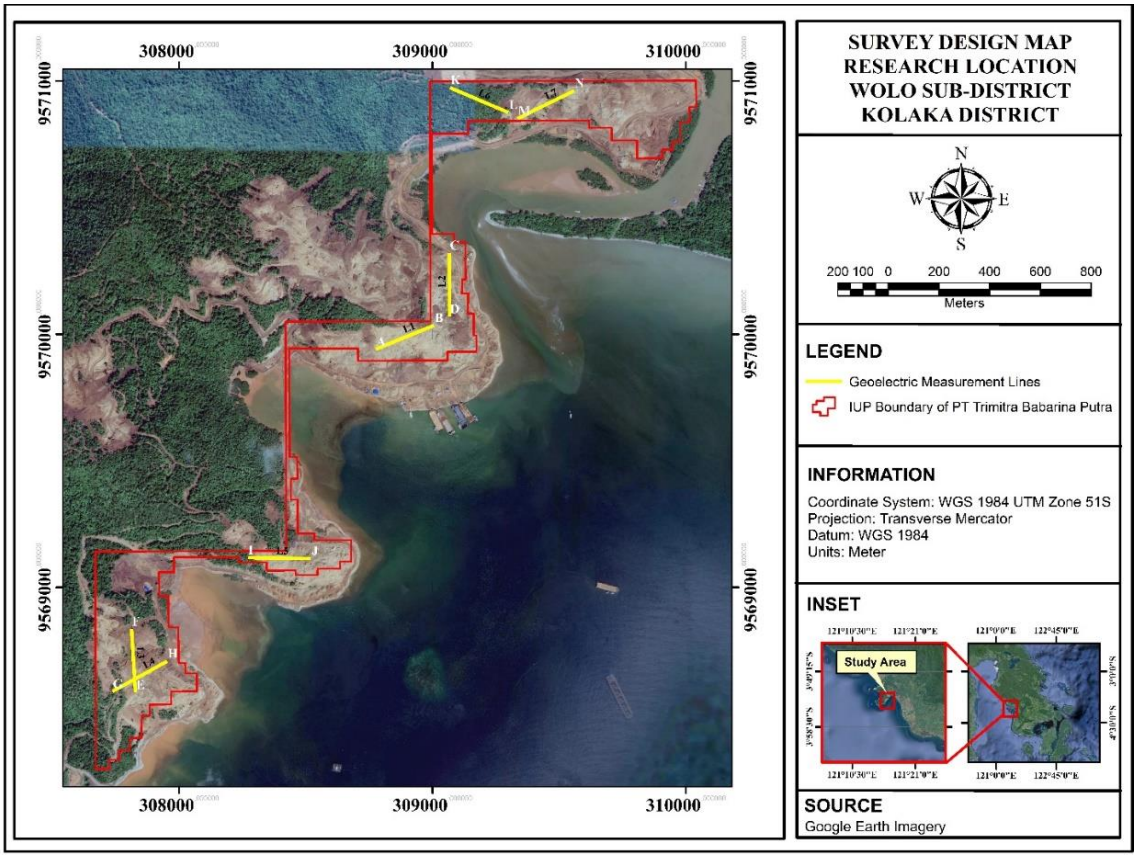

Figure 5. Research Location Map.

Results and Discussion

Line 1

Based on the two-dimensional resistivity cross-section model on line 1 (Figure 6), it can be seen from the span of 0 - 190 meters horizontally while vertically at a depth of 2.50 - 39.6 meters. The distribution of resistivity values on this line ranges from 16.5 to 17984 Ohm-meters with 6 iterations and an RMS error of 9.8%. Iteration is done several times to reduce the error value. The resistivity values vary from low resistivity values to high resistivity values. The lithology layer can be distinguished by looking at the resistivity value that has been obtained from the results of data processing and looking at geological information consisting of regional geological maps, and rock outcrops.

Line 1 with a resistivity value of 16.5 – 122 Ohm-meters is identified as a top soil layer with an average depth from the surface to 13 meters, its physical appearance is yellow-brownish. The resistivity value of 200 – 2438 Ohm-meters is identified as a serpentinite rock layer with a depth from the surface to 18.5 m and at a depth of 32 m. Rock outcrops are seen at 30 m, 60 – 100 m, 130 – 145 m, and 160 – 170 m. This rock layer has undergone a serpentinization process that changes the mineral composition, chemistry, and texture of rocks in ultrabasic rocks when there is interaction between rocks and hydrothermal fluids through them (Permana et al., 2017). The resistivity value of 3000 – 17984 Ohm-meters is identified as a bedrock layer or the lowest layer with constituent rocks dominated by peridotite rocks at a depth of 34.5 to 39.6 meters and the thickness of this layer is 5.1 meters. This rock layer still has the physical properties of its original rock and has not undergone a serpentinization process.

Line 2

Based on the two-dimensional resistivity cross-section model on line 2 (Figure 7), it

can be seen from the span of 0 - 190 meters horizontally while vertically at a depth of 2.50 – 39.6 meters. The distribution of resistivity values on this line ranges from 16.5 to 17984 Ohm-meters with 5 iterations and an RMS error of 13.0%. Iteration is done several times to reduce the error value. The resistivity values vary from low resistivity values to high resistivity values. This is because each layer has a different element content. The lithology layer can be distinguished by looking at the resistivity value that has been obtained from the results of data processing and looking at geological information consisting of regional geological maps, and rock outcrops.

Line 2 with a resistivity value of 16.5 – 122 Ohm-meters is identified as a top soil layer with an average depth from the surface of up to 13 meters, its physical appearance is yellow-brownish and has outcrops of peridotite rocks that come to the surface. The resistivity value of 200 – 2438 Ohm-meters is identified as a serpentinite rock layer with a depth from the surface to 18.5 m and at a depth of 32 m. Rock outcrops are seen at 35 – 70 m, 90 – 108 m, 123 – 147 m, and 165 – 175 m. This rock layer has undergone a serpentinization process that changes the mineral composition, chemistry, and texture of rocks in ultrabasic rocks when there is interaction between rocks and hydrothermal fluids through them (Permana et al., 2017). The resistivity value of 3000 – 17984 Ohm-meters is identified as the bedrock layer or the lowest layer with the constituent rocks dominated by peridotite rocks at a depth of 34.5 to 39.6 meters and the thickness of this layer is 5.1 meters. Rock outcrops of peridotite meter 20 – 30 m. This rock layer still has the physical properties of its original rock and has not undergone the serpentinization process.

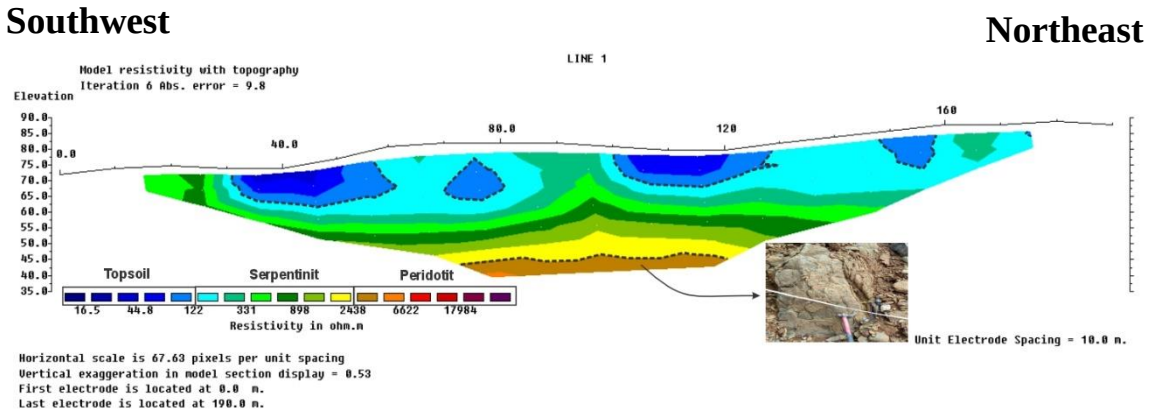

Figure 6. 2D resistivity cross section model of line 1 with topography.

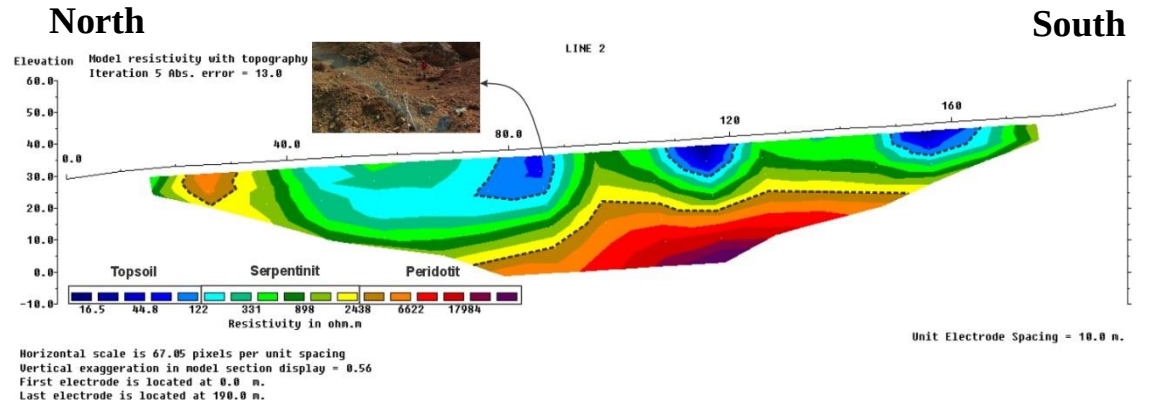

Figure 7. 2D resistivity cross section model of line 2 with topography.

Line 3

Based on the two-dimensional resistivity cross-section model on line 3 (Figure 8), it can be seen from the span of 0 - 200 meters horizontally while vertically at a depth of 2.50 – 39.6 meters. The variation of resistivity values on this line ranges from 16.5 to 17984 Ohm-meters with 5 iterations and the RMS error is 19.6%. Iteration is done several times to reduce the error value. The resistivity values vary from low resistivity values to high resistivity values. This is because each layer contains different elements and materials. The lithology layer can be distinguished by looking at the resistivity value that has been obtained from the data processing results and looking at the geological information of the study area consisting of regional geological maps, and rock outcrops.

Line 3 with an average depth from the surface to 25 meters is identified as a soil layer, the distribution of resistivity values ranges from 16.5 – 122 Ohm-meters, the physical appearance is yellow-brownish and has outcrops of peridotite that is serpentinized to the surface. From the surface to 32 m and at a depth of 39.6 m it is identified as a serpentinite rock layer, the resistivity value distribution is 200 – 2438 Ohm-meters. Rock outcrops are seen at 20 – 30 m, 40 – 50 m, 90 – 105 m, 135 – 155 m and 175 m. This rock layer has undergone a serpentinization process that changes the mineral composition, chemistry, and texture of rocks in ultrabasic rocks when there is interaction between rocks and hydrothermal fluids through them (Permana et al., 2017). At a depth of 40 m to more, it is identified as the bedrock layer or the lowest layer with its constituent rocks dominated by peridotite rocks with a resistivity value of 3000 – 17984 Ohm-meters. This rock layer still has the physical properties of its original rock and has not undergone a serpentinization process.

Line 4

Based on the two-dimensional resistivity cross section model on line 4 (Figure 9), it can be seen from the span of 0 – 190 meters horizontally while vertically at a depth of 2.50 – 39.6 meters. Obtained variations in resistivity values on this line ranged from 16.5 to 17984 Ohm-meters with 5 iterations and an RMS error of 14.8%. Iteration is done several times to reduce the error value. The resistivity values vary from low resistivity values to high resistivity values. This is caused by each layer having different element and material content.

Line 4 with an average depth from the surface to 12.8 meters is identified as a soil layer, the distribution of its resistivity values ranges from 16.5 – 122 Ohm-meters, its physical appearance is yellow-brownish. From the surface to 13 m and at a depth of 32 m is identified as a serpentinite rock layer, the distribution of resistivity values is 200 - 2438 Ohm-meters. The rock outcrops are seen at 20 – 45 m, 65 – 75 m, 90 – 110 m, 125 m and 140 – 145 m. This rock layer has undergone a serpentinization process that changes the mineral composition, chemistry, and rock texture in ultrabasic rocks when there is interaction between the rock and the hydrothermal fluid through it (Permana et al., 2017). At a depth of 34.5 to 39.6 meters and a thickness of 5.1 meters, this layer is identified as a bedrock layer or the lowest layer with constituent rocks dominated by peridotite rocks with a resistivity value of 3000 – 17984 Ohm-meters. This rock layer still has the physical properties of its original rock and has not undergone a serpentinization process.

Interpreting the lithologic layers requires literature studies and field observations. Mentioned in regional geology, Wolo sub-district is included in the Mekongga complex (Pzm), alluvium (Qa) and ultramafic complex (Ku). The research site is included in the ultramafic complex with its constituent rocks identified as serpentinite and peridotite rocks. The soil layer is the opening soil or the topmost

layer. The soil is hollow due to land that has been previously stripped. The presence of veins in ultramafic rocks is evidence that the rocks have been serpentinized into serpentinite rocks seen in the rock outcrops. The degree of serpentinization is divided into three categories (low, medium, high) based on the type of serpentine vein (Jaya et al., 2024). An understanding of serpentinization is important in knowing the composition of the bedrock, determining the temperature and pressure conditions under which the hydration process took place, and determining the location of serpentinization in continental crust, oceanic crust, or both (Jaya et al., 2024). Most ultramafic rocks were originally peridotite rocks with pyroxene and olivine mineral compositions that formed in the upper mantle and then transformed into serpentinite, completely or partially. The uses of peridotite rocks are that they can be utilized in the metallurgical, chemical and construction industries and can be used as raw materials in the refractory industry and abrasive industry. The existence of peridotite rocks is reinforced by observations in the field as evidenced by the presence of rock outcrops.

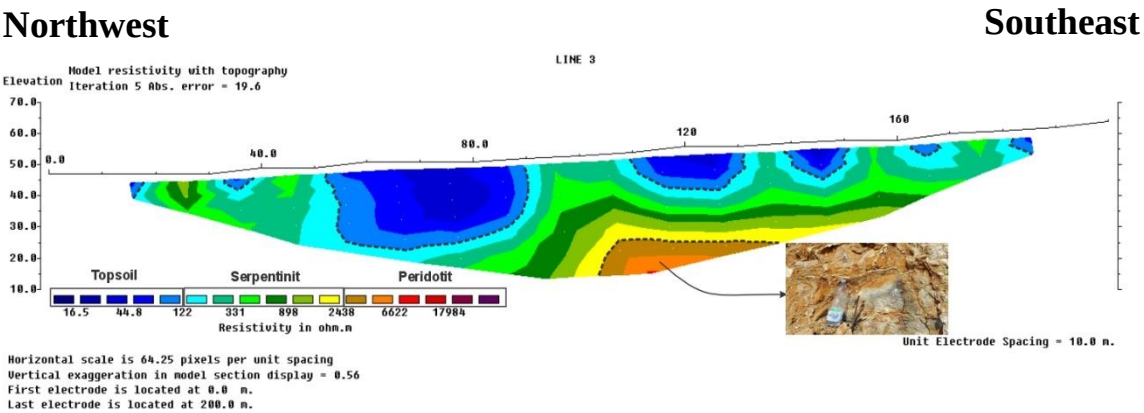

Figure 8. 2D resistivity cross section model of line 3 with topography.

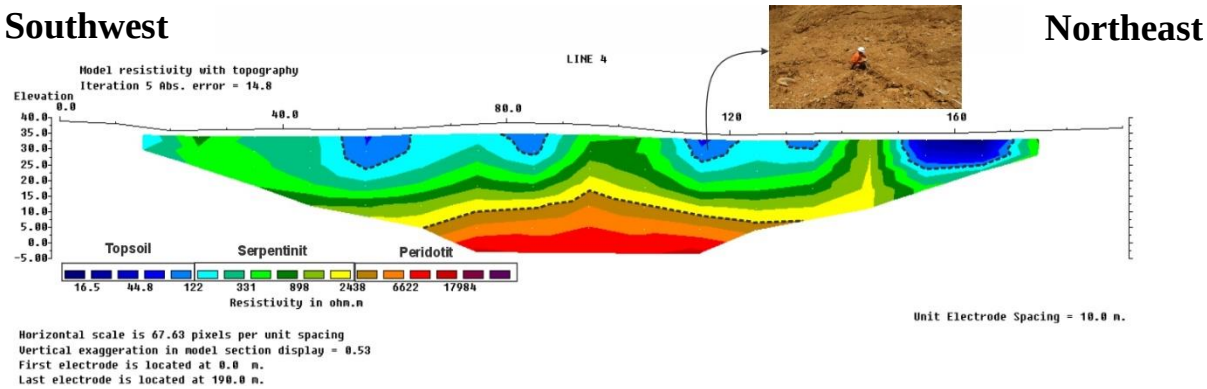

Figure 9. 2D resistivity cross section model of line 4 with topography.

Conclusion

The presence of peridotite bedrock in the mining area of PT Tri Mitra Babarina Putra has a resistivity value between 3000 – 17984 Ohm-meters. Peridotite bedrock in the research area on all four lines has a depth and thickness that is almost uniform. lines 1 and 2 and 4 are at a depth of 34.5 – 39.6 meters with a thickness of up to 5.1 meters. and line 3 peridotite bedrock is at a depth of 40 m to more. There are 3 layers in the study area, which are, soil/ overburden layer with a resistivity value of 16.5 – 122 Ohm-meters, serpentinite rock layer with a resistivity value of 200 – 2438 Ohm-meters and peridotite bedrock layer with a resistivity value of 3000 – 17984 Ohm-meters.

Acknowledgments

The author would like to thank PT. Tri Mitra Babarina Putra for granting research permission and thanks to all those who have helped the author so that it is well completed.

Author Contribution

The idea of this topic was recommended by Syamsul Razak Haraty and Erzam Salahuddin Hasan as supervisors and helped to review the manuscript. reference collection, field survey, data processing, data analysis and interpretation were done by Muhammad Gusan.

Conflict of Interest

This research has no donation from any party or organization.

References

Akhasanullatief, F., & Sehah, S. (2022). Interpretasi Sebaran Batuan Andesit di Desa Karangcegak Kecamatan Utasari Kabupaten Purbalingga Berdasarkan Data Resistivitas dengan Konfigurasi Wenner-Schlumberger. *Bulletin of Scientific Contribution: GEOLOGY*, 17(1), 15–22. https://jurnal.unpad.ac.id/bsc/article/view/39043

Amin, M., Tambun, B., & Halawa, A. (2023). Identifikasi Lapisan Aquifer Berdasarkan Metoda Geolistrik Konfigurasi Wenner Schlumberger Di Desa Petuaran Hilir Kecamatan Pegajahan Kabupaten Serdang Bedagai. *Jurnal Teknologi Informasi dan Industri*, 3(2), 167–177. https://ejurnal.istp.ac.id/index.php/jtii/article/view/304

Amir, A., Jahidin, J., & Rubaiyn A. (2022). Aplikasi Metode Resistivitas Konfigurasi Wenner Schlumberger Untuk Analisa Keterdapatan Batu Gamping Di Bawah Permukaan Pada Blok A Area Penambangan Pt. Ansaf Inti Resources Desa Tondowatu, Kabupaten Konawe Utara. *Jurnal Rekayasa Geofisika Indonesia*, 4(02), 105–199. https://doi.org/10.56099/jrgi.v4i02.27517

Anggriawan, P., Ngkoimani, L. O., & Suryawan, A. (2021). Studi Geomorfologgi Karst Daerah Labengki, Kecamatan Lasolo Kepulauan, Kabupaten Konawe Utara, Provinsi Sulawesi Tenggara. *Jurnal Ophiolite Geologi Terapan*, 03(02), 50–62. https://doi.org/10.56099/ophiolite.v3i2.23375

Ariputra Y. F., Putra Y. S., & Muhardi, M. (2021). Aplikasi Metode Geolistrik Resistivitas Untuk Mengidentifikasi Lapisan Bawah Permukaan Jalan Rasau Jaya, Kabupaten Kubu Raya. *Journal Online of Physics*, 7(1), 47–51. https://doi.org/10.22437/jop.v7i1.14632

Asdar M. F., Okto A., & Ngkoimani L. O. (2022). Karakteristik Batuan Ultramafik Daerah Tamainusi, Kecamatan Soyo Jaya, Kabupaten Morowali Utara, Provinsi Sulawesi Tengah. *Jurnal Geologi Terapan*, 04(02), 57–68. https://doi.org/10.56099/ophiolite.v4i2.28635

BPS Kabupaten Kolaka. (2023). *Kecamatan Wolo dalam Angka (Wolo Sub District in Figures).* Kolaka: BPS Kabupaten Kolaka.

BPS Sulawesi Tenggara. (2018). *Kabupaten Kolaka.* kolaka: sultra.bps.go.id.

Erwin, R., Hasria, H., Okto, A., Bahdad, B., Arisona, A., & Hamimu, L. (2023). Kandungan dan Ketebalan Endapan Nikel Laterit Di Kecamatan Langgikima Kabupaten Konawe Utara Provinsi Sulawesi Tenggara. *Jurnal Geomine*, 11(1), 22–41. https://jurnal.fti.umi.ac.id/index.php/JG/article/view/148

Hasria, H., Ramadhan A. M., Okto A., Masri, M., Bahdad, B., Ngkoimani L. O., & Azzaman M. A. (2022). Analisis Petrografi dan Geokimia Batuan Ultramafik Kompleks Ofiolit Kecamatan Andowia Kabupaten Konawe Utara, Provinsi Sulawesi Tenggara. *Jurnal Geosapta*, 8(2), 91–97. https://doi.org/10.20527/jg.v8i2.14112

Hati, A. P., Jahidin, J., & Hasan, E. S. (2022). Identifikasi Sebaran Batu Gamping Bawah Permukaan Dengan Menggunakan Metode Resistivitas Konfigurasi Wenner Schlumberger Pada Blok B Area Penambangan Pt. Ansaf Inti Resources Desa Tondowatu Kabupaten Konawe Utara. *Jurnal Rekayasa Geofisika Indonesia*, 4(02), 76–85. https://doi.org/10.56099/jrgi.v4i02.27524

Hermawan, O. R., & Putra, D. P. E. (2016). The Effectiveness of Wenner-Schlumberger and Dipole-dipole Array of 2D Geoelectrical Survey to Detect The Occurring of Groundwater in the Gunung Kidul Karst Aquifer System. *Journal of Applied Geology*, *1*(2), 71–81. https://doi.org/10.22146/jag.26963

Jaya, R. I. M. C., Masri., Juarsan, L. I., Haraty, S. R., Pramadana, R., & Hasria, H. (2024). Studi paragenesis serpentin pada batuan utramafik Kompleks Ofiolit Daerah Baula dan Pomalaa, Sulawesi Tenggara. *Jurnal Geologi dan Sumberdaya Mineral*, 25(2), 95–106. https://doi.org/10.33332/jgsm.geologi.v25i2.761

Jeremiarta, R. E., Sutarto, S., Setiawan, J., & Ardian P, F. (2022). Hubungan Karakteristik Batuan Dasar Terhadap Kadar Ni Pada Zona Laterit Di Daerah Wulu, Kabupaten Buton Tengah, Sulawesi Tenggara. *Jurnal Ilmiah Geologi PANGEA*, *9*(2), 1–9. https://doi.org/10.31315/jigp.v9i2.9502

Musrifin, L., Hasria, H., & Okto, A. (2021). Karakteristik Batuan Dasar Pada Profil Nikel Laterit PT. Baula Petra Buana, Desa Roraya, Kecamatan Tinanggea, Kabupaten Konawe Selatan, Sulawesi Tenggara. *Jurnal Ophiolite Geologi Terapan*, 03(02), 102–112. https://doi.org/10.56099/ophiolite.v3i2.23394

Nugroho, M. W., & Afiatna, F. A. N. F. (2021). *Pendekatan Metode Geolistrik dalam Perencanaan Pondasi.* Penerbit Samudra Biru. https://eprints.unhasy.ac.id/115/2/4.BUKU%20ISBN_Pendekatan%20Metode%20Geolistrik.pdf

Pambudi R. R., Nurul M., Prihadita W. P., & Mulyasari, R. (2022). Analisis Kelongsoran dengan Metode Geolistrik Konfigurasi Wenner-Schlumberger dan Wenner-Alpha di Jalan Raya Suban Bandar Lampung. *Jurnal Geocelebes*, 6(2), 108–116. https://doi.org/10.20956/geocelebes.v6i2.17903

Panjaitan, S. R., & Jusfarida, J. (2022). Pemetaan Geologi Untuk Menentukan Zona Akuifer Air Tanah Menggunakan Geolistrik Konfigurasi Wenner Di Desa Wonosemi, Kecamatan Banjarejo, Kabupaten Blora, Jawa Tengah. *Prosiding Seminar Nasional Sains dan Teknologi Terapan X*, 1–9. https://ejurnal.itats.ac.id/sntekpan/article/view/3570

Permana, M. R. (2017). *Studi Geologi Dan Alterasi Hidrotermal Pada Prospek Sentul Dan Buluroto, Kabupaten Trenggalek, Provinsi Jawa Timur.* Universitas Gadjah Mada.

Pratama, W., & Rustadi, R. (2019a). Aplikasi Metode Geolistrik Resistivitas Konfigurasi Wenner-Schlumberger Untuk Mengidentifikasi Litologi Batuan Bawah Permukaan Dan Fluida Panas Bumi Way Ratai di

Area Manifestasi Padok Di Kecamatan Padang Cermin Kabupaten Pesawaran Propinsi Lampung. *Jurnal Geofisika Eksplorasi*, 5(1), 30–44. https://doi.org/10.23960/jge.v5i1.21

Pratama, I. E., Muhtar, I. J., Syamsuddin, S., & Aswad, S. (2019b). Identifikasi Batuan Dasar Daerah Pantai Lumpue Kota Parepare Menggunakan Metode Geolistrik Konfigurasi Wenner. *Jurnal Geocelebes*, 3(1), 47–50. https://doi.org/10.20956/geocelebes.v3i1.6397

Puspita, R., Ninasafitri, N., & Ente, M. R. (2022). Karakteristik Batuan Ultramafik Dan Penyebaran Nikel Laterit Pada Daerah Siuna Kecamatan Pagimana Kabupaten Banggai, Sulawesi Tengah. *Jurnal Geocelebes*, 6(1), 93–107. https://doi.org/10.20956/geocelebes.v6i1.18523

Rachman, A. N., Oktariza, N., & Muzani, M. (2020). Struktur Geologi Pulau Sulawesi. *JAGAT (Jurnal Geografi Aplikasi dan Teknologi)*, 4(2), 9–18. https://ojs.uho.ac.id/index.php/jagat/article/view/12883

Sapina, E., Handayani, L., & Pebralia, J. (2023). Identifikasi Struktur Lapisan Tanah Pada Lahan Gambut Dengan Metode Resistivitas Konfigurasi Wenner-Schlumberger. *JGE (Jurnal Geofisika Eksplorasi)*, 09(02), 142–149. https://doi.org/10.23960/jge.v9i2.270

Saputra, F., Baskoro, S. A., Supriyadi, S., & Priyantari, N. (2020). Aplikasi metode geolistrik resistivitas konfigurasi wenner dan wenner-schlumberger pada daerah mata air panas Kali Sengon di Desa Blawan-Ijen. *Berkala Sainstek*, VIII(1), 20–24. https://doi.org/10.19184/bst.v8i1.11991

Sihombing, J., Lepong, P., & Supriyanto, S. (2023). Eksplorasi Batuan Andesit Berdasarkan Interpretasi Data Resistivitas Di Desa Petangis, Kecamatan Batu Engau, Kabupaten Paser. *Geosains Kutai Basin*, 6(2), 105–113. https://doi.org/10.30872/geofisunmul.v6i2.1126

Telford, W. M., Geldart, L. P., & Sheriff, R. E. (1990). *Applied Geophysics Second Edition.* Cambridge University Press.

Thorffata, D. S., Sutarto, S., & Soesilo, J. (2022). Geologi Dan Karakteristik Batuan Dasar Terhadap Endapan Nikel Laterit Di Daerah Watupari, Kecamatan Routa, Kabupaten Konawe, Provinsi Sulawesi Tenggara. *Jurnal Ilmiah Geologi Pangea*, 9(1), 110–117. https://doi.org/10.31315/jigp.v9i1.9574

Yuristina, A. P., Supriyadi, S., & Khumaedi, K. (2015). Pendugaan Persebaran Air Bawah Permukaan Metode Geolistrik Konfigurasi Wenner-Schlumberger di Desa Tanggungarjo Kabupaten Grobogan. *Unnes Physics Journal*, 4(1), 75–82. https://journal.unnes.ac.id/sju/upj/article/view/7070

Indexing and Abstracting

GEOFISIKA
UNIVERSITAS HASANUDDIN

ISSN 2579-5546